Technische Universität Dresden

Structure and Properties of Twin Boundaries in Ni-Mn-Ga Alloys

Robert Chulist

der Fakultät Mathematik und Naturwissenschaften der

Technischen Universität Dresden

zur Erlangung des akademischen Grades eines

Doktor rerum naturalium

(Dr. rer. nat.)

vorgelegte Dissertation

Eingereicht am 31. Januar 2011

Contents

Symbols and abbreviations

Symbols:

Ga	gallium
Mn	manganese
Ni	nickel
Ni_2MnGa	the stoichiometric Ni-Mn-Ga alloy
$L2_1$	ordered structure in ternary system of Heusler alloy
B2'	partially ordered structure in ternary system of Heusler alloy
5M	five layered martensite
7M	seven layered martensite
NM	non-modulated martensite

Abbreviations:

MSMA	magnetic shape memory alloy
MFIS	magnetic field induced strain
MIR	magnetically induced reorientation
MIPT	magnetically induced phase transformation
DS	directional solidification

HR   hot rolling

HE   hot extrusion

HPT   high pressure torsion

EBSD   electron backscatter diffraction

SEM   scanning electron microscope

HESR   high-energy synchrotron radiation

CS   coordinate system

PF   pole figure

IPF   inverse pole figure

ODF   orientation distribution function

K-S   Kurdjumov - Sachs

N-W   Nishiyama – Wassermann

Abstract

Ni-Mn-Ga alloys close to the stoichiometric composition Ni_2MnGa belong to the quite new family of ferromagnetic shape memory alloys. These alloys are characterized by the magnetic field induced strain (MFIS) based on the comparably easy motion of twin boundaries under a magnetic field. They are mostly chosen as a potential candidate for practical application especially promising for actuators and sensors because they are showing the largest MFIS so far. Depending on the chemical composition and heat treatment, at least three martensitic structures can be distinguished in the Ni-Mn-Ga system. However, the effect mentioned above only exists in two modulated structures. Since for the intended application of MFIS in technology polycrystalline materials seem to be more appropriate in contrast to single crystals, the specific polycrystalline aspects are considered. Factors important for decreasing the twinning stress and increasing the twinning strain of polycrystalline Ni-Mn-Ga alloys are texturing, adjusting the structure by annealing and training by thermomechanical treatments.

To achieve pronounced MFIS in polycrystals, fabrication processes are needed to produce specific strong textures. The material texturing has been obtained by directional solidification and plastic deformation by hot rolling and hot extrusion as well as high pressure torsion (HPT). To examine the texture of coarse-grained Ni-Mn-Ga alloys (due to a solidification process or dynamic recrystallization), diffraction of synchrotron radiation and neutrons was applied. The texture results show that the texture of Ni-Mn-Ga subjected to directional solidification, hot rolling and hot extrusion is a fibre or weak biaxial texture. However, local synchrotron measurements reveal that the global fibre texture of the hot extruded sample is a "cyclic" fibre texture, i.e. it is composed of components related to the radial direction rotating around the extrusion axis. This allows finding regions with a strong texture component. The texture after HPT is characterized by a strong cube

component with the cube favourably oriented.

The initial microstructure of the Ni-Mn-Ga alloys is a typical self-accommodated microstructure of martensite. High resolution EBSD mappings show macro, micro twins and two types of microstructure. The twin plane is determined to be {110}. In a typical martensitic transformation the high-temperature phase has a higher crystallographic symmetry than the low-temperature phase. Consequently, austenite may transform to several martensitic variants, the number of which depends on the change of symmetry during transformation. Generally, in a cubic-to-tetragonal transformation (5M case) three variants can form with the c-axis oriented close to the three main cubic axes of austenite. However, close examination of the high resolution EBSD mapping reveals that more than just three orientations, as expected from the Bain model, exist in $Ni_{50}Mn_{29}Ga_{21}$. Each of three Bain variants may be split in some twin relations in different regions of the sample which differ from each other by about few degrees creating a much higher number of variants.

The training process, as the last step in the preparation procedure of Ni-Mn-Ga alloys, consists of multi-axis compression finally leading to a single-variant state. Compression of polycrystalline samples leads to motion of those twin boundaries changing the volume fraction of particular martensitic variants in such a way that the shortest axis (c-axis) becomes preferentially aligned parallel to the compression axis. It allows reducing the twinning stress and maximizing the twinning strain. To understand the training process in more detail, the interaction of the twin variants with the neighbourhood of parent austenite grains was investigated.

1

Chapter 1

Introduction

1.1 Background

Due to their application potential, intelligent smart active and adaptive systems have arisen much interest. Smart behaviour such as change of shape, stiffness, colour, optical properties, or viscosity in response to its environment by external stimuli provides sensing and actuating functions. Intelligent materials can be classified according to type of response and activation, including stress, temperature, moisture, pH, electric or magnetic fields. Magnetic shape memory alloys (MSMAs) like Ni-Mn-Ga belong to these materials due to a shape change in response to a significant structural orientation change in the magnetic field.

Large magnetic field induced strain (MFIS) [1, 2, 3] can be realized either by a magnetically induced phase transformation (MIPT) or a magnetically induced reorientation (MIR). In MIPT, reported in several alloy systems like Ni-Mn-Ga-Fe and Ni-Mn-In [4], the martensitic transformation is initiated by application of a magnetic field due to a lowering of the transformation temperature which allows starting the martensitic phase transformation early. In contrast, MIR is due to an easy twin boundary motion and a high magnetocrystalline anisotropy in the martensitic state. Both possibilities make MSMAs suitable for a large number of technological applications like actuators or sensors. Since the discovery of 0.2% MFIS in a Ni-Mn-Ga alloy by Ulakko et al. in 1996 [1], with regard to this effect, several other alloy systems have been investigated like Co-Ni-Al, Co-Ni-Ga, Ni-Fe-Ga and Fe-Pd. However up to now, MFIS has mainly been reported for Ni-Mn-Ga [5, 6, 7]. The key characteristic making this material so attractive is the large MFIS observed in single crystals. Since for broad technical applications growth of single crystals is quite time consuming and cost intensive it is necessary to investigate polycrystalline samples on

their suitability for MFIS. To approach single crystals behavior, fabrication processes of polycrystals are needed which produce a strong texture. In general, twin boundary motion is affected by parameters such as order, modulation and grain size. Therefore, it is the task of this thesis to systematically investigate the effect of these parameters on MFIS in Ni-Mn-Ga alloys, especially in the five-layered phase. Factors important for decreasing the twinning stress and increasing the twinning strain of polycrystalline Ni-Mn-Ga alloys can be controlled by texturing, annealing and training processes. The training process, last step in the preparation procedure of Ni-Mn-Ga alloys, leads to a single-variant state allowing to reduce the twinning stress and maximize the twinning strain.

1.2 Martensitic transformation

The shape memory effect is strongly linked to martensitic phase transformations, i.e. first order, diffusion-less phase transformations where the lattice structure is changed by homogeneous deformation of the parent phase. The change of the lattice parameters is discontinuous with temperature. In displacive transformations each atom moves a very small distance but the macroscopic strain is quite large. As in mechanical twinning there is an invariant plane, also called habit plane, with respect to which a coordinated motion of atoms takes place creating mirror orientations. However, in contrast to mechanical twinning, martensitic transformations involve a lattice shear on both sides of the invariant plane and the term "parent lattice" is reserved for the austenite.

To minimize the strain energy the austenite transforms to several martensitic variants allowing large local shears to be accommodated with minimal macroscopic shear. Variants are single orientations created from the austenite. Originally, the name martensite was used to describe the "hard" microstructure found in quenched steels which is of great technological importance for steels because it combines an outstanding strength with high toughness. However, compared to shape memory alloys the shape memory effect is not observed in steels because in these materials the transition is not reversible (non-thermoelastic). The martensitic structure has also been found in many other materials including nonferrous metallic alloys, pure metals, ceramics, minerals and polymers. In a typical martensitic transformation the high-temperature phase (also called austenite as

in steel) has a higher crystallographic symmetry than the low-temperature phase (called martensite). Consequently, austenite may transform to several martensitic variants, the number of which depends on the change of symmetry during transformation. In a cubic-to-tetragonal transformation three variants can form with the c-axis oriented close to the three main cubic axes of austenite (Fig. 1.1).
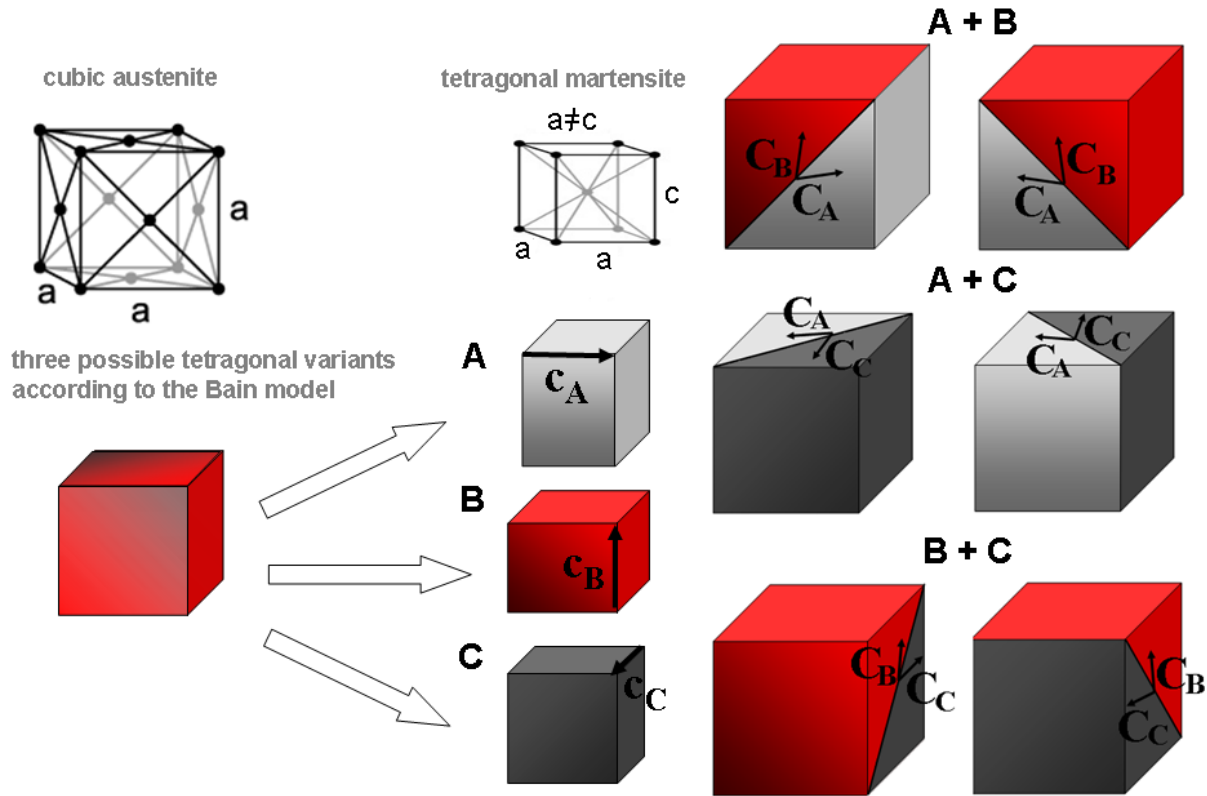

Figure 1.1: Three martensitic variants according to the Bain model and six different twins in tetragonal 5M Ni-Mn-Ga

There are a few models in the literature describing the orientation relationship between austenite and martensite. The three most important models considering the cubic-to-tetragonal transition are: Bain [8], Kurdjumov-Sachs [9] and Nishiyama-Wassermann [10, 11]. They describe this transition just as a rotation of some angle about a specific axis. Nevertheless, none of them is able to describe this phenomenon accurately in the Ni-Mn-Ga 5M structure. Therefore, the orientation relationship between austenite and martensite is examined thoroughly in this thesis. The martensitic transformation temperature in Ni-Mn-Ga alloys strongly depends on the alloy chemical composition [12, 13, 14] and generally increases with increasing average number of valence electrons.

1.3 Crystal structure

The crystal structure of Ni-Mn-Ga alloys has been studied by X-ray, electron and neutron diffraction. As X-ray atomic scattering factors of the elements Ni, Mn and Ga are close to each other compared to neutron scattering factors, neutron diffraction has been used as a powerful tool to determine the crystal structure of Ni-Mn-Ga. However, despite of several investigations, details of the crystal structure of martensite are still far from being understood. This problem is mainly addressed to modulated phases where the character and nature of modulation are constantly discussed in the literature.
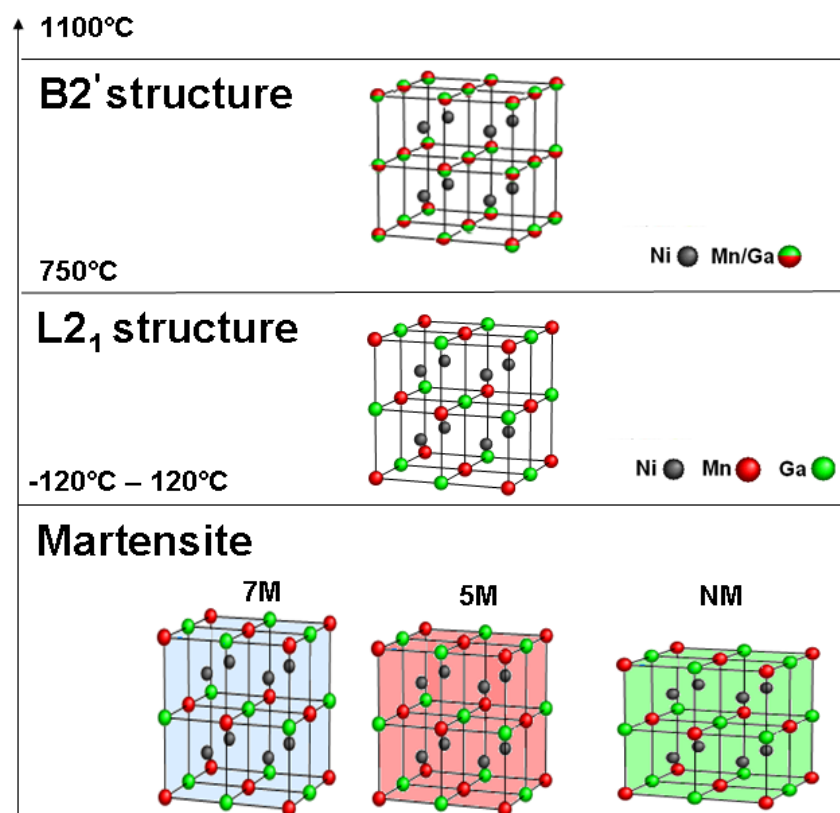

Figure 1.2: Schematic illustration of all phases in the Ni-Mn-Ga system

During cooling from high temperatures, Ni-Mn-Ga alloys experience different phase transitions, from B2´ via $L2_1$ austenite to martensitic structures (Fig. 1.2). A systematic study carried out by Brown et al. [15] reports that the high-temperature austenitic parent phase has a cubic $L2_1$ Heusler structure with a lattice parameter of about 5.82Å. The $L2_1$ structure belongs to the space group Fm3m, no. 225 with atom positions: Ni - 8c (0.25, 0.25, 0.25), Mn - 4a (0, 0, 0) and Ga - 4b (0.5, 0.5, 0.5). This order arises from the partially

disordered B2´ phase at about 750°C where Ni atoms occupy sites on one sublattice while Mn and Ga atoms are randomly distributed on the other (see Fig. 1.2)[16].

Depending on the chemical composition and heat treatment at least three martensitic structures can be distinguished in the Ni-Mn-Ga system: seven-layered modulated (7M, monoclinic approximately orthorhombic), five-layered modulated (5M) and non-modulated (NM), (both tetragonal) structures [1, 12, 17]. Martynov [17] interpreted the 7M structure as monoclinic with the lattice parameters a = 6.14 Å, b = 5.78 Å, c = 5.51 Å, γ = 90.5° and NM as tetragonal with a = 5.52 Å and c = 6.44 Å. For the 5M martensite Pons et al. [18] report that the unit cell is body-centred tetragonal with a = 5.90 Å and c = 5.54 Å. It should be noted that the lattice parameters of the modulated phases are given as average values of the 5M and 7M structures excluding modulation. The MFIS effect mentioned above only exists in the two modulated structures. The lowest observed twinning stress for the non-modulated martensitic phase is much higher ($\approx$ 15MPa) than that required for MFIS. Moreover, an uniaxial magnetic anisotropy [19] does not exist in the NM structure. Therefore much attention has been paid to the modulation, which can play a basic role during motion of twin boundaries. In brief, the modulation can be described as a periodic shuffling of atomic planes along the <110] direction [18, 20] and in diffraction patterns it is observed as extra spots along this direction (four and six extra spots in the 5M and 7M structure, respectively) [21, 22, 23].

Moreover, the nature of modulation determines the crystal structure of both modulated lattices. There are two approaches of modulation: one concept proposes sinusoidal shifts of atom position in one direction [18] while the other considers the layered structure as nano-twinning [24, 25]. Recent research tends to describe the modulation as nano-twinning, providing only small distortion of the tetragonal 5M structure. Thus, in order to determine the exact crystal structure of modulated phases, it is necessary to study the character of modulation and behaviour during twin boundary motion. Figure 1.3 presents the stability of the above mentioned phases as a function of temperature and e/a ratio. During cooling from high temperatures the martensitic phases occur in a specific sequence, namely: 5M=>7M=>NM.
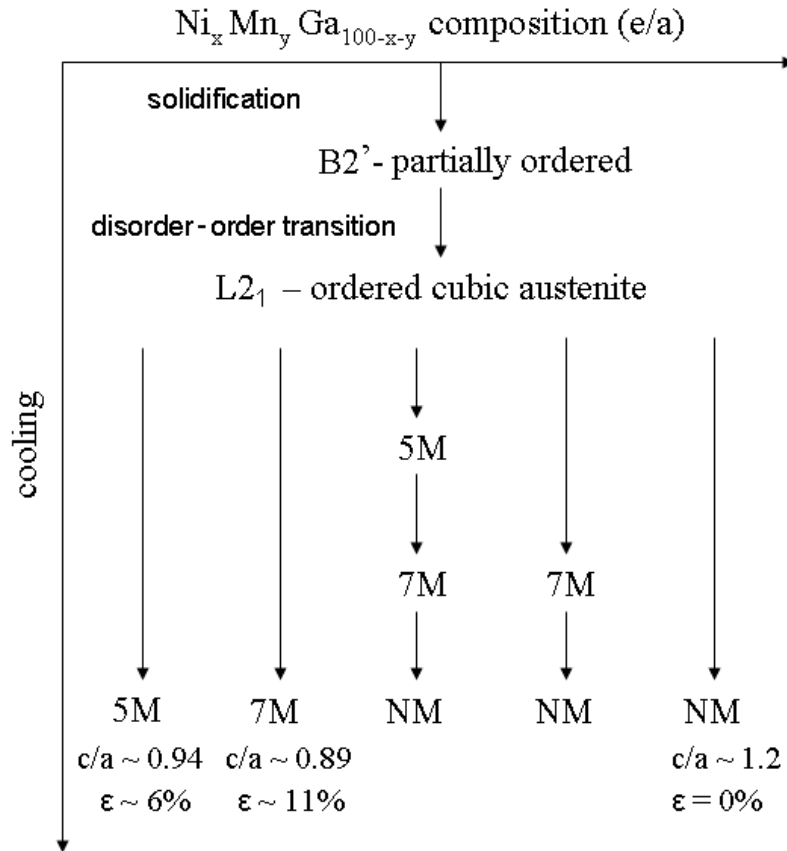
Figure 1.3: Phases in Ni-Mn-Ga alloys as a function of temperature and e/a ratio (according to [4])

1.4 Twinning and twin boundary motion

Besides crystallographic slip, deformation twinning is the most prevalent mechanism of plastic deformation in many materials. However in contrast to slip, twinning is a highly coordinated process. The parent lattice is reoriented by homogeneous atom displacement, which is equivalent to simple shear of the lattice. Similar to martensitic transitions, each atom moves only a small distance relative to its neighbours but the macroscopic effect is quite large. A twin plane is a highly symmetric interface that acts as mirror for the lattice on both sides. In the classic definition the relationship between twin and parent lattice has to comply with an invariant plane and can be realized either by a reflection in some plane or by a rotation of 180° about some axis. These operations are [26]:

- reflection in K_1

- rotation of 180° about η_1

- reflection in the plane normal to $\eta_{|1}$

- rotation of 180° about the direction normal to K_1,

with

K_1 first invariant plane

K_2 second invariant plane also called conjugate plane

$\eta_{|1}$ shear direction

$\eta_{|2}$ conjugate shear direction

S   shear plane

being the twinning elements in the classical theory of deformation twinning based on minimum shear and shuffle of atoms. Additionally, in the 5M structure the twinning relationship can be satisfied by rotation of 86.4° about the <100] common a-axis. This approach is commonly used here in the subsequent chapters. For 5M Ni-Mn-Ga polycrystals the twinning elements were determined to be: $K_1 = \{101)$, $K_2 = \{10\bar{1})$, $\eta_1 = <10\bar{1}]$, $\eta_2 = <101]$ and $S = \{100)$. Fig. 1.4 shows the geometry of twinning.
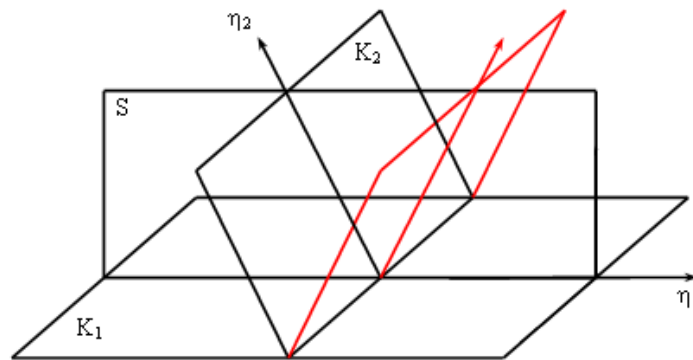
Figure 1.4: Geometry of twinning: the invariant twin planes are K_1 and K_2, the shear and conjugate shear directions are η_1 and η_2, respectively.

The martensitic transformation, which is similar to twinning, in addition involves a change of crystal structure. There also exists an invariant plane, with respect to which the lattice is sheared. As consequence of the energy minimization during martensitic transformation, twin boundaries are formed separating the martensitic variants, which fit together at the

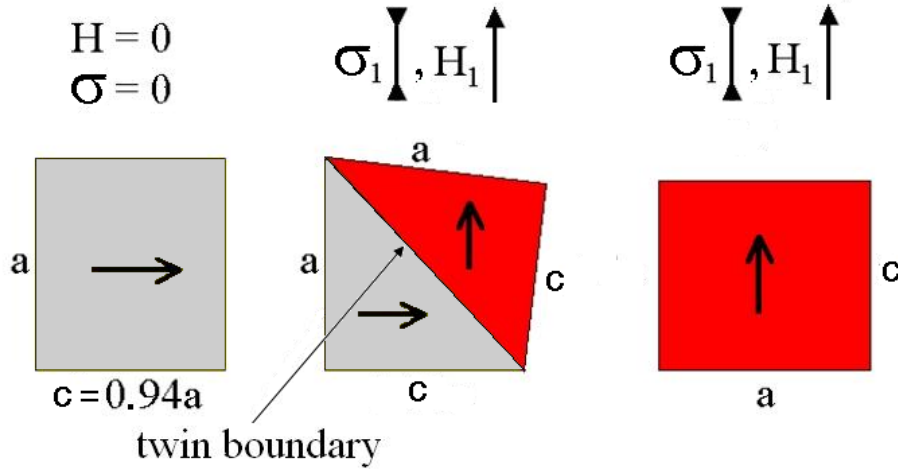**Figure 1.5:** Schematic diagram showing MIR in the 5M structure. The red variant grows at cost of the grey variant by moving the twin boundary with a magnetic field (H) or mechanical compressive stress (σ).

twin plane without distortion. These twin boundaries can be easily moved by a mechanical stress changing the volume fraction of particular variants. Compression of single crystals in the two-variant state, i.e. with different c-axis directions, leads to the alignment of the c-axis (shorter lattice parameter) along the compression direction. Due to the tetragonal 5M and approximately orthorhombic 7M structure, a macroscopic strain occurs by twin boundary motion exchanging the a- and c-axis (Fig. 1.5). As the c-axis is the magnetic easy direction, this effect can also be achieved by application of a magnetic field.

Theoretical MFIS values in the Ni-Mn-Ga system are given by the a/c ratio of the lattice parameters (eq. 1.1) and are in good agreement with maximum observed values. The lattice parameters used are expressed with respect to the so-called cubic coordinate system (see Chapter 1.6). In the modulated structures the theoretical maximum strains for 5M and 7M is 6% and 10%, respectively, while the maximum mechanical induced strain for NM martensite is about 20%.

$$\varepsilon_{\max} = 1 - \frac{c}{a} \qquad (1.1)$$

1.5 Magnetic properties of Ni-Mn-Ga alloys

It is the prerequisite for MFIS in the Ni-Mn-Ga system that the alloys must have the twinned ferromagnetic martensitic microstructure in the range of working temperature. This means that the reversible martensitic transformation has to take place below the Curie temperature (Tc). For Ni-Mn-Ga alloys Tc is reported to be around 370K [27, 28]. Since it is weakly dependent on composition [29, 30], almost the whole range of useful Ni-Mn-Ga compositions has a martensitic structure below Tc.

Another crucial parameter for MFIS is the magnetic anisotropy, which leads to twin boundary motion under an applied magnetic field. Magnetic anisotropy is the dependency of the internal energy of a system on the direction of the spontaneous magnetization. In general, the magnetic anisotropy is related to the crystal symmetry of a material and this is known as magnetocrystalline anisotropy. The magnetocrystalline anisotropy energy is defined as the work required to rotate the magnetization from the magnetic easy axis to the hard one and is described as:

$$E = K_1\alpha_1^2 + K_2\alpha_2^2 + K_3\alpha_3^2 \tag{1.2}$$

with:

K_i magnetic anisotropy constants

α_i direction cosines of magnetization

For the 5M structure with uniaxial anisotropy relation 1.2 simplifies to:

$$E = K_1 sin^2\theta + K_2 sin^4\theta \tag{1.3}$$

with:

θ angle between magnetization direction and magnetic field

For the 5M and 7M structures K_1 is about 1.7×10^5 J/m^3, and the easy axis of magnetization is along the c-axis which is the shortest lattice parameter. Due to the strong anisotropy, the magnetization vectors correspond to the easy magnetization axis in each martensite
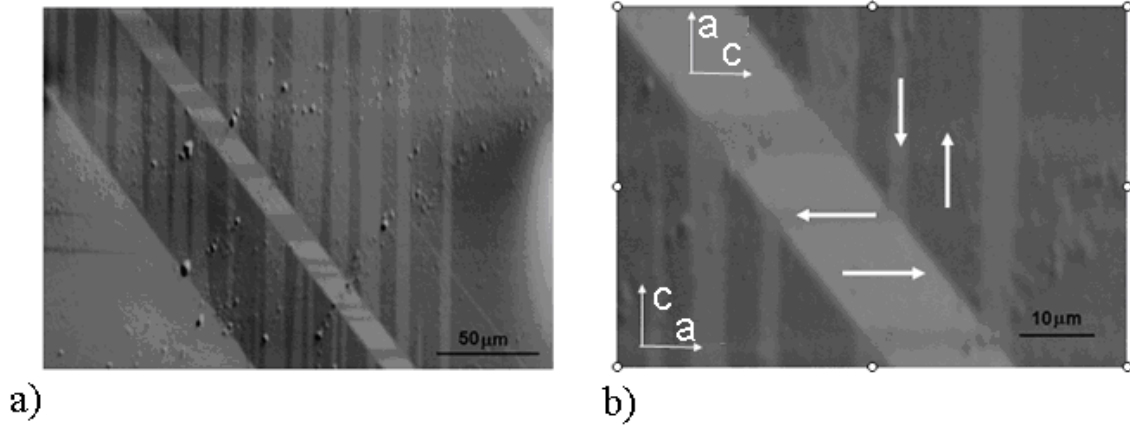
Figure 1.6: The magnetic domain structure in a 5M single crystal imaged with type II magnetic contrast. The orientation of the magnetic easy axis is marked in (b).

variant. This means that the magnetization inside the domains is aligned with the c-axis. An example is shown in Fig. 1.6, where 90° and 180° magnetic domain boundaries are depicted with type II magnetic contrast in the SEM.

1.6 Conventions of coordinate system in the 5M structure

There are two coordinate systems (CS) commonly accepted in the literature, in which the structure of 5M martensite is expressed:

- tetragonal CS related to the martensitic principle axes (marked with T)

- cubic CS

From the crystallographic point of view only the first CS is correct because it is constructed on the basis of the lowest number of atoms (smallest unit cell) and is used to determine orientations by EBSD (see Chapter 3.2). The so-called cubic coordinate system is also built up of a tetragonal lattice but with more atoms and rotated by 45° about the c-axis in such a way that the martensitic principal axes are aligned with the axes of the unit cell of the cubic parent $L2_1$ phase (Fig. 1.7). It should be mentioned, that all planes and directions mentioned in this thesis are given in the so-called cubic CS. Usually this CS is chosen for description of MFIS (see eq. 1.1). Note that the c-axis expressed in the cubic
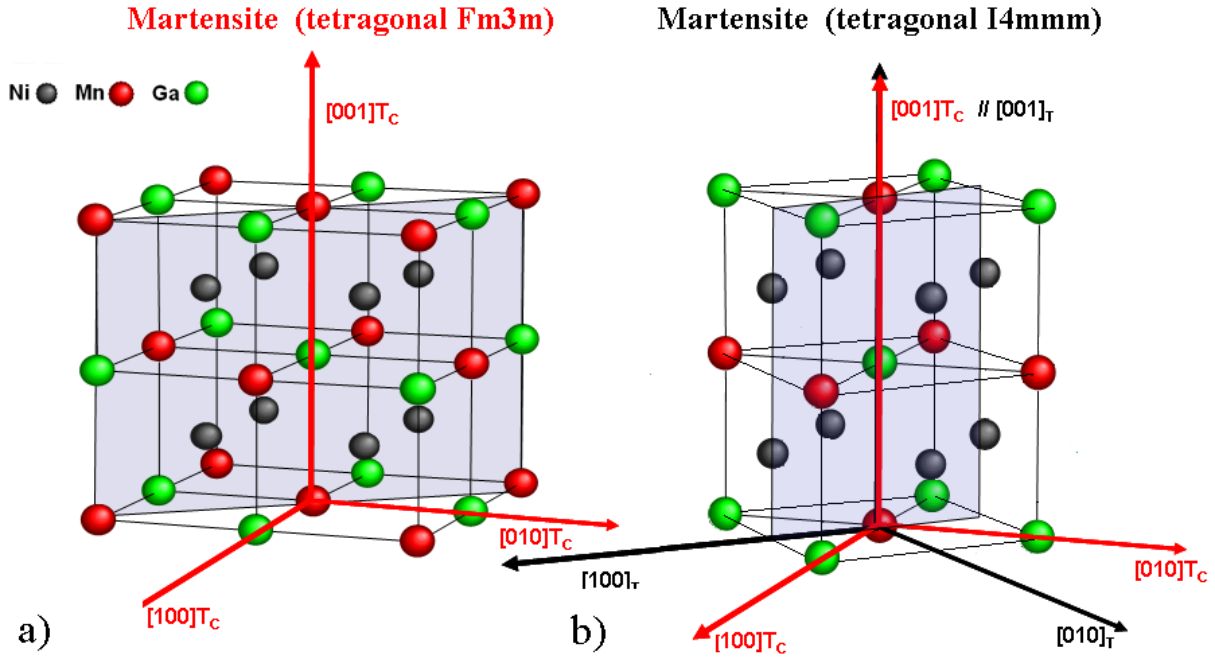
Figure 1.7: Two concepts of coordinate system: cubic (a) and tetragonal (b).

CS is the shortest lattice parameter while in the tetragonal CS it is the longest one often providing confusion in MFIS estimation.

The cubic CS is also chosen here for texture description. Since generally the texture is formed in the high-temperature cubic phase, it is easy to compare it with other metallic compounds with cubic structure, which do not undergo the martensitic transformation. Additionally, the tetragonal CS causes difficulties in the interpretation of texture. A good example is the <100> fibre texture in the cubic CS, which in the tetragonal CS is described as biaxial [001] and <110] fibre texture making the texture description more complex.

It should be also mentioned that the lattice parameters as well as planes and directions expressed in both CSs differ from each other. The transformation matrices to calculate any direction or plane in the tetragonal CS are given by eqs. 1.4 and 1.5, respectively.

$$
\begin{bmatrix} u_T \\ v_T \\ w_T \end{bmatrix} = \begin{bmatrix} 1 & -1 & 0 \\ 1 & 1 & 0 \\ 0 & 0 & 2 \end{bmatrix} * \begin{bmatrix} u_C \\ v_C \\ w_C \end{bmatrix} \tag{1.4}
$$

$$\begin{bmatrix} h_T \\ k_T \\ l_T \end{bmatrix} = \begin{bmatrix} 1 & -1 & 0 \\ 1 & 1 & 0 \\ 0 & 0 & 2 \end{bmatrix} * \begin{bmatrix} h_C \\ k_C \\ l_C \end{bmatrix} \tag{1.5}$$

1.7 Objectives

It is the main goal of the present thesis to establish the conditions under which MFIS can be achieved in polycrystalline Ni-Mn-Ga alloys. To develop new MFIS materials, respectively optimize the MFIS effect of known materials, it is a challenge to understand the physical processes determining the motion of twin boundaries in these materials. Twin boundary motion, in general, is affected by parameters such as order, modulation, grain size and texture. Therefore, it is the task of the work to systematically investigate the effect of these parameters on the MFIS in Ni-Mn-Ga alloys. In particular, the study comprises the microstructural investigations on polycrystalline samples. Such experiments allow revealing the martensitic microstructure and relationship between martensitic variants. Moreover, it allows observing twin boundary motion and, especially, directly seeing twin-twin and twin-grain boundary interactions (including other twin boundaries) and possible crack formation.

Texture is also an important object of interest. It determines the amount of strain to be achieved, which in a randomly textured sample is about 20% of that of a suitable oriented single crystal. With suitable type and strength of texture this percentage can be increased. Therefore, different processing routes like directional solidification (DS), casting plus hot rolling (HR), casting plus hot extrusion (HE) and casting, hot extrusion plus high pressure torsion (HPT) are used to obtain the texture desired. Texture is a crucial structural parameter of polycrystalline Ni-Mn-Ga alloys, which has to be optimized. Another important aspect with respect to the main goal is the training process of single as well as polycrystalline Ni-Mn-Ga. Up to now, it was not really evident why this process is needed. As polycrystalline samples are quite brittle, special care has to be taken during training to avoid microcrack formation.

This work was carried out within the priority program SPP 1239 "Magnetic shape Memory: Change of microstructure and shape of solid materials by external magnetic

fields" of the German Research Society (DFG) in cooperation with the Institute for Metallic Materials IFW Dresden and Fraunhofer Institute for Machine Tools and Forming Technology, Chemnitz. To produce and optimize the MFIS in Ni-Mn-Ga alloys extended cooperation of these three institutes was required. This includes experience in materials preparation and macroscopic characterization of IFW Dresden (Dr. S. Roth), experience in materials processing and engineering of Fraunhofer Institute (Dr. A. Böhm) as well as experience with microstructural and textural characterization of metals or intermetallics of the Institute of Structural Physics, TU Dresden (Prof. W. Skrotzki). Combination of these expertises allowed characterizing in great detail the real structure of Ni-Mn-Ga alloys.

2 Chapter 2
State of the art

So far the Heusler alloy Ni_2MnGa close to stoichiometric composition yields the largest MFIS. This alloy shows length changes of the order of 10% for moderate magnetic fields of about 1T at frequencies of the order of 1 kHz [1, 6]. The length change is produced by the movement of twin boundaries originating in this alloy from the transformation of the high-temperature cubic phase (austenite) to the low-temperature non-modulated (NM) and modulated (5M), both tetragonal, or (7M) monoclinic or even higher modulated phases (martensite) [18, 24, 25]. Applying a magnetic field leads to growth of those twin variants having the smallest inclination of the easy axis of magnetization with the magnetic field, i.e. which lower the magnetization energy.

Important for MFIS is the existence of a strong magnetic anisotropy making a simple rotation of the magnetization direction difficult, and a low twinning stress as well as an appropriate orientation of the twins. The composition, structure and microstructure of the alloy have to be adjusted to meet these prerequisites. The type of the magnetic anisotropy is determined by the c/a ratio of the tetragonal (or "nearly tetragonal", orthorhombic or monoclinic) martensite. The c/a ratio depends on composition [31], but various martensitic structures can also be found for the same composition depending on the sample type (powder, bulk) [32, 33].

Twinning can be achieved by applying a mechanical stress. Compression tests done on single crystalline samples of differently modulated structures (5M, 7M, NM) [34, 35, 36] in general show stress-strain curves with weak work-hardening. The stresses at the onset of deformation range from 0.1 [37] to 2 MPa and the maximum strains obtained by twinning range from 5.5 to 10.1%, depending on the c/a ratio, and are lowest in the 5M and 7M structures, while corresponding values are 7 to 15 MPa and 17 to 20.5% in the NM structure. Deformation experiments were carried out at different temperatures

[38, 39, 40, 41]. Twinning has also been produced by applying a magnetic field [6, 42]. The magnetic fields to induce twinning are 0.5 T and 0.4 T for the 5M and 7M structure, respectively. Twinning can be blocked by a compressive stress of the order of 2 MPa applied orthogonal to the magnetic field [2].

A dislocation model was proposed for MFIS in Ni_2MnGa based on the motion of 0.144 <111> type twinning dislocations on {112} type planes [43] (here referred to the tetragonal CS). Successive shear operations of twinning dislocations on {112} planes result in the reorientation of a microtwin. Calculations show that the application of a 0.4 T magnetic field can induce a shear stress of approximately 2.7 MPa on the twinning dislocations, a value exceeding the Peierls and yield stress for Ni_2MnGa single crystals. Twinning dislocations were detected by [44] while [45] based on their observations explained twin boundary motion by an atomic mechanism. Impurities and inclusions may impede the motion of the twin boundaries, e.g. by interaction with twinning dislocations. It was reported that very small amounts of sulphur (~ 100 atomic ppm) lead to formation of MnS precipitates in Ni-Mn-Ga-alloys [46], while oxygen leads to MnO precipitates [47]. Therefore, the amount of inclusions has to be reduced by avoiding oxidation and refining the starting materials, especially by extracting sulphur from the manganese, whereas size and distribution of these precipitates are to be controlled by proper annealing.

To study MFIS, so far mainly single crystalline samples have been used. However, because of economic reasons for technical applications only polycrystalline alloys or composites seem to be appropriate. The length change of polycrystalline aggregates is significantly lower than that of single crystals. For a random orientation distribution it is 21%, it amounts to 50% when the normal of the twin boundary is parallel to the magnetic field [48, 49]. According to investigations on twinning in metals [50], the twinning stress follows a Hall-Petch relation, i.e. with decreasing grain size the twinning stress increases and hence MFIS becomes more difficult to realize. This has been confirmed for polycrystalline Ni-Mn-Ga samples. Material texturing was obtained by using directional solidification [51, 52], rapid solidification through planar flow casting [53], plastic deformation by hot forging [54], hot rolling [51, 55, 56], hot extrusion [57, 58], high pressure torsion [59] and additional heat treatments for grain growth [60]. The movement of twin boundaries in polycrystalline samples was clearly shown in [61, 62]. Similar to single crystals, adjusting the

structure [63] and training [62] is important. Coarse-grained polycrystals with solidification texture show MFIS as large as 1% after proper treatment including two step annealing and mechanical training [64].

3

Materials, processes and experimental methods

To achieve pronounced MFIS in polycrystals, fabrication processes are needed to produce specific strong textures. Materials fabricated with directional solidification or plastic deformation like hot rolling, hot extrusion and high pressure torsion (at high temperature to avoid brittle fracture) have a coarse-grained microstructure due to solidification or dynamic recrystallization. Therefore, to investigate the texture of a coarse-grained material with a good grain statistics high energy X-ray and neutron diffraction were used. On the other hand to reveal fine martensitic microstructures, electron backscatter diffraction (EBSD) in the scanning electron microscope (SEM) was applied. The combination of both techniques was mainly used to systematically investigate the effect of the above mentioned parameters on MFIS in Ni-Mn-Ga alloys.

3.1 Materials and processes

The main criterion for the selection of materials for MFIS is the actuation performance. As mentioned above, the Ni-Mn-Ga Heusler alloys so far are giving the largest MFIS. These alloys show length changes up to 10% and 6% for 7M and 5M structure, respectively. At first sight due to the larger MFIS, the 7M structure seems to be more suitable for technical application. However, because of the following problems the 5M structure with exact composition $Ni_{50}Mn_{29}Ga_{21}$ was chosen. 7M martensite is highly limited to a narrow temperature and composition range. Additionally, due to internal stresses in 7M polycrystals, the NM phase may occur acting as barrier for twin boundary motion [51]. Therefore, investigations on 5M Ni-Mn-Ga predominate in recent research. The

single crystals investigated were prepared by the Bridgman method and supplied by the company Adaptamat. The polycrystalline samples were prepared from prealloys by induction melting of pure elements [65]. The martensitic transition of $Ni_{50}Mn_{29}Ga_{21}$ takes place at a temperature of 328 K. The individual fabrication processes are described in the following chapters.

3.1.1 Directional solidification

Pronounced material texturing has been produced by directional solidification (DS). DS was carried out under Ar atmosphere. A prealloy was prepared by induction melting of pure elements (Ni 99.98, Mn 99.8, Ga 99.999) [65]. The alloy was annealed for 48 h at 1273 K under (Ar/5% H_2) atmosphere for homogenization. The casting process was performed in an Indrudet S investment casting machine followed by furnace-cooling to room temperature. The principle of the experimental setup is as follows. A hot mold is mounted on a copper cooling plate. To avoid heating of the cooling plate by the hot mold, an insulation ring is placed between the mold and the plate. When the melt is cast into the mold, a temperature gradient and thereby a heat flow through the melt toward the bottom is generated. This causes DS in opposite direction. Coarse columnar grain growth was achieved by using a hot mold with a cooled copper plate at the bottom. The mold was heated in a separate furnace to a temperature close to melting. The cylindrical sample cut from the cast ingot above about 1 *cm* from the bottom had a diameter and height of 8 *mm* and 15 *mm*, respectively.

3.1.2 Hot rolling

Another route to obtain texture is plastic deformation by hot rolling (HR). To perform HR a master alloy of composition $Ni_{50}Mn_{29}Ga_{21}$ produced by induction melting in Ar atmosphere followed by casting into a cold copper mold was prepared. The mass loss was negligible, hence the composition is assumed to be the intended one. Subsequently, the ingot ($7.9 \times 11.9 \times 44 \, mm^3$) canned in steel was rolled at a temperature of 1273 K up to 50% reduction and then air-cooled to room temperature. No crack formation was observed during processing. For textural and microstructural investigation the sample

with dimensions of $10 \times 15 \times 3\,mm^3$ was cut by spark erosion from the rolled sheet.

3.1.3 Hot extrusion

An important technological process to achieve specific strong textures is hot extrusion (HE). The initial material was prepared in the same way as in the hot rolled case. Cast $Ni_{50}Mn_{29}Ga_{21}$ sample was hot-extruded through a round die. To decrease friction during extrusion, the cylindrical ingot ($100\,mm$ length, $35\,mm$ diameter) was canned in stainless steel. Direct extrusion processing was done at 1273 K with an extrusion ratio of 4/1. The extruded rods were air-cooled. For the texture measurements three cylindrical samples with height and diameter of 10 mm were cut from the extruded rod at the front, middle and end. Additionally, five different samples as shown in Fig. 4.29 where cut for EBSD and synchrotron radiation measurements.

3.1.4 High pressure torsion

An advanced fabrication process applied is high pressure torsion (HPT). As starting material the hot extruded sample was used. From the extruded rod at half length in the centre, a cylindrical sample with length and diameter of 10 mm was cut by spark erosion. High strain torsion of the sample with torsion axis parallel to the extrusion axis was done with a Paterson rock deformation machine [66] at 1073 K under a confining pressure of 400 MPa. The maximum shear strain and shear strain rate applied were about 3 and $2 \times 10^{-4} s^{-1}$, respectively. The pressure produced by Argon gas creates large contact forces between the parts of the sample assembly as well as between the internal load cell and the upper end of the sample assembly. Due to this, a torque can be transmitted to the sample by friction through the movement of the torsion actuator. The torque is limited by possible slipping between the components of the sample column. The shear stress – shear strain curve for the surface of the sample was calculated from the measured torque and twist data according to the procedure given in [66, 67]. After some undefined oscillations the shear stress at a shear strain of about 2 reaches a steady state value of about 18 MPa, which is the maximum shear stress acting in the torsion sample. The shear strain increases from zero in the centre of the bar to a maximum at the edge according to [68].

3.2 Experimental methods

3.2.1 Electron backscatter diffraction

In the last decade electron backscatter diffraction (EBSD) has become a well-established technique for obtaining microstructural and crystallographic information in the scanning electron microscope (SEM). EBSD reveals grain orientation, grain size, grain boundary character, micro texture, and allows phase identification. The nominal angular resolution limit is about 0.5° and the spatial resolution in modern field emission SEMs is about 40 nm.

The EBSD experiments are mostly used for crystal orientation mappings (also called orientation imaging, TSL Companies). In crystal orientation mapping, the electron beam is scanned over the sample measuring the orientation from the diffraction pattern at each point. The experimental setup and indexing process are shown in Fig. 3.1. A sample commonly tilted at 70° is irradiated by an electron beam forming a diffraction pattern of Kikuchi lines on a phosphor screen. Special computer software analyzes these Kikuchi lines using the Hough transform and compares them with theoretical Kikuchi lines for a known crystal structure to get the best orientation fit. These data can be used to show the crystallite orientations (here referred to as texture) of the material as well as their spatial distribution. For microstructure and texture investigations of Ni-Mn-Ga single and polycrystals two SEMs (Zeiss Ultra 55 at TU Dresden and Zeiss Supra 25 at Fraunhofer Institute for Machine Tools and Forming Technology in cooperation with Dr. A. Böhm) were used.

Usually, electron microscopic investigations require special preparation steps. As EBSD patterns are formed in a surface layer of $10 - 50 \ nm$, any residual surface deformation introduced during the preparation must be minimized in order to maximize pattern quality. To achieve this, several preparation steps were used:

- mounting of the samples into a two-component epoxy system consisting of a conducting and insolating layer

- mechanical grinding with SiC papers (up to 2000 size)

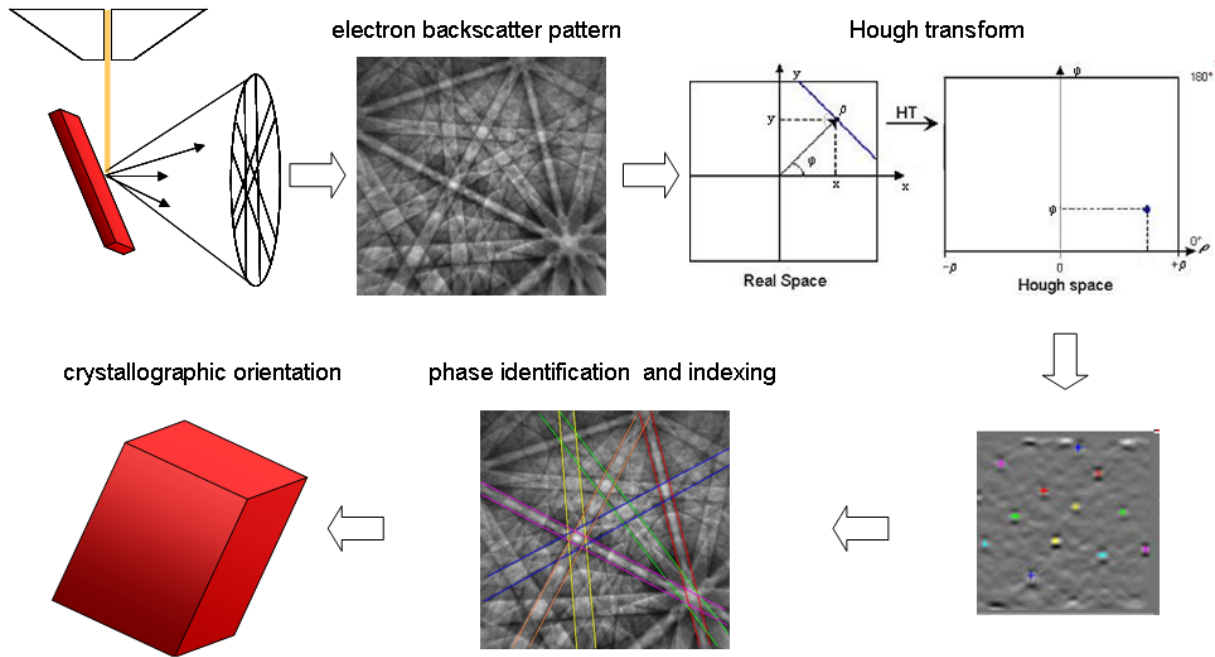- polishing with alumina suspension (particle size 1.0 and 0.3 μm)

Figure 3.1: Experimental EBSD setup and indexing procedure

- electro-polishing using a mixture of nitric acid and ethanol (volume ratio 1:3) and polishing parameters: T = 273K, U = 8V and t = 90s.

3.2.2 High energy synchrotron radiation

Diffraction with high-energy synchrotron radiation (HESR) is a quite new experimental method to determine textures of materials. The high penetration depth of synchrotron radiation opens the possibility to investigate representative large sample volumes. HESR wavelengths in the range of 0.1Å can penetrate deep into the materials allowing measurements in transmission geometry. Additionally, HESR texture measurements with an area detector based on Debye-Scherrer ring analyses are extremely time-saving. The main part of the experimental setup of texture measurements with HESR is shown in Fig. 3.2. The collimated X-ray beam transmits through the sample volume (red area) and a Debye-Scherrer ring pattern is recorded on a flat area detector. Each Debye-Scherrer ring corresponds to a family of lattice planes (hkl) and its intensity is transformed with a special software into a corresponding pole figure. In order to obtain the complete texture information, the sample is rotated on a goniometer around the ω axis by 180°. A detailed description of the synchrotron texture measurement is given in [69]. The texture
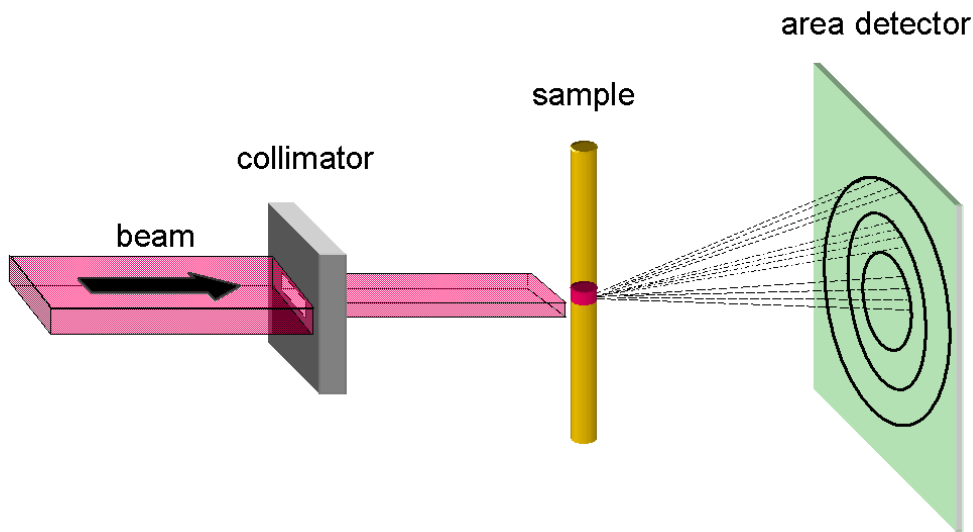
Figure 3.2: Experimental setup for texture measurements by HESR (schematic diagram made by R. Tamm)

measurements with HESR (100 keV) [70] on Ni-Mn-Ga alloys were carried out using the beam line W2 and the GKSS materials science beam line HARWI-II at DESY in Hamburg, Germany.

3.2.3 Neutron diffraction

The geometrical aspects of neutron and X-ray diffraction are the same but in contrast to X-rays, which are scattered by electrons, neutrons are mainly scattered by the atomic nuclei and magnetic moments. Due to their low attenuation by most materials, neutrons penetrate deeply into the samples. Additionally, neutron as well as HESR texture measurements do not require any special sample preparation. Thus, neutron diffraction may be used to measure textures of coarse-grained materials. The texture measurements with neutron diffraction (9.3 keV) on Ni-Mn-Ga alloys were carried out at GKSS Research Centre Geesthacht, Germany.

3.2.4 Training experiments

To achieve MFIS in Ni-Mn-Ga alloys, a training process has to be applied. This process consists of successively compressing mostly cuboid samples along two or three axes. As a result the twinning stress is reduced and the twinning strain is maximized. Training

of polycrystals was performed in an Instron 8562 testing machine at room temperature under a compressive stress up to 30 MPa at a strain rate of 10^{-3} s^{-1}. The training process on single crystals using the same parameters was carried out in an Instron 5566 testing machine in cooperation with Prof. M. Szczerba at AGH University of Science and Technology, Faculty of Non-Ferrous Metals, Cracow, Poland.

3.3 Representation of texture

3.3.1 Coordinate systems

In order to describe an orientation of a crystallite in a polycrystal, it is necessary to establish two coordinate systems (CSs), one related to the crystal and another one related to the sample taking into account the geometry of fabrication, deformation process or relevant directions related to the external shape of the specimen. Usually, Cartesian right-hand CSs are used for both the crystallite and the sample (Fig. 3.3). For example in Fig. 3.4c, for a rolled sample the rolling direction RD and normal direction ND are parallel to X_s and Z_s, respectively. Generally, in cubic, tetragonal and orthorhombic materials the crystal CS is fixed to the basis vectors a, b and c of the Bravais lattice. Commonly, the following representations of texture are used: pole figures, inverse pole figures, sections of the orientation distribution function and ideal components. These are described in the next subsections.

3.3.2 Pole figure and inverse pole figure

A pole figure (PF) represents the projection of specific crystallographic directions of grains in the sample CS. In the stereographic projection, illustrated in Fig. 3.4a, a direction (dashed line) cutting the sphere at point P is projected from the south pole S into the equatorial plane at the point P'. Different PFs illustrating the same crystal orientation are shown in Fig 3.4b. The inverse pole figure (IPF) represents the distribution of a selected sample direction in the crystal CS (Fig. 3.5). An IPF is a convenient way to show fibre textures.
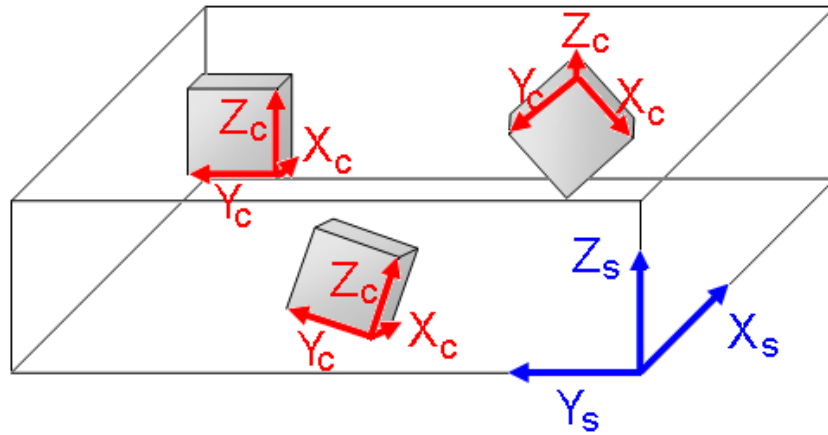
Figure 3.3: Relationship between crystal (red) and sample coordinate system (blue) with three unit cells differently oriented
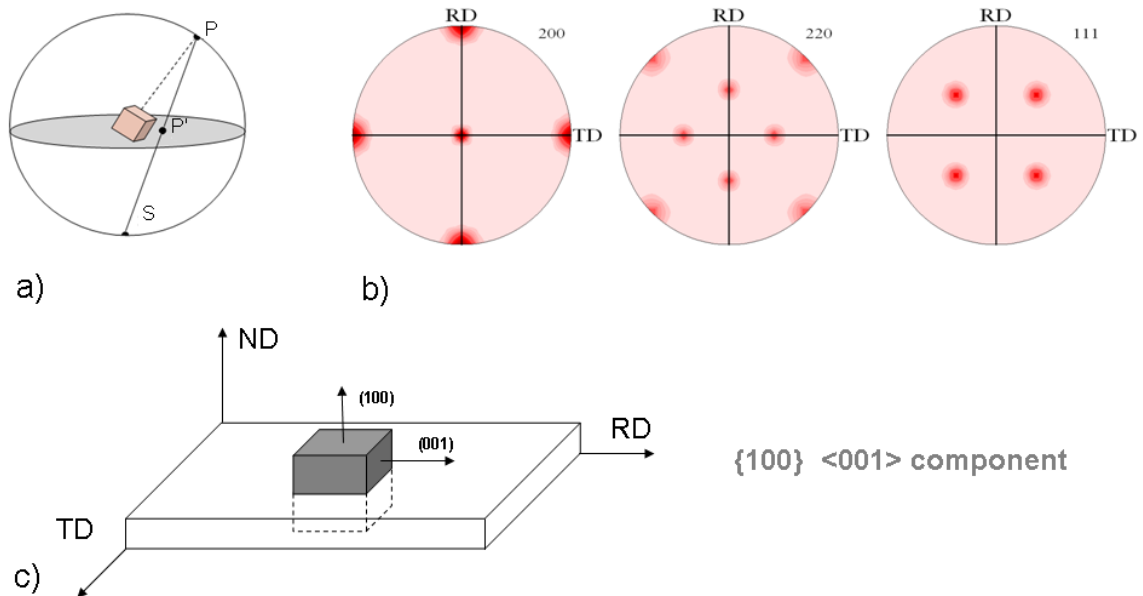

Figure 3.4: Stereographic projection of a <100> crystal direction (a). (200), (220) and (111) pole figures showing the {100} <001> ideal component (b) and the same component placed in a rolled sheet of a metal (c)
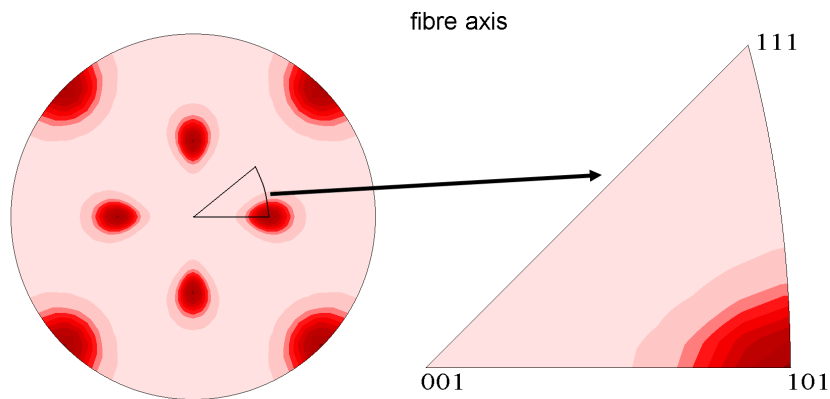
Figure 3.5: Inverse pole figure of an ideal <110> fibre texture (a) and a reduced triangle due to cubic crystal symmetry (b)

3.3.3 Orientation distribution function

An orientation g is unambiguously defined by a set of three angles φ_1, Φ and φ_2. These so-called Euler angles represent successive rotations of the crystal CS with respect to the sample CS, for example according to the Bunge notation [71]). Any orientation g represents a point in the three-dimensional orientation space spanned by the three Euler angles. The volume fraction of grains with orientations between g and g + dg is given by [72]:

$$\frac{dV}{V} = f(g)dg$$

where:

f(g)   orientation distribution function (ODF)

g   orientation $(\varphi_1, \Phi, \varphi_2)$

dV   volume of crystallites with orientations between g and g+dg

V   sample volume

The intensity (strength) of texture is given in multiples of a random distribution (mrd). For triclinic crystal and sample symmetry, the ODF is defined in the range of $0° - 360°$

for φ_1 and φ_2 and 0 –180° for Φ. In the case of cubic sample and crystal symmetry it can be reduced to 0° – 90° for all Euler angles. Any three-dimensional ODF can be expressed
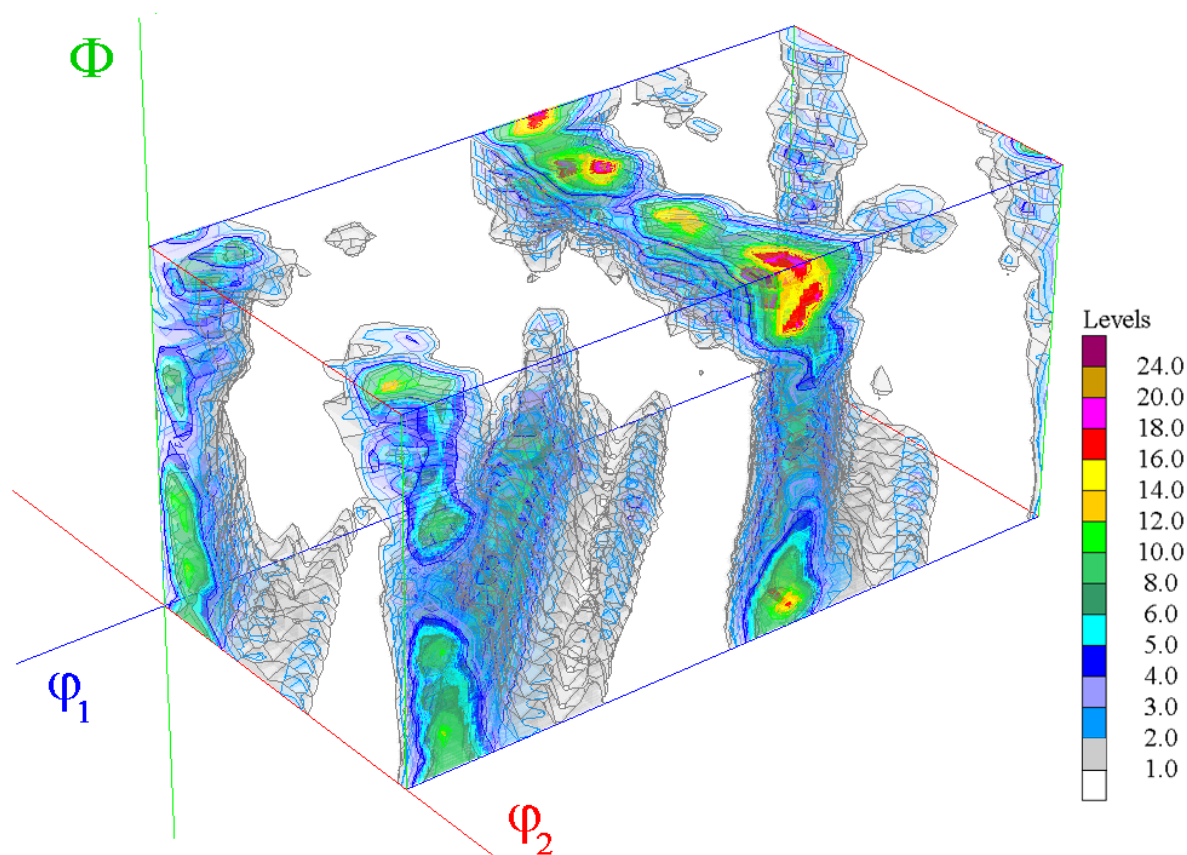

Figure 3.6: Shear texture after HPT at 1073K of 5M Ni-Mn-Ga represented as three-dimensional ODF. Intensities are given in multiples of a random distribution (mrd).

by two-dimensional cross sections through the Eulerian space. These sections simplify the texture analysis, especially when sections are used which contain the most important components. Additionally, a key figure allows better interpretation of textures.

3.3.4 Ideal orientation

A practical way to describe an orientation is via crystal plane and direction aligned parallel to principal planes and directions of the sample. It is expressed with Miller indices, for example, for the ideal cube component described as {100} <001> (Fig. 3.4c) the {100} plane corresponds to the rolling plane normal (ND) while the <001> direction is parallel to the rolling direction (RD). The indices for the plane and direction are rounded to the nearest low index. Ideal orientations of fcc metals deformed by simple shear are given in
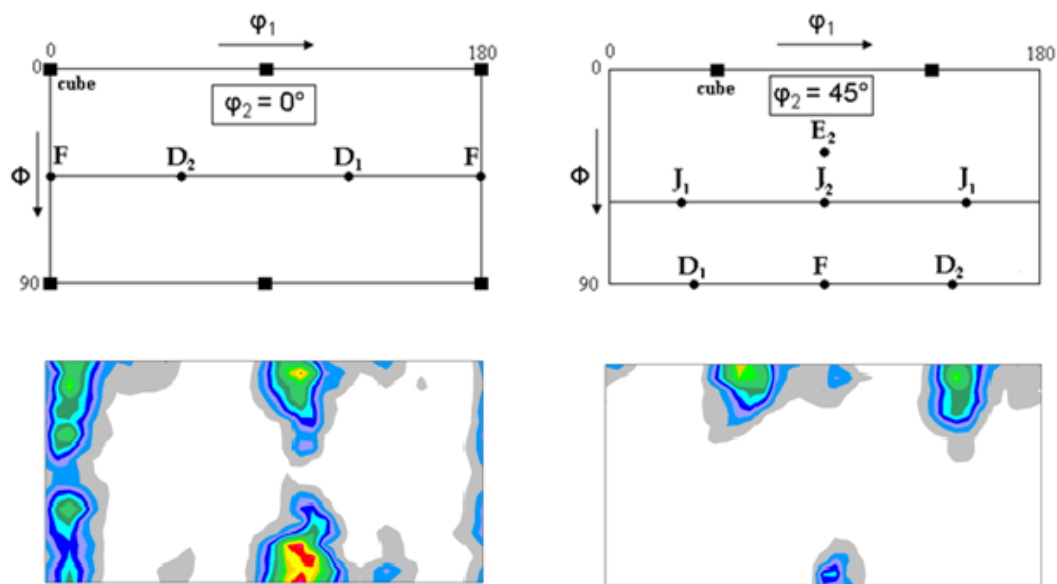
the key figure of Fig. 3.7 and in table 4.2.

Figure 3.7: ODF sections at $\varphi_2 = 0°$ and $\varphi_2 = 45°$ of Fig. 3.6. The key figure gives the ideal components of simple shear of bct metals plus the cube component.

Chapter 4

4 Results and discussion

4.1 Microstructure of Ni$_{50}$Mn$_{29}$Ga$_{21}$

A very interesting feature of the martensitic transformation is the microstructure it produces. In a martensitic transformation the lattice of the high-temperature austenite phase has a higher crystallographic symmetry than that of the low-temperature martensite phase. Consequently, austenite may transform to several martensitic variants, with the number depending on the change of symmetry during transformation. In a cubic-to-tetragonal transformation three variants may form with the c-axis approximately oriented parallel to the three main cubic axes of austenite. Different regions of the crystal transform to different martensitic variants in such a way that there is no macroscopic change in shape allowing large shears to be accommodated with minimal macroscopic shear. This characteristic feature is called self-accommodation.

The arrangement of variants can occur on different length scale, from a few nanometres up to a few millimetres depending on grain size, specimen size, change of lattice parameters (austenite-martensite) and processing. The initial microstructure of Ni-Mn-Ga alloys is a typical self-accommodated martensitic microstructure containing a mixture of variants. The Ni-Mn-Ga polycrystals investigated consist of macro and micro twins (Figs. 4.1, 4.2). The coarse twin lamellae extend through the whole parent austenitic grains while the fine lamellae frequently cross the coarse variants in a zig-zag manner with mirror symmetry (Fig. 4.1b). This kind of microstructure was observed in all polycrystals investigated. It should be mentioned that the fine twin lamellae can only be resolved by EBSD at high magnification (Fig. 4.1b). It is obvious that there exists a hierarchy in twin formation. At first the coarse twin lamellae are formed (shown in Fig. 4.1a) and subsequently the fine twins develop (Fig. 4.1b). This is concluded from the fact that the fine twins are not
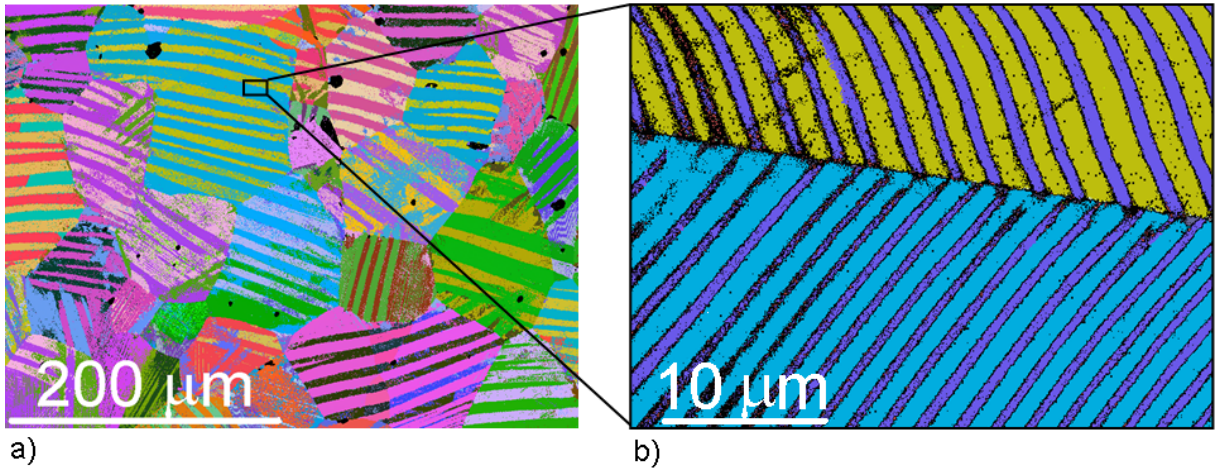
continuous across the coarse lamellae.

Figure 4.1: Macro (a) and micro twins (b) in a hot extruded 5M Ni-Mn-Ga alloy

To investigate the relationship between macro and micro twins a bicrystal was used. The bicrystal also consists of macro and micro twins [62] (Fig. 4.2a). The twin planes are within about 2° parallel to {1 0 1}. Close examination of the microstructure (for example in Figs. 4.2a, b) shows that the fine lamellae are twin related with respect to the macro twins and create a so-called "twins within twins" structure.

The initial orientation mapping reveals a distribution of three different martensitic variants in both parent austenitic grains. These martensitic variants with c-axis approximately parallel to the main cubic axes of the parent austenite originate from the cubic-to-tetragonal transformation according to the Bain model. All three variants of the tetragonal unit cell revealed in the pole figures of the bicrystal are displayed in Fig. 4.2c. The c-axis and a-axes, short (5.51 Å) and long (5.91Å) lattice parameter, represent [001] and <100] directions. Since the twin plane is of {1 0 1} type, the trace of this plane should be placed exactly in between two c-axes. To demonstrate this, the stereographic projection has been used. For example within grain 1, the trace of the twin plane between the pink and blue orientation is indicated as a black line (Fig. 4.2b). The black dashed line shows how this plane crosses the flat surface and corresponds very well to the orientation mapping on the left hand side (Fig. 4.2a).

Similarly, the other traces of twin planes (red and green) correspond to the orientation mapping. It should be noted that the green line marks the macro (main) twins and the red and black lines mark the micro (fine) twins. As mentioned above the twin planes

(by means of two-surface trace analysis on two perpendicular surfaces of the bicrystal) were also geometrically determined to be {101}. Besides the so called "twins within twins" structure another type of microstructure can be observed in Ni$_{50}$Mn$_{29}$Ga$_{21}$ alloys. Orientation mapping shows that the boundary plane of one of the micro twins is far away from ideal position (Figs. 4.3a, b, the ideal position is marked with a red line), while the second micro twin and the main twin remain unchanged. In this configuration the micro twin planes look like a mirror image with respect to the main twin boundary on both perpendicular surfaces (Fig. 4.3c) but in fact one of them is not twin related.
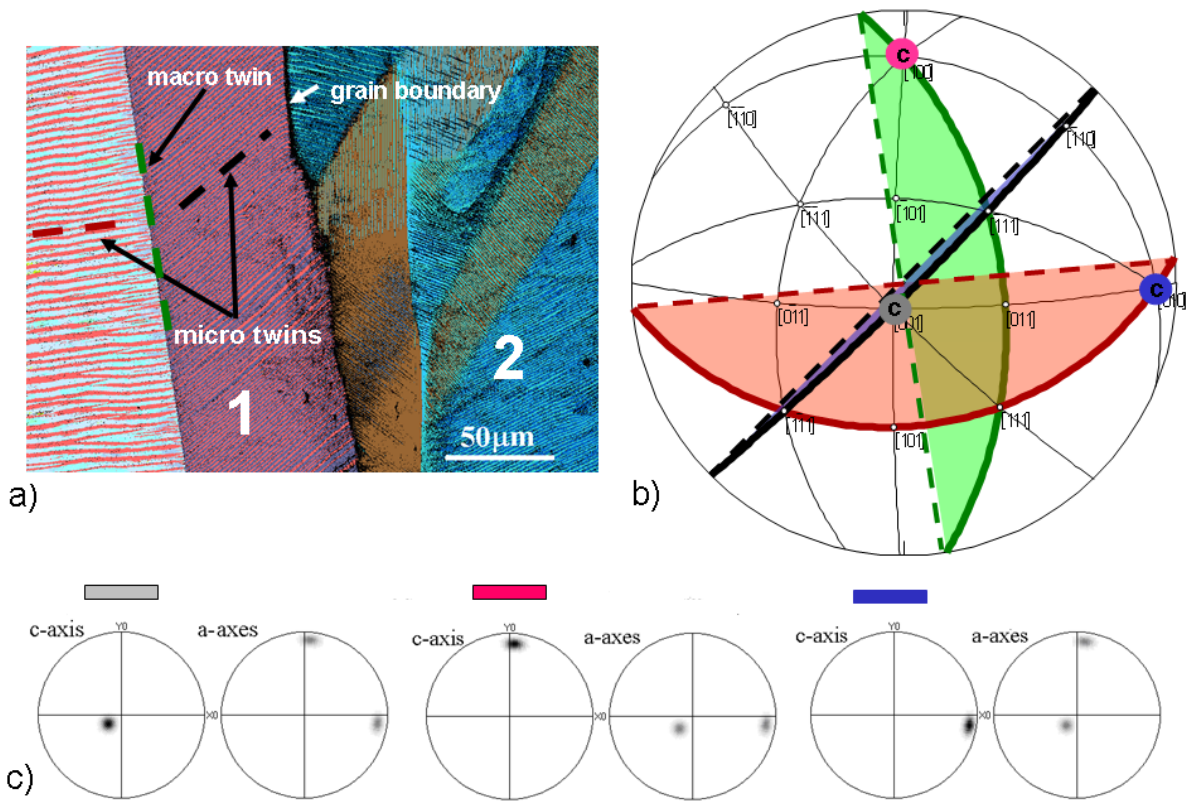

Figure 4.2: Orientation mapping (a) and stereographic projection with indication of twin traces in grain 1 (b) of the bicrystal. Pole figures of differently coloured areas of the tetragonal 5M phase of grain 1 (c). The c-axis and a-axes (short and long lattice parameter) represent [001] and <100] directions of the tetragonal 5M structure, respectively. 1 and 2 denote the two grains of the bicrystal.

The second plane is about 3° away from {1 1 0), which is not equivalent to the {1 0 1) twin plane in the tetragonal system. However, the traces of these planes look like a mirror image with respect to the main twin boundary on both sides of this plane but crystallographically they are not twin related. Furthermore, in Fig. 4.2a characteristic
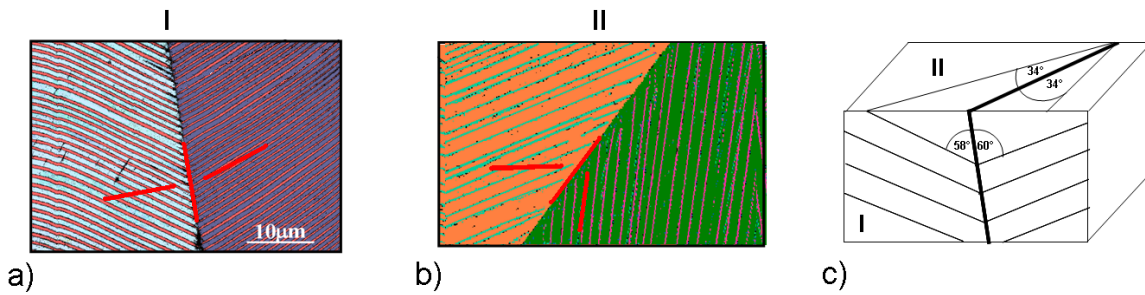
Figure 4.3: Orientation mapping on two perpendicular surfaces (I and II) of the 5M Ni-Mn-Ga bicrystal (a, b). Schematic diagram showing the angles between micro and macro twins (c)

branching of the micro twins is observed due to lowering of the elastic energy at the macro twin boundary. Branching is favoured by a small interface energy, large grain size and soft elastic behaviour in the martensite [73].

4.2 Microstructure of Ni$_{50}$Mn$_{30}$Ga$_{20}$

As mentioned above, the 7M martensite is highly limited to a narrow temperature and composition range. Additionally, due to internal stresses in 7M polycrystals, the NM phase may occur acting as barrier for twin boundary motion. It is known that for Ni$_{50}$Mn$_{30}$Ga$_{20}$
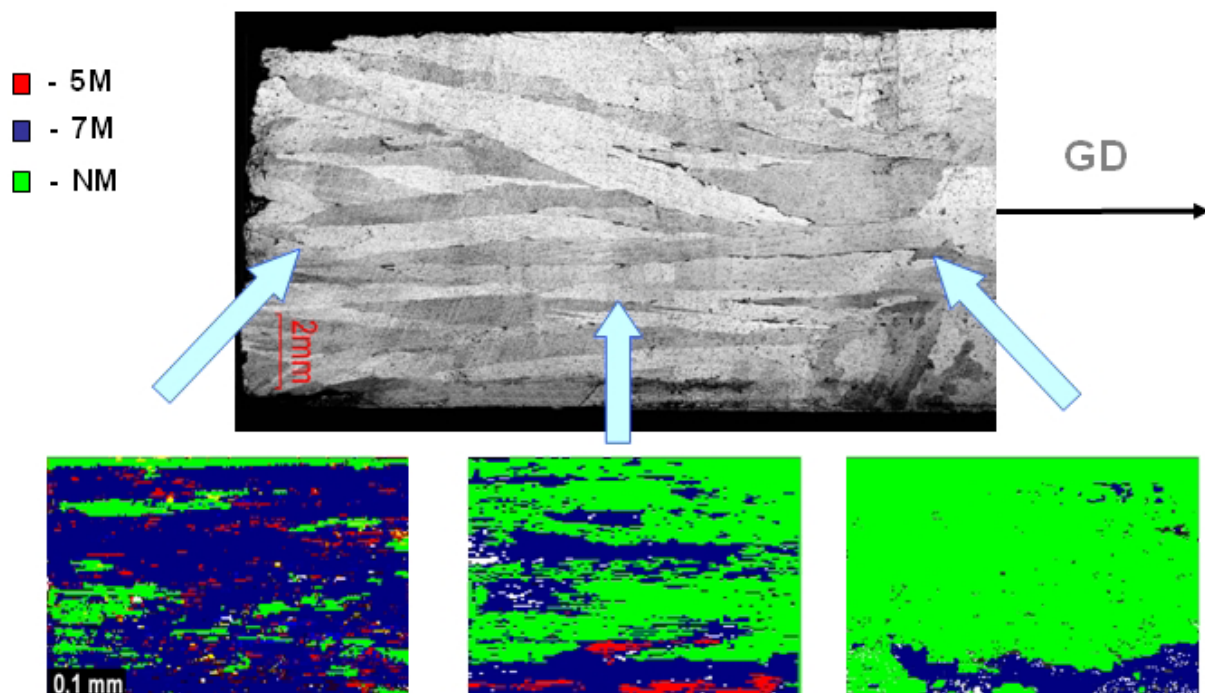

Figure 4.4: BSE image of the microstructure of DS Ni$_{30}$Mn$_{30}$Ga$_{20}$ polycrystals with EBSD mappings showing the local distribution of different phases (5M red, 7M blue, NM green)

single crystals the 7M structure can be achieved by thermo-mechanical treatment. However, this composition chosen to be only 7M structure, is difficult to achieve in polycrystals. X-ray or neutron diffraction diffractograms of bulk samples show that the as-cast and as-rolled polycrystals used simultaneously contain two martensitic phases (NM and 7M, [51]). This can be clearly seen in the EBSD mapping of the directionally solidified sample characterized by long columnar grains (Fig. 4.4) where 7M and NM phases exist in different regions of the ingot their volume fractions varying along the growth direction. In the lower part of the ingot 7M dominates while in the upper part it is NM. Minor existence of 5M is also recognized. Coexisting different martensitic phases have also been found by high resolution transmision electron microscopy. Additional heat treatment increases the portion of the 7M structure. Nevertheless, it does not remove the NM phase completely. Therefore, furthere investigations were only carried out on Ni-Mn-Ga alloys with 5M martensite at room temperature and nominal composition of $Ni_{50}Mn_{29}Ga_{21}$.

4.3 Relationship between austenite and martensitic variants

There are few models in the literature describing the orientation relationship between austenite and martensite. The most important models considering the fcc to bct transition are those proposed by Bain [8], Kurdjumov-Sachs [9] and Nishiyama-Wassermann [10, 11]. All of them describe this transition just as a rotation by some angle about a specific axis. The Bain description is the simplest one explaining the fcc to bct transformation as a 45° rotation about the main cubic axes of the austenite. The lattice relationship is given by:

$$\{001\}_A \parallel \{001\}_T \text{ and } <100>_A \parallel <110>_T$$

There exist three possible martensitic variants for this orientation relationship depicted in the pole figures of Fig. 4.5. However, high resolution EBSD mapping reveals that there exist more than just three orientations in $Ni_{50}Mn_{29}Ga_{21}$. As shown for a HPT sample (Fig. 4.6), the blue variant is split into three orientations, which differ from each other by about 4° to 8° (Figs. 4.6a, b). This is possible because the three blue orientations create three twin relations in the different regions of the sample (A, B, C). For example in region
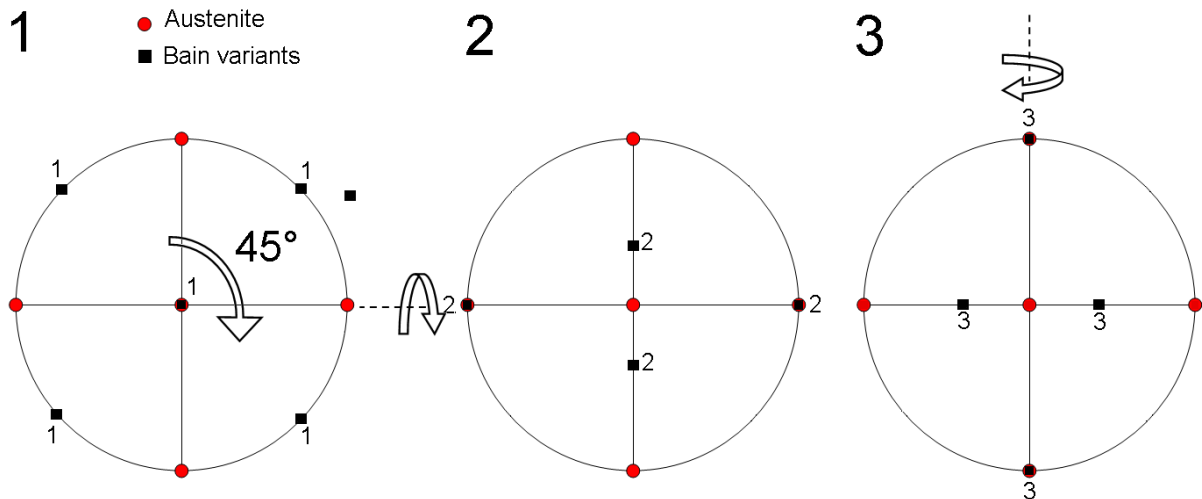
Figure 4.5: Illustration of the three Bain variants

A the first blue orientation is twin related to the pink one by a rotation of 86.6° around the common a-axis (Figs. 4.7a, b). In region B the second blue orientation satisfying the twin relation with the green orientation is also rotated by 86.5° but around the common a-axis of the blue and green variant (Figs. 4.7c, d). In region C the third blue orientation creates again a twin with the pink one, however, in this case the blue variant is rotated 86.6° in opposite direction (Figs. 4.7e, f). Based on this, it can be concluded that between two variants one of them can be adjusted in four different ways, which correspond to four orientations. The permutation of the three Bain variants gives at least twelve orientations in 5M $Ni_{50}Mn_{29}Ga_{21}$ polycrystals. Thus, the three transformed orientations according to the Bain model are too rudimentary for general use but nevertheless provide a good basis for understanding the more complicated case.
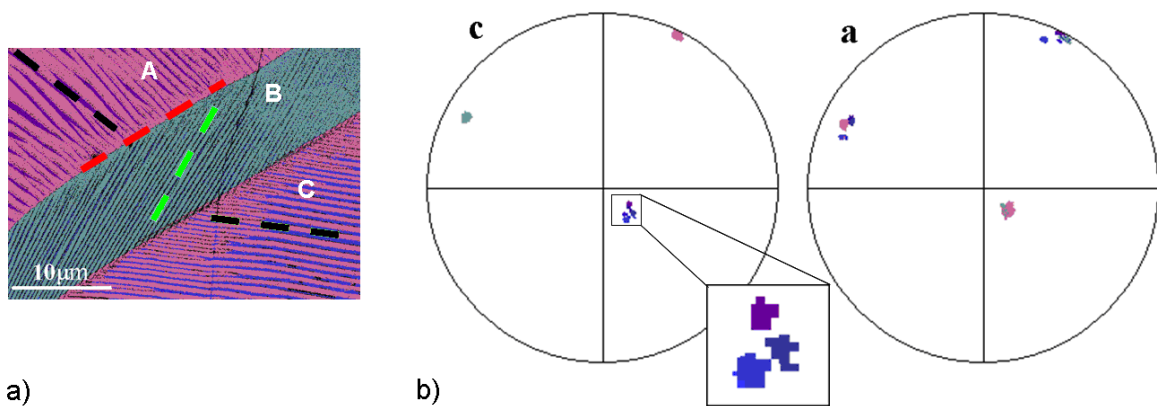

a)   b)

Figure 4.6: EBSD mapping (a) and c- and a- axis pole figures of $Ni_{50}Mn_{29}Ga_{21}$ after HPT (b)

Two more complex models were presented by Nishiyama – Wassermann (N-W) and Kurdjumov – Sachs (K-S). The first one describs the relationship between austenite and martensite as rotation of 95.27° about a common $<1+\sqrt{2}+\sqrt{3}, -1+\sqrt{2}+\sqrt{3}, \sqrt{2}>$ axis satisfying the following orientation relationship:

$$\{111\}_A \parallel \{011\}_T \text{ and } <11\bar{2}>_A \parallel <01\bar{1}>_T$$

It gives twelve possible martensitic variants. Kurdjumov-Sachs explain this transformation as a simple shear resulting in a rotation of 90° about the $<112>$ direction. Since there are twelve $<112>$ rotations possible and two senses of rotation, twenty four variants may be created from one austenitic orientation. The orientation relationship is given as:

$$\{111\}_A \parallel \{110\}_T \text{ and } <101>_A \parallel <1\bar{1}1>_T$$

Fig. 4.8 presents the result of the above three models. As can be clearly seen, one Bain variant is an average of four N-W or eight K-S variants. Nevertheless, none of both models describes this phenomenon accurately in the Ni-Mn-Ga 5M structure. For example, in Fig. 4.9a the orientation is shown of an austenitic grain and its corresponding four martensitic variants measured with EBSD.

To measure this, first the orientation of the martensite was taken and then the sample was heated up above the martensite-austenite transformation temperature and measured again in the austenitic state with EBSD. For comparison with the above mentioned models, the whole coordinate system was rotated in such a way that the measured austenite had a cubic orientation. As can be seen in Fig. 4.9a, the measured variants do not have the ideal orientation of any of the models. The maximum deviation from N-W is about 5° and from K-S 4°, which seems to be quite large especially because the minimum difference between two K-S and two N-W variants is 6.59° and 10.42°, respectively.

Therefore, a new model is proposed for the 5M structure. It is explained in the cubic CS by means of rotations about the c- and a-axes. As shown in Fig. 4.10, at first just one martensitic variant (green) arises by rotation of 3.6° about $<110>$. Subsequently, the next variants follow the twin relationship. The second variant (brown) is rotated by 86.5° around the common a-axis. The third and fourth variants (violet) follow the twin relationship as described before. In other words, this approach is based on three steps. The first step is a rotation of 3.6° around $<110>$. Since there are six $<110>$ directions
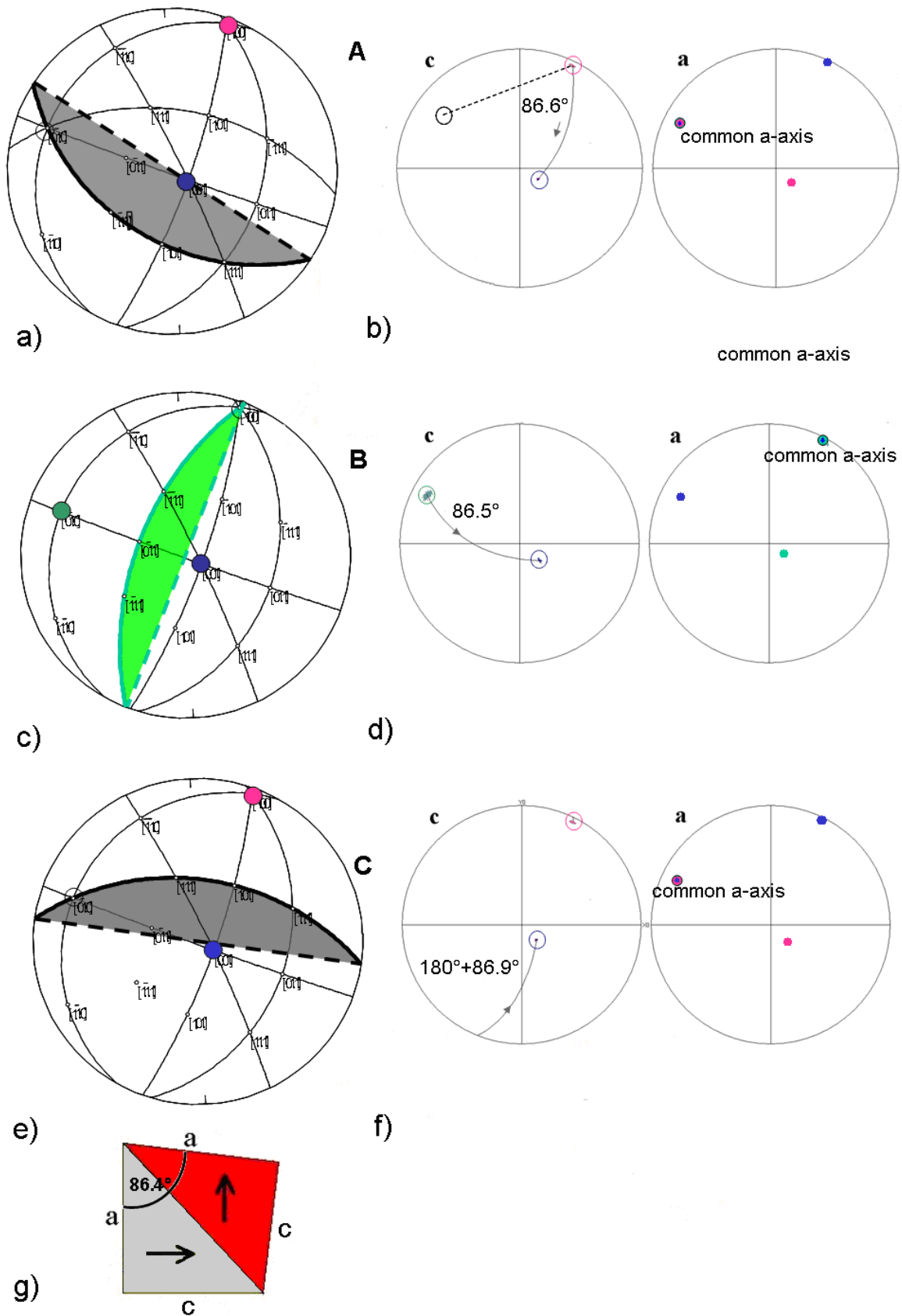
Figure 4.7: EBSD stereographic projection with indication of twin traces in regions marked A, B, C (a, b, c, d, e, f) and illustration of the ideal twin relationship in 5M Ni-Mn-Ga alloys (g)
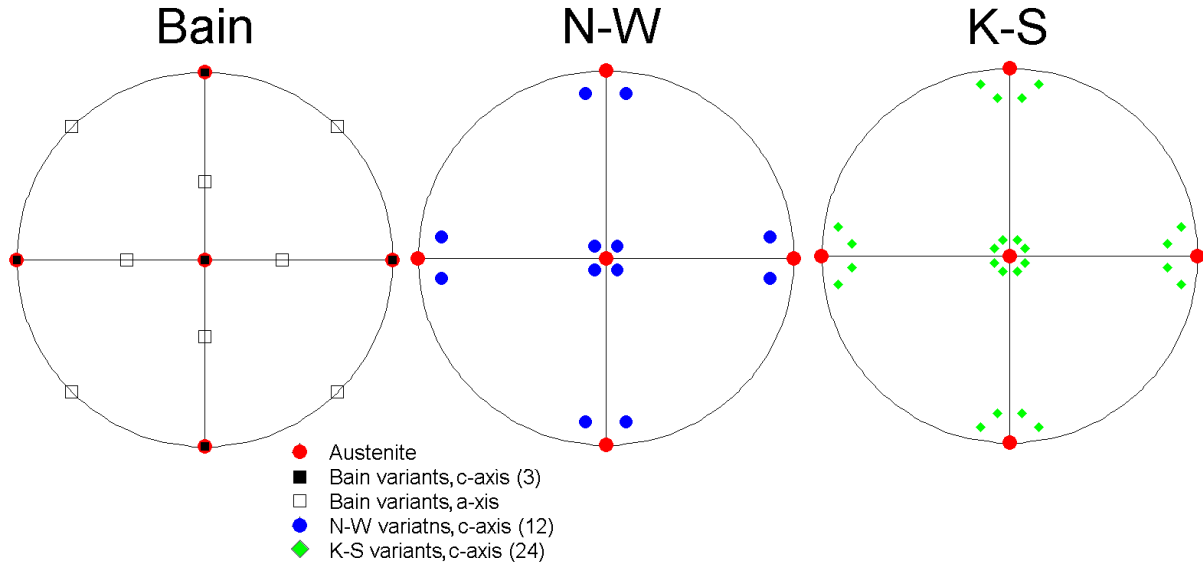
Figure 4.8: (001) pole figures demonstrating the three models (Bain, N-W and K-S) with respect to an initial austenite cube orientation

and two senses of rotation, the first main martensitic variant can be rotated in twelve ways (four of them are depicted in Fig. 4.10 with orange circles). During the second step, the second variant arises creating the macro twins. Similarly, as found before, the second variant can be adjusted in four different ways, which corresponds to four orientations.

The same holds for the third step where the micro twins are created. There are again four possibilities to adapt the micro twins. However, half of them overlap with variants which can be formed in the second step. As a result, an austenitic orientation can be adjusted by martensitic variants in 96 possible ways ($12 \times 4 \times 2$). Using this method, the simulated positions of the martensitic variants do not deviate more than 0.5° from the theoretical positions, which is the nominal angular resolution of EBSD. Note that in the 5M structure there usually occur only few variants within a parent austenitic grain. However, these four or five martensitic orientations can be adapted in 96 different ways. This model also was confirmed by the measured martensite orientations. This is possible because the initial orientation of austenite can be calculated from two measured martensitic orientations. As the martensite can be calculated from the austenite using the transformation matrix (rotation of some degree about some axis), the austenitic orientation can be calculated in the opposite way using the matrix transposition. Both measured martensitic variants give several possible austenitic solutions but just the common orientation is the
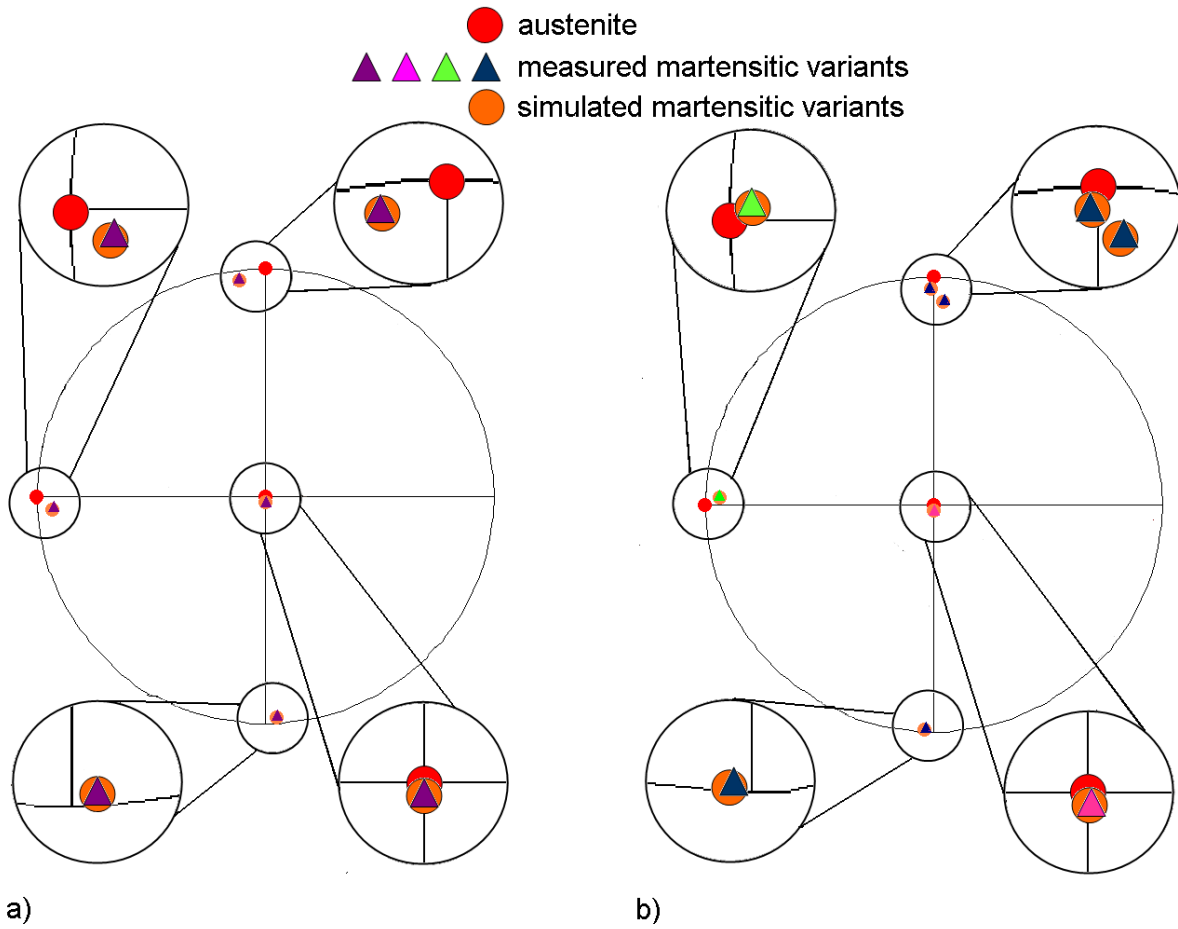
Figure 4.9: Measured and simulated positions of the c-axis of martensitic variants in a DS sample (a) and calculated austenite orientation for 5M Ni-Mn-Ga deformed by HPT (b)
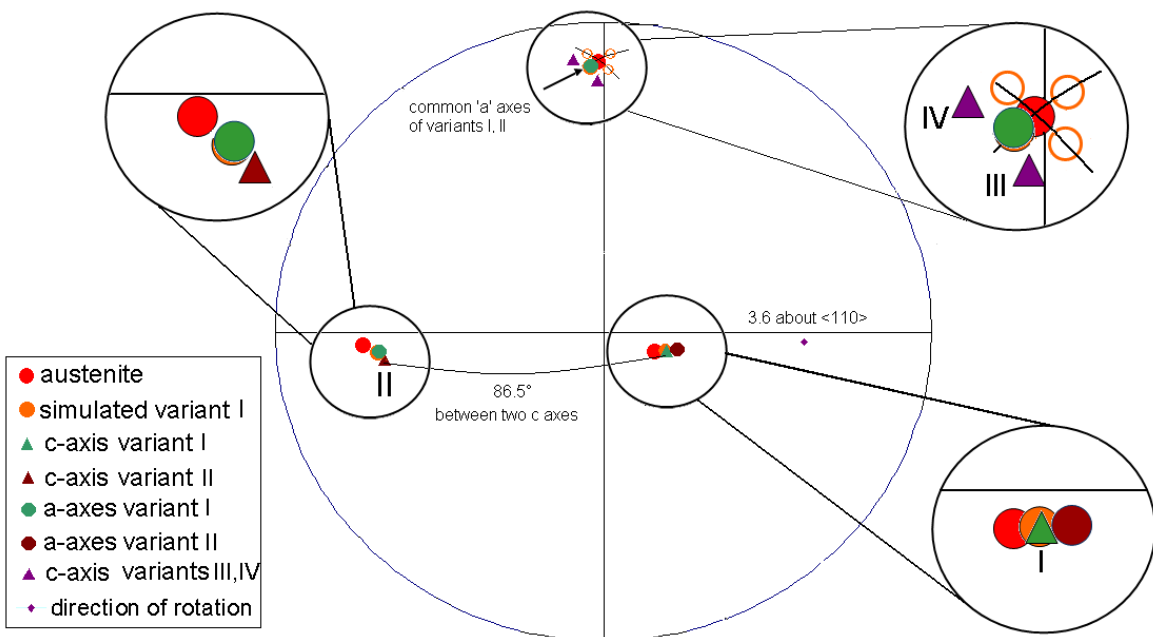

Figure 4.10: Austenite-martensite orientation relationship in DS 5M Ni-Mn-Ga

correct one, from which martensite arises. An example for such a calculation matching very well with experiment is shown in Fig. 4.9b for a HPT sample.

4.4 Direction of modulation during twin boundary motion

The lowest observed twinning stress in Ni-Mn-Ga alloys can only be found in two modulated structures (5M, 7M) [37]. The twinning stress of the third, non-modulated (NM), martensitic phase is much higher than those measured for the modulated structures [74]. Additionally, because of the absence of a uniaxial magnetic anisotropy [19], MFIS does not exist in the NM structure. Therefore, much attention has been paid to the modulation, which can play a basic role during motion of twin boundaries. As mentioned above the modulation can be described as a periodic shuffling of atomic planes along the <110] direction [18, 20] and in diffraction patterns it is observed as extra spots along this direction (four and six extra spots in the 5M and 7M structure, respectively). The nature, stability and role of the modulation are described by Zayak et al. [21, 22, 23].
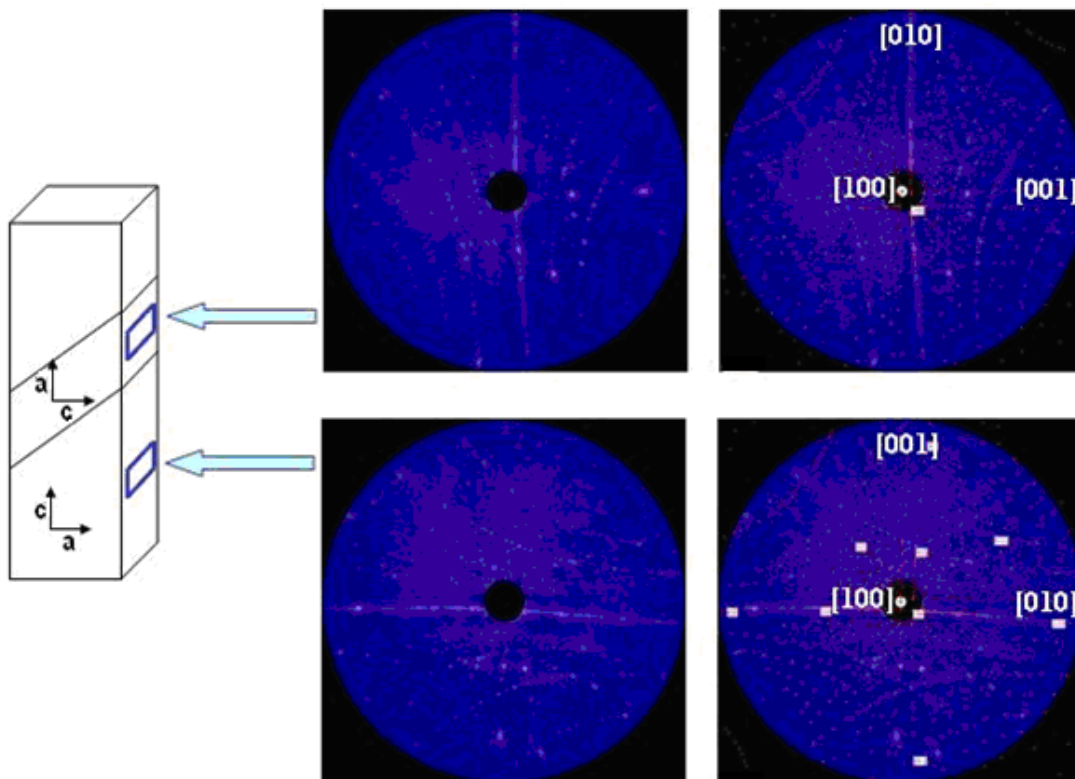
Figure 4.11: Laue diffraction pattern of the single crystal with 5M structure and orientation analysis

Figure 4.12: X-ray diffraction of a 5M single crystal with twin band (c-axis differently oriented). The modulation is only visible when the beam is parallel to the c-axis.

Figure 4.13: X-ray diffraction of a 5M single crystal with twin band (c-axis differently oriented). Upper diffraction pattern shows a twin relation.
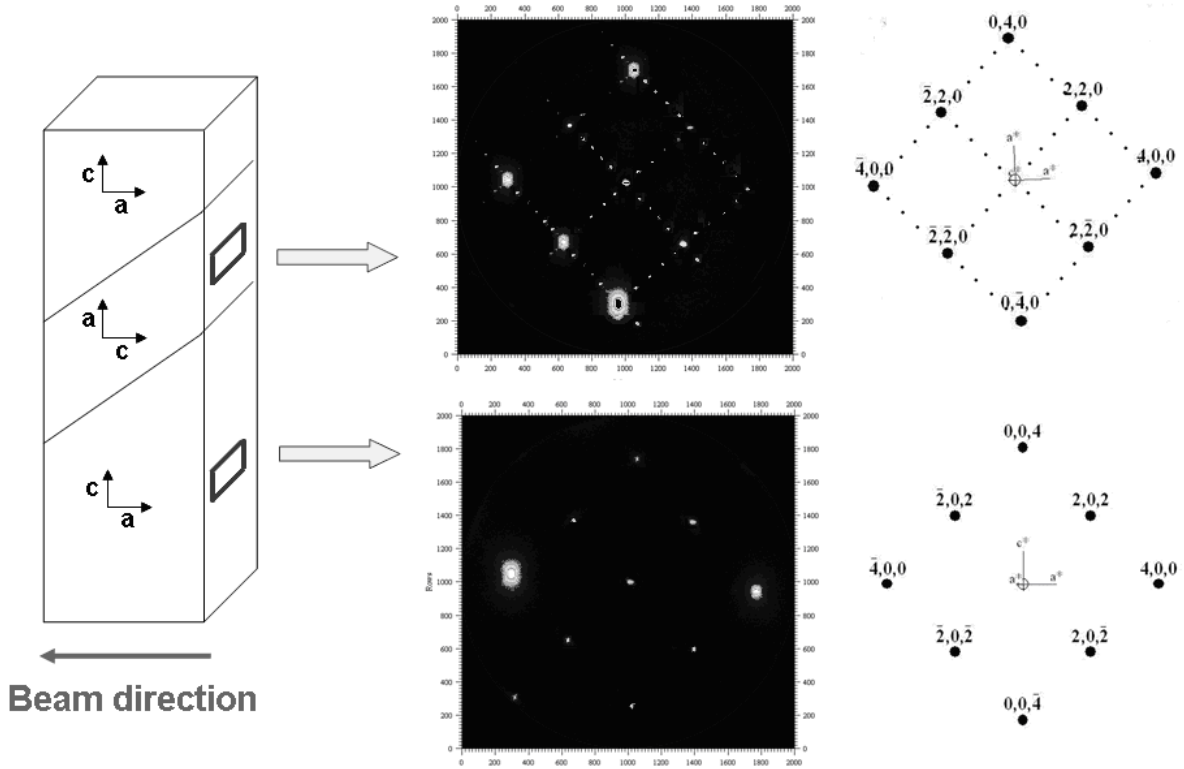
Figure 4.14: X-ray diffraction of a 7M single crystal with twin band (c-axis differently oriented). The modulation is only visible when the beam is parallel to the c-axis.
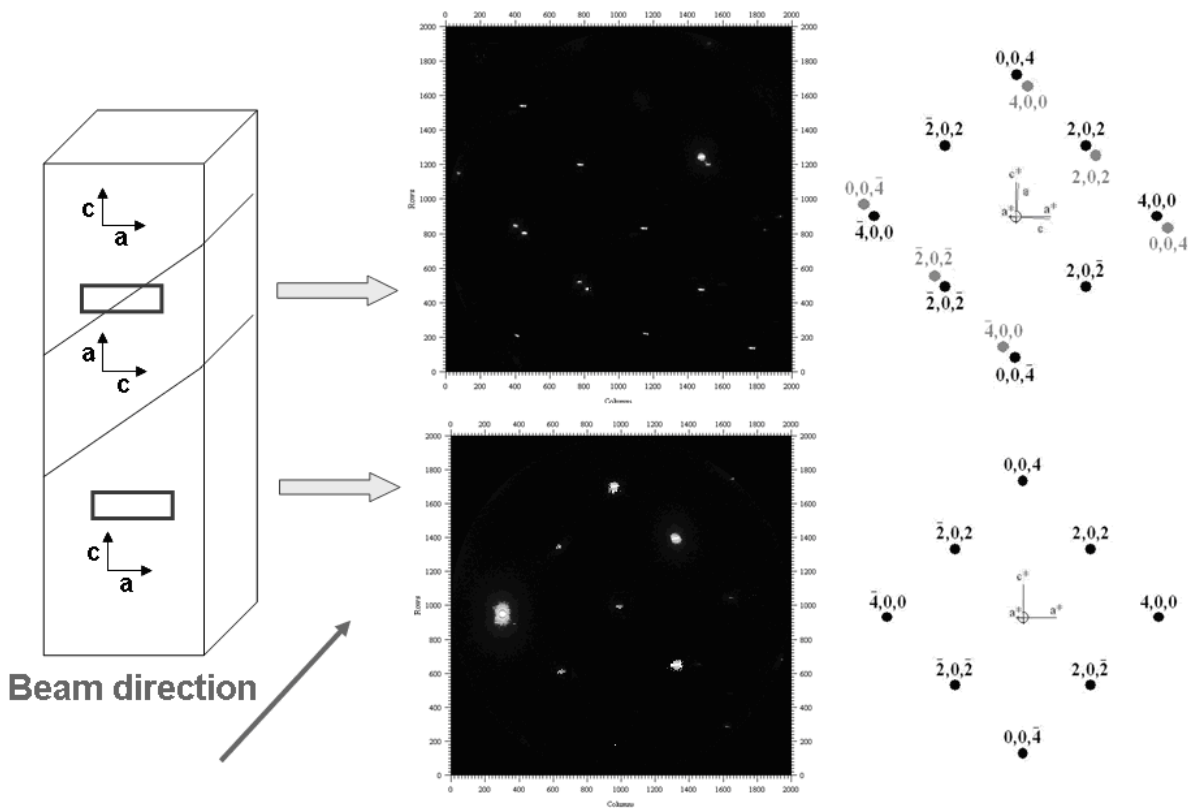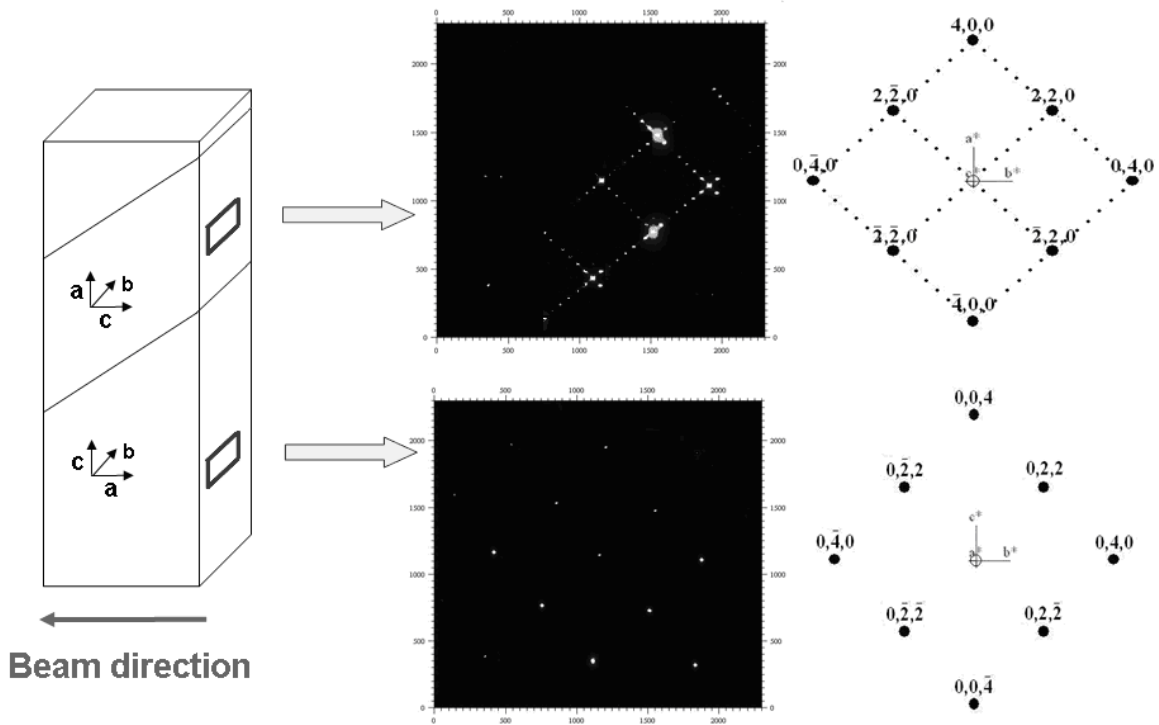
To study the effect of twin boundary motion on modulation, Ni-Mn-Ga single crystals with five-layer (5M) and seven-layer (7M) martensitic structures at room temperature were chosen. The single crystals prepared by the Bridgman method were supplied by company Adaptamat. After slight deformation, the orientation of the single crystals was determined by means of Laue diffraction patterns in undeformed and deformed areas representing two martensitic variants related by twin relationship. The change of the direction of modulation was measured by diffraction of HESR (100 keV). To do this, before and after deformation the single crystals were X-rayed at two specific places. Since the modulation is only visible when the beam direction is parallel to the c-axis the samples were transmitted by X-rays along those directions, which are parallel to the main tetragonal (5M) and orthorhombic (7M) axes (possible c-axis localization) to find optimal diffraction parameters. As mentioned above, the modulations in the 5M and 7M structure can be distinguished because of the presence of four (5M) or six (7M) extra spots along the <110] direction between the main reflections (Figs. 4.12 and 4.14). The tetragonal and orthorhombic unit cell dimensions are given in following order $a > c$ and $a > b > c$, respectively.

Synchrotron diffraction in transmission of a sample volume of $3 \times 3 \times 0.5\,mm^3$ under different directions shows that the structure modulation takes place on {110) planes and that during twin boundary motion the c-axis orientation changes and with this also the direction of modulation with respect to the initial single crystal reference system (Fig. 4.13). This result clearly demonstrates that the direction of modulation is crystallographically fixed normal to the c-axis. While on the one hand this may be a trivial result, on the other hand it shows that different atom movements are taking place during twin boundary motion in modulated structures compared to non-modulated ones. This may be the reason for the much lower stresses (about an order of magnitude) observed for twin boundary motion in modulated structures. Modulation along the <110] directions has already been shown by Ge et al. [75] with high resolution transmission electron microscopy. The different modulation directions belong to different areas in the single crystal and are separated by a facetted interface [75]. Figs. 4.12 and 4.14 present such situation with two directions of modulation (normal to (110) and ($\bar{1}$10)). During twin boundary motion the c-axis orientation changes and with this also the direction of modulation with respect to the initial single crystal reference system (Figs. 4.12 - 4.14). A schematic sketch of this process is shown in Fig. 4.15 for the 7M structure.
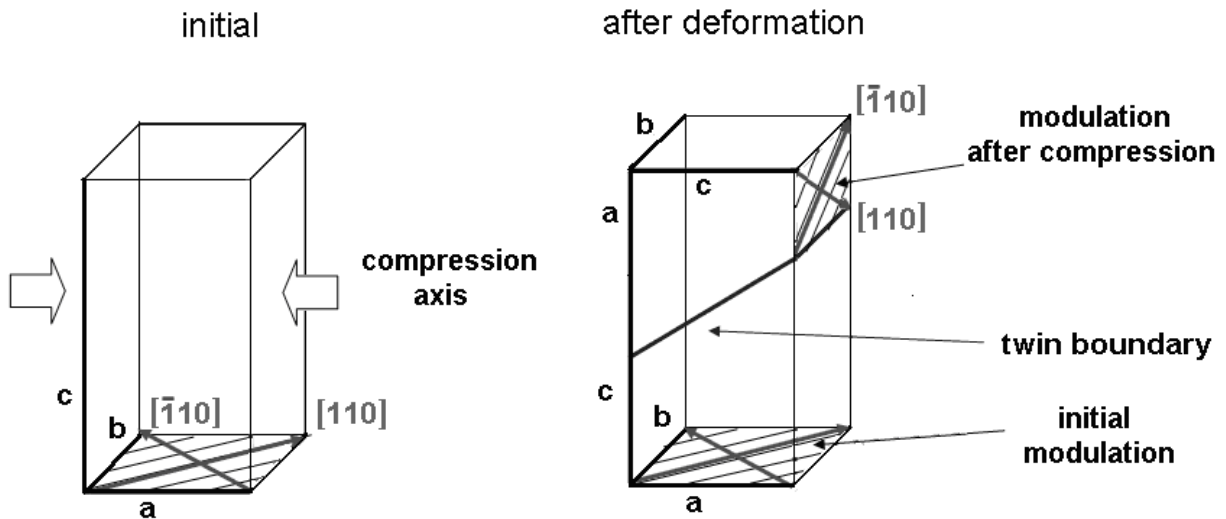

Figure 4.15: Change of direction of modulation in a 7M structure during twin boundary motion induced by compression in a-direction

The modulation is only visible when the beam direction is parallel to the c-axis. If the beam direction is along the a-axis the characteristic diffraction features of modulation

are absent. Initially, the modulation is on the {110) plane in one variant while after deformation it is still on the {110) plane but in the variant generated by twinning. The modulation direction obeys the twinning relation. Additionally, in Fig. 4.13 the upper diffraction pattern shows additional spots due to twinning. The non-split spots belong to the common (202) plane. The results clearly demonstrate that the direction of modulation in the 5M and 7M structure is crystallographically fixed normal to the c-axis. Thus, during twin boundary motion in modulated structures different atom movements have to take place compared to non-modulated ones. This may be the reason for the much lower stresses observed for twin boundary motion in modulated structures because of a more "flexible" lattice. Note that in the 7M structure there also occurs another type of twinning system on {110) planes. However, motion of these twins only switches the a- and b-axes while the c-axis remains unchanged. In other words the direction of modulation does not change.

4.5 Training process

In order to achieve MFIS in Ni-Mn-Ga alloys, a training process has to be applied. This process consists of successively compressing mostly cuboid samples along two or three axes up to a certain stress. A cuboid sample is used due to the geometry allowing successive compression along three axes normal to each other. Compression along these axes results in the motion of the twin boundaries changing the volume fraction of particular martensitic variants. As a result the twinning stress is reduced and the twinning strain is maximized. It is the aim of repeated compression to eliminate those variants with c-axis perpendicular to the compression axes. A lot of training processes have been applied to single crystals and polycrystals prepared in different ways. However, the main conclusion which can be drawn is, that the training process should lead to one type of twin or a single-variant state.

4.5.1 Training of single crystals

Calculations according to [3, 4] show that the application of a 0.4 T magnetic field can induce a shear stress of approximately 2.7 MPa. Therefore, the main goal of training is to

reduce the twinning stress below this limit. An example for a stress-strain curve of an untrained 7M Ni-Mn-Ga single crystal is given in Fig. 4.16 with the red line indicating the maximum magnetic stress, which can be achieved with a magnetic field. As can be clearly seen, the twin boundaries can not be moved with a magnetic field because of the high twinning stress level caused by a complex martensitic microstructure (see chapter 4.1). Thus, the training process has to be done first mechanically. Typical stress-strain curves for training of a single crystal are shown in Fig 4.17. After six cycles along two axes (1 and 2) the single crystal is well trained. A cycle defines successive compressions along two or three axes depending on the training type. The subscript "1", "2" or "3" is added to the number of cycles denoting the axis, along which compression was performed. Fig. 4.17 demonstrates that with increasing number of cycles the twinning stress decreases. After the second cycle the twinning stress is dramatically reduced. Further compressions lead to a plateau stress of about 0.5 MPa. Now a magnetic field should produce MFIS. A detailed examination of the training process applied to a Ni-Mn-Ga bi-crystal is presented in the next chapter.

4.5.2 Training of a bicrystal

To investigate in detail well defined twin-grain boundary interactions including twin-twin interactions, a training process of a bi-crystal was studied. A bi-crystal was chosen due to its simplicity. The change of microstructure (i.e. martensitic variant distribution) during training was investigated by EBSD on two perpendicular surfaces. A cuboid sample was cut in such a way that one grain (1) of the bicrystal (Fig. 4-2c) had the <100> axes parallel to the specimen edges. The bicrystal is characterized by a general high angle grain boundary with rotation of about 60° about the <1 2 3> axis and different martensitic variants within the two grains. The volume fraction of grain 1 of the bicrystal is about 0.6. The initial microstructure of the bicrystal investigated is a typical self-accommodated microstructure of martensite (Fig. 4.18). The microstructure of the deformed sample is shown in Fig. 4.3. The orientations of four twin-related martensitic variants of grain 1 on surface II are presented by different colours described in Fig. 4.19e. To simplify Fig. 4.19e, the orientations are characterized just by the c-axis (c_A, c_B, c_C, c_D). After the
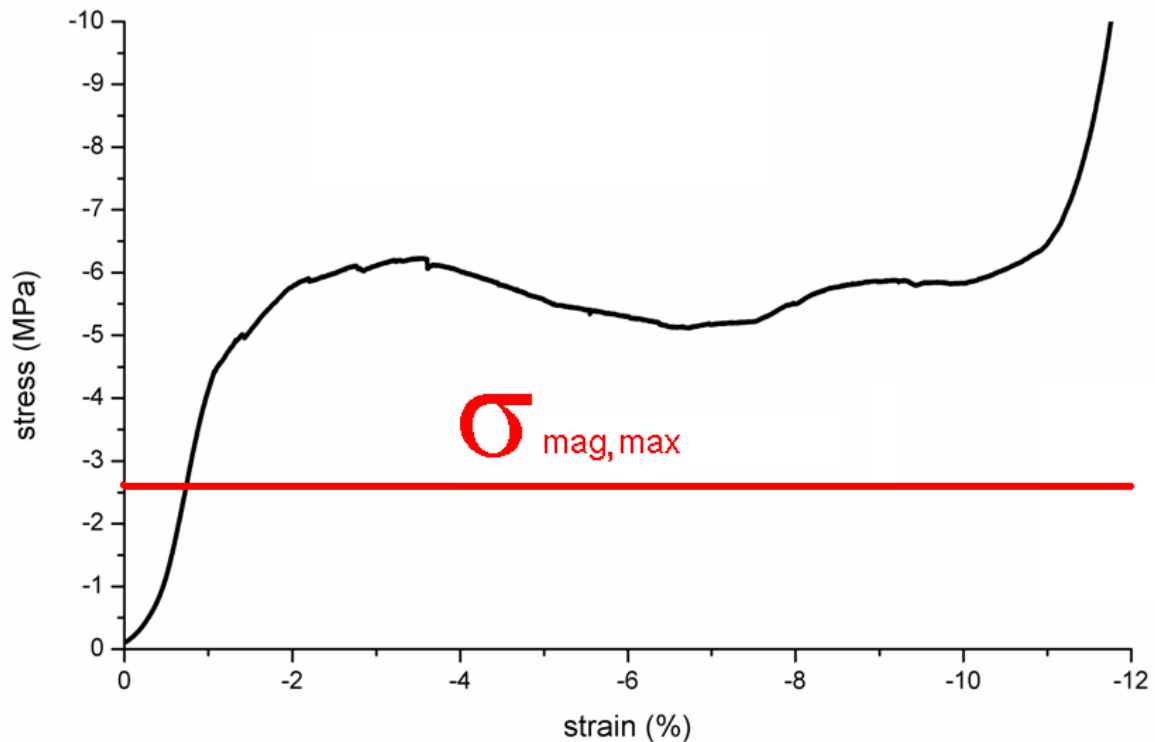
Figure 4.16: Stress-strain curve for an untrained 7M Ni-Mn-Ga single crystal. σ mag, max is the maximum magnetic stress, which can be applied by a magnetic field.

first compression step the twin boundaries between variants A (green) and B (orange) (called main twin) move to the left in such a way that the volume fraction of variant B increases (Figs. 4.19a, b) because this variant has the c-axis (the shorter lattice parameter) along the compression direction. Moreover, the fine blue twins become more regular and thicker. This clearly shows that the fine twins can be moved, too. The next compression step results in the motion of the main twin boundary in opposite direction increasing the volume fraction of the dark green variant (Fig. 4.19c).

Additionally, after the first cycle (compression along two directions) many fine twins disappeared. After the second cycle they disappeared completely (Fig. 4.19d). This result corresponds to the strong decrease of the flow stress in the stress - strain curve below the maximum magnetic stress, which can be applied by a magnetic field (Fig. 4.20a). Thus, the fine twins are responsible for the high stress at the beginning of training. This means that during the training process the orientations not belonging to the main twin (C and D) are removed and then the main twin boundary can be moved easily. Finally, the training
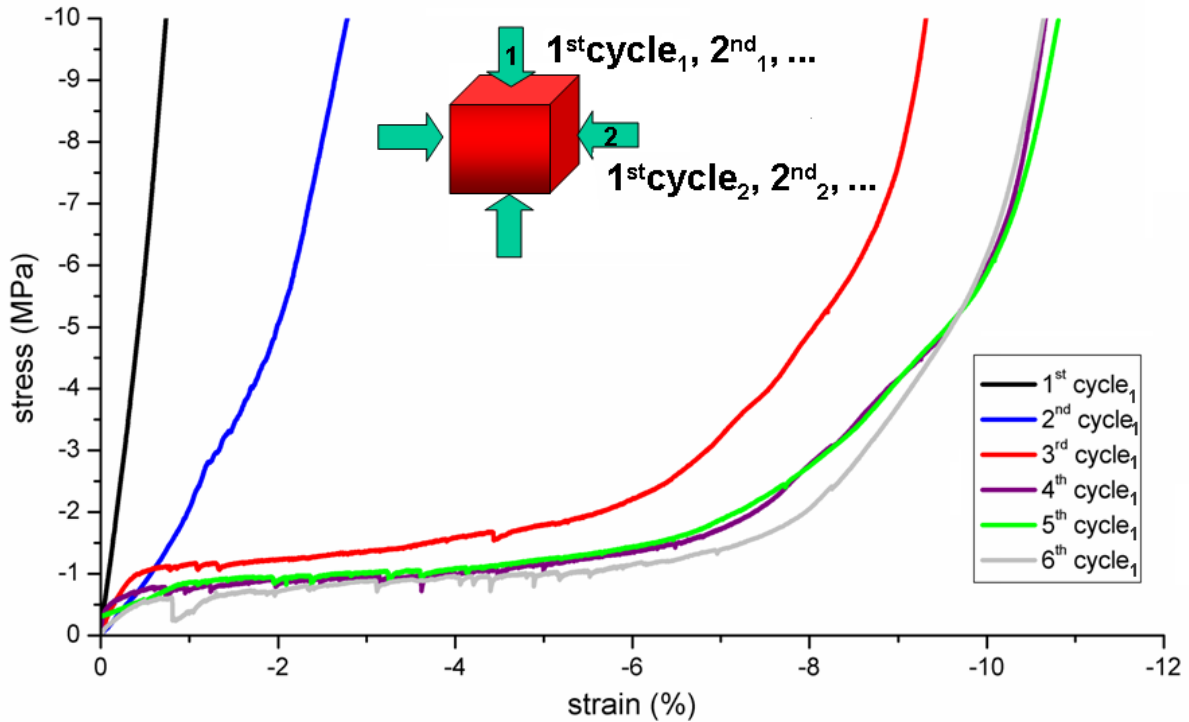
Figure 4.17: Stress-strain curve for successive compression cycles of a 7M Ni-Mn-Ga single crystal

process creates one type of twin or a single-variant state. Within grain 2 a reorientation of variants is also observed leading to a reduction of the micro twins and increasing the volume fraction of that variant with the c-axis nearest oriented to the compression axis. It should be mentioned that in some macro twins two micro twin variants were found, which are aligned with their twin planes perpendicular to each other, so-called "crossing boundaries" (Fig. 4.19f). Compression of these micro twins results in the motion of the main twin boundary removing the crossing boundaries, too (Fig. 4.19g). This clearly shows that the training process eliminates this type of barrier as well.

Moreover, the training process should be done just along two axes with respect to the main (macro) twins. In this case horizontally and vertically, i.e. parallel to the c-axes of the orange and dark green variants. This is because in general there is only one type of macro twin extending through the whole parent austenitic grain [57, 59] while even three different types of micro twins exist. Compression along the third direction related to the c-axes of the micro twins causes the motion and expansion of twins crossing each other,
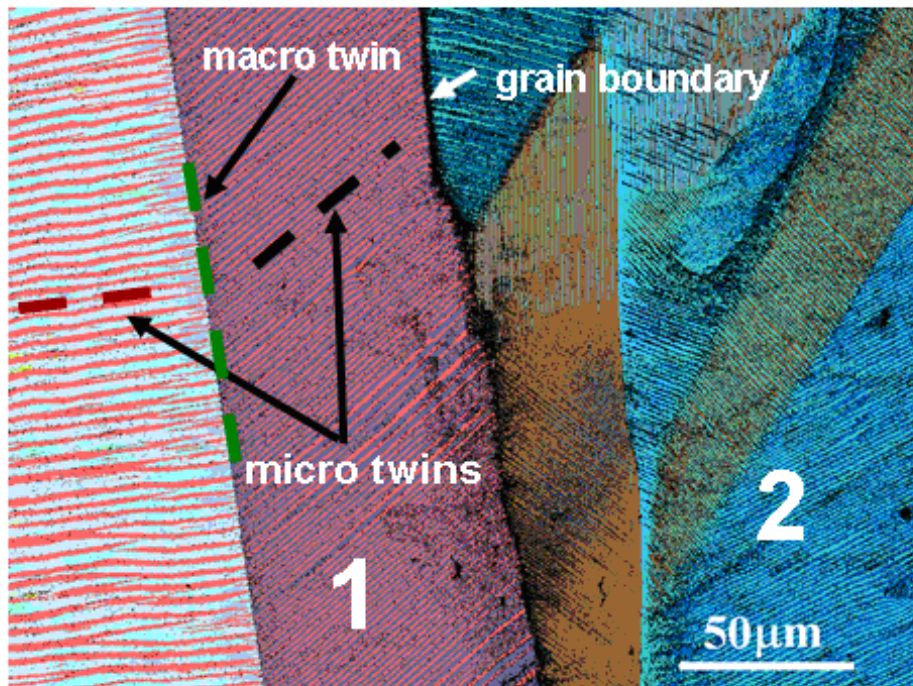
Figure 4.18: Orientation mapping with indication of twin traces in grain 1 of the bicrystal

which makes the training process much more complicated. This is clearly demonstrated in the stress strain curve of Fig. 4.20b where compression along all three directions is less effective in comparison to compression along two axes. The repeated training of the same bicrystal was possible by heating up the sample above the martensite-austenite transformation temperature. Cooling leads again to a self-accommodated microstructure. According to Fig. 4.20b three axes training leads to an increasing number of cycles required to achieve the desired stress reduction and strain maximization. Thus, the fastest way to train Ni-Mn-Ga 5M single or polycrystals is training just along two axes with respect to the main (macro) twins.

During the training process new twins are formed close to the grain boundary (Fig. 4.21b). These twins may compensate the different shape changes of both grains during deformation. As polycrystalline intermetallic samples are quite brittle at low temperatures, the formation of these additional twin boundaries allows accommodating certain strain components, thus preventing the formation of micro-cracks at the grain boundary. Beside the stress level limiting crack formation, it is well promising to investigate also the effect of temperature during training. On the one hand, training at higher temperatures reduces
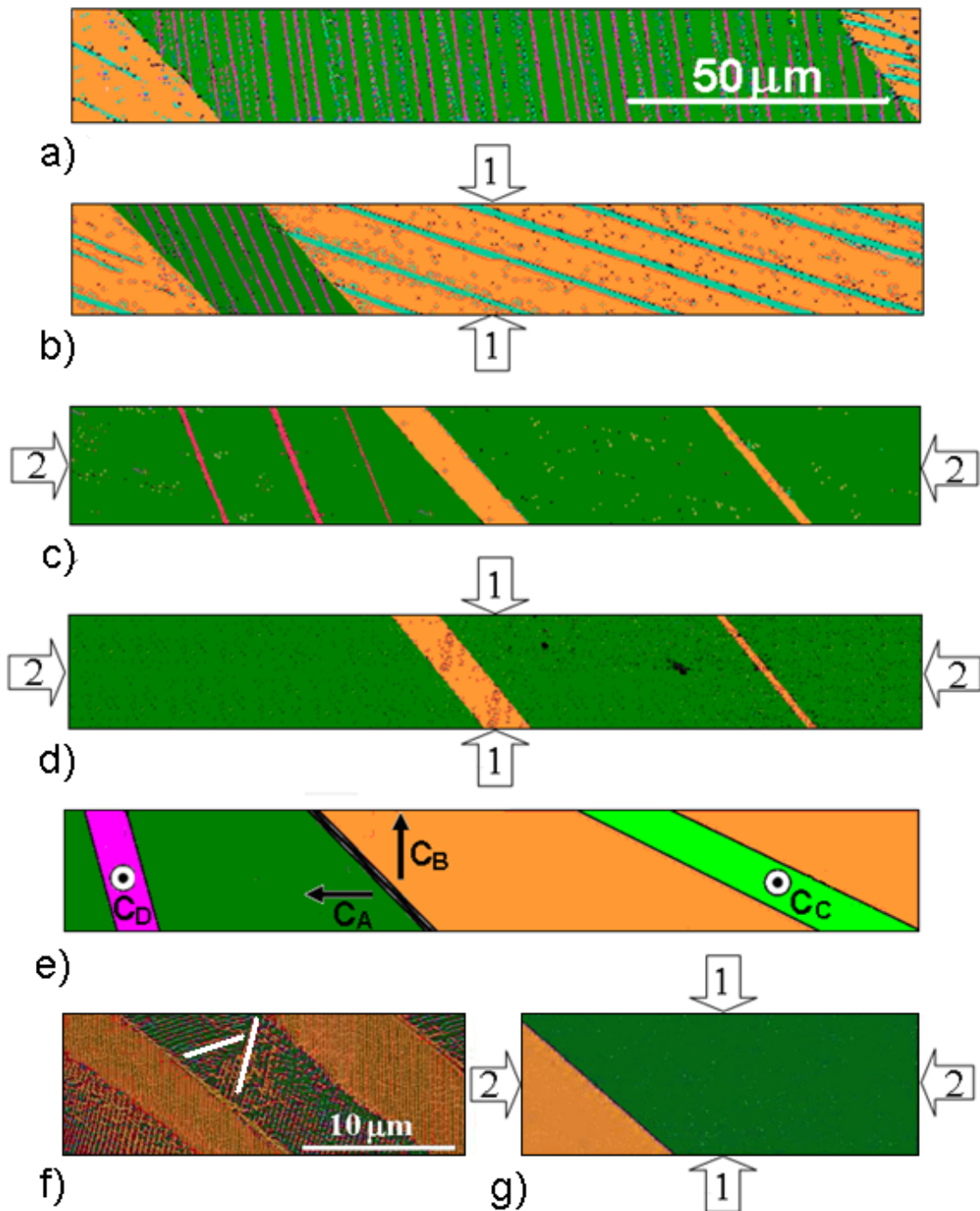
Figure 4.19: Orientation mapping of an undeformed (a) and deformed area (b: 1st cycle$_1$, c: 1st cycle$_2$, d: 2nd cycle$_2$) of the bicrystal taken from the same area during successive compression cycles. The arrows show the direction of compression. The black spots are not indexed. The EBSD colour code corresponds to the orientation of the c-axes (e). Example of so-called "crossing boundaries" (f) marked with white lines and the same area after two cycles of deformation (g).

Figure 4.20: Stress-strain curves of a 5M Ni-Mn-Ga bicrystal for successive compression steps (three cycles) (a) and comparison of the second cycle along the first direction with and without including the third compression axis (b). $\sigma_{mag,\,max}$ is the maximum magnetic stress, which can be applied by a magnetic field.

the twinning stress, on the other hand, it allows an easier formation of new martensitic variants. Therefore, this will be a future task to find the conditions of "safe" training.
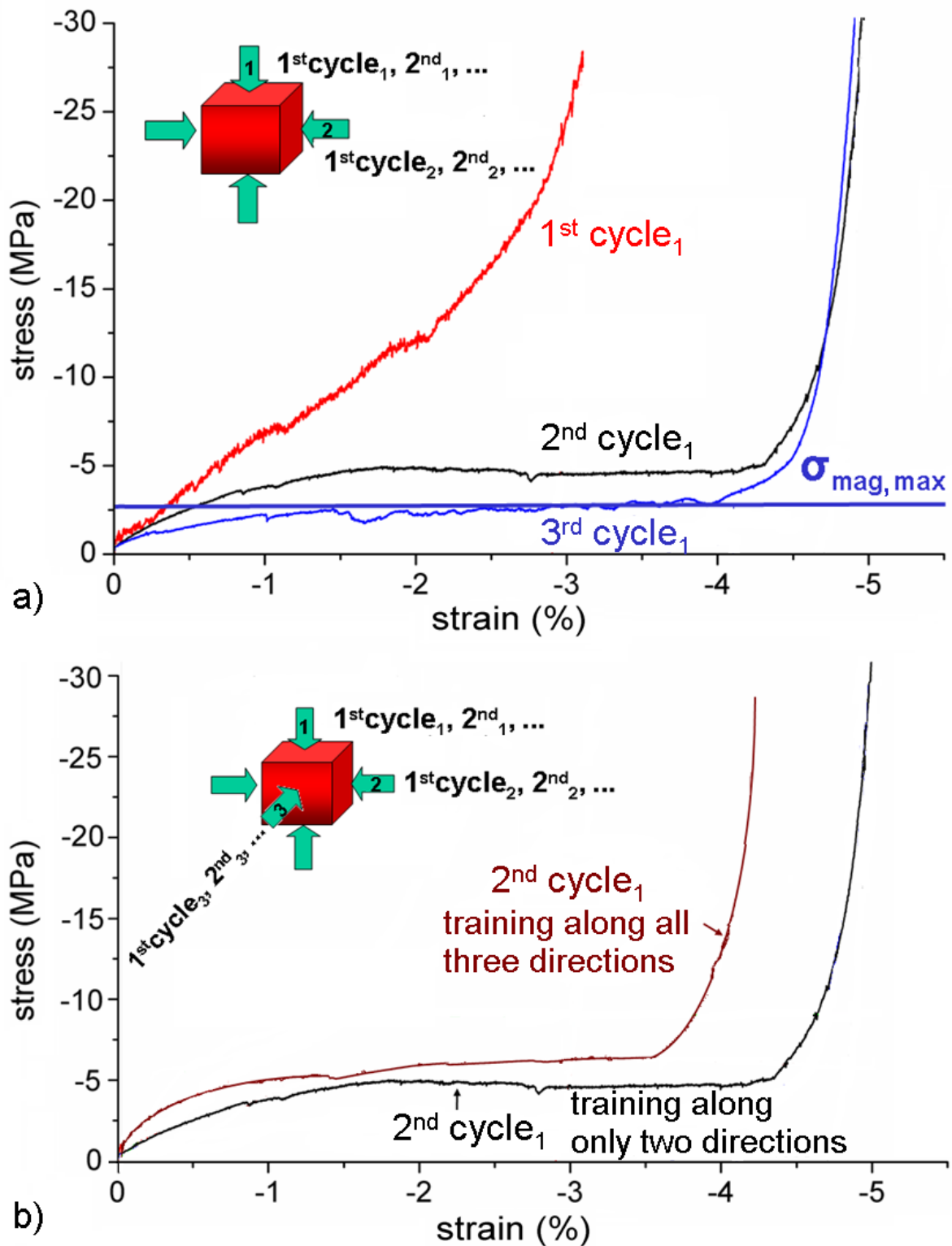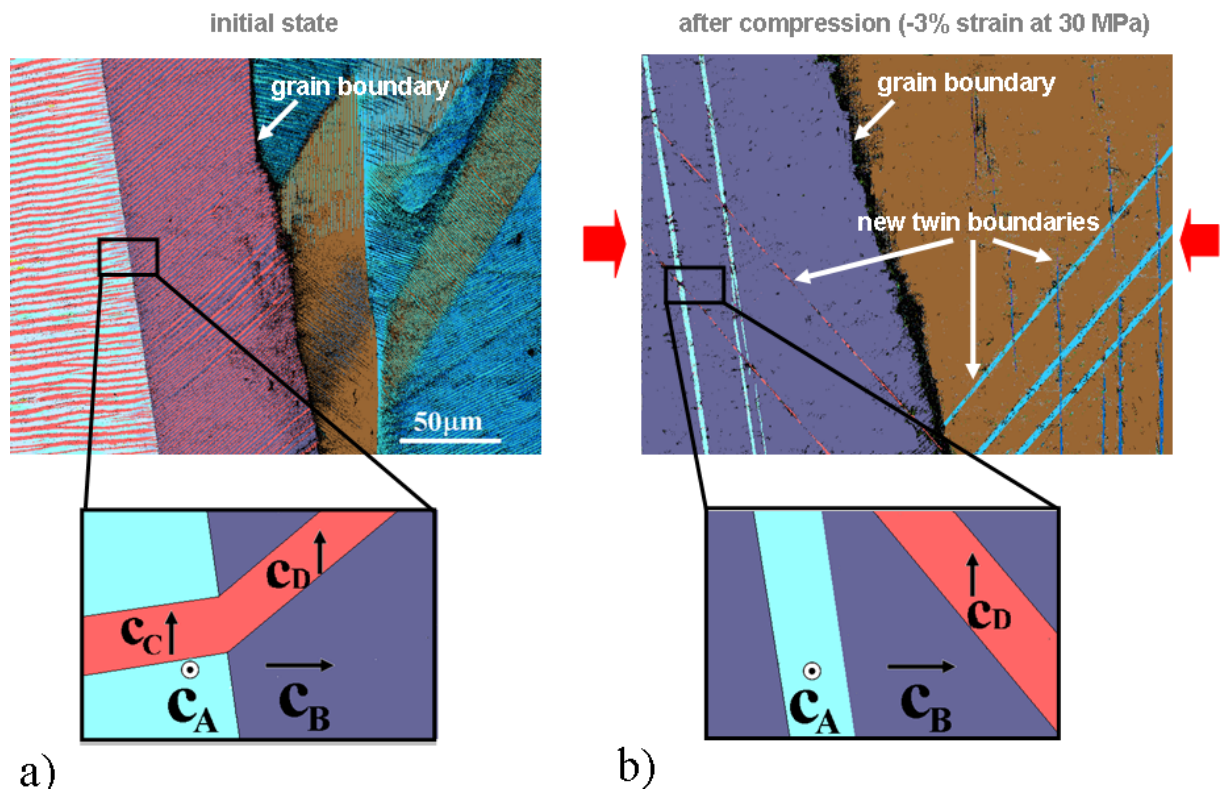

Figure 4.21: EBSD mapping of an undeformed (a) and deformed (b) bi-crystal taken at the grain boundary showing change of twin arrangement

4.5.3 Training of polycrystals and Hall-Petch relationship

To summarize the training results, the stress-strain curves of trained samples fabricated by different processes are demonstrated in Fig. 4.22. As can be seen, with increasing grain size the twinning stress decreases while the twinning strain increases. This clearly shows that for MFIS a coarse-grained microstructure is preferred and that the twinning stress in polycrystalline Ni-Mn-Ga alloys obeys a Hall–Petch type relationship. It should be noted that the materials have been fabricated with different processes leading to different types and strengths of texture. The effect of texture on the stress - strain curve is not clear, because texture and grain size cannot be investigated independently. However, by comparing the hot extruded and HPT sample with comparable grain size an effect of texture can be observed.

Figure 4.22: Hall-Petch relationship for twinning in trained 5M Ni-Mn-Ga alloys

4.6 Texture

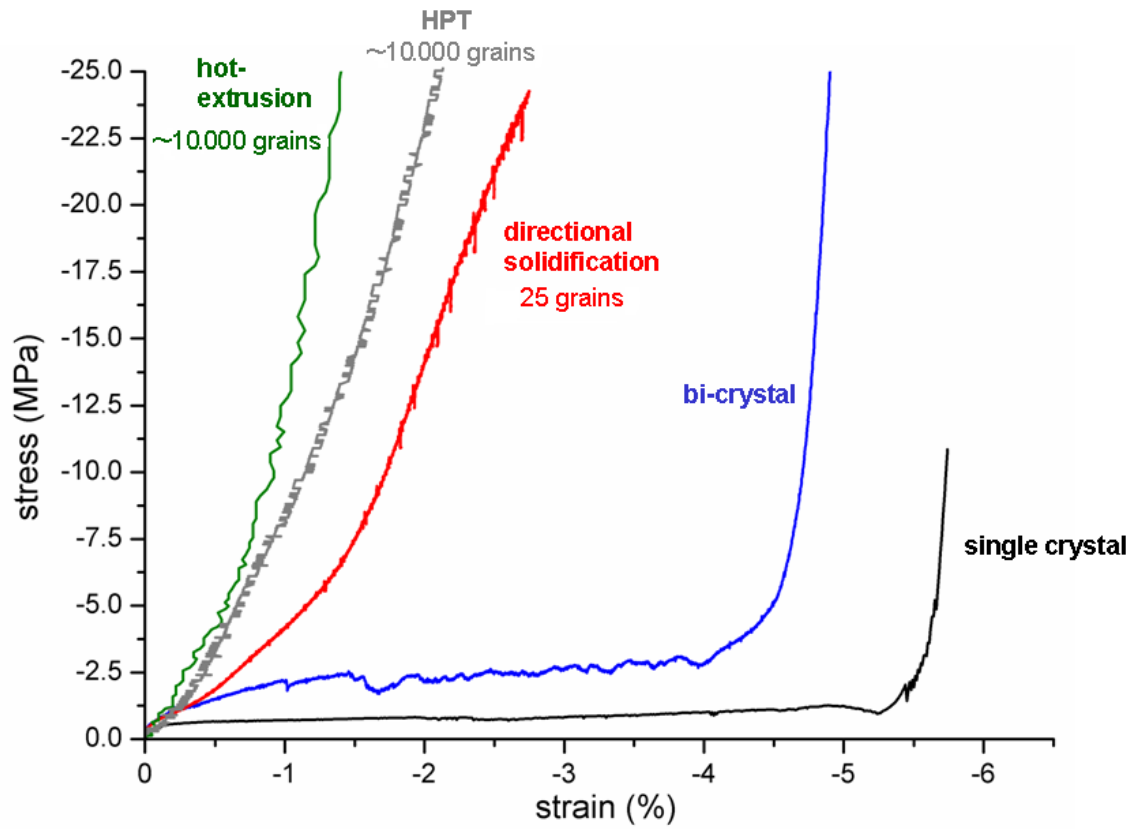To achieve pronounced MFIS in polycrystals, fabrication processes are needed to produce specific strong textures. Texture is generally defined as the crystallographic orientation distribution in a polycrystalline sample [76, 77, 78]. Texture affects various unidirectional properties directly related to anisotropy like Young's modulus, strength, ductility, magnetization or thermal expansion. In the extreme case of a random texture the polycrystals become isotropic while for a strong single texture component it approaches the anisotropy of a single crystal.

Texture also has an important influence on MFIS and twinning stress of polycrystalline Ni-Mn-Ga alloys. It determines the maximum amount of strain to be achieved, which in a randomly textured sample is about 20% of that of a suitable oriented single crystal. A strong biaxial texture increases this percentage. In contrast to fibre textures, where just one direction is preferred, biaxial textures are very important for MFIS because there are three preferred directions along which MFIS can be realized. If there is just one preferred direction, the magnetic field can move the twin boundaries along one axis but it is difficult to move them back because the other directions (or other c-axes) are distributed randomly normal to the fibre axis. Therefore, in the case of fibre textures, only a one-way (not resettable) effect can be observed. Thus, texture is a crucial structural parameter of polycrystalline Ni-Mn-Ga alloys, which has to be optimized. Different fabrication processes lead to different texture evolution allowing to produce the type of texture desired. Material texturing has been obtained by directional solidification [51] and plastic deformation by hot rolling and hot extrusion [57] as well as high pressure torsion (HPT) [59]. These processes were also followed by thermo-mechanical treatments. Texture analysis is discussed with respect to both, the parent phase (austenite) and the directly related martensitic phase considering variant selection.

To examine the texture of coarse-grained Ni-Mn-Ga alloys, diffraction of synchrotron radiation and neutrons was applied. Both techniques have been provided in transmission geometry. Additionally, to determine the local texture, EBSD in the SEM was used. Processing of the texture data was done with the Labotex software. It should be noted that all planes and directions mentioned in this chapter are given in the so-called "cubic

coordinate system", which is related to the cubic axes of the parent L2$_1$ phase (see Chapter 1.6).

4.6.1 Directional solidification texture

The first process to produce material texturing was directional solidification. The cast sample had a diameter and length of 10 mm and 50 mm, respectively. The crystallite growth is supposed to occur along the direction of the heat flow, preferentially in <100>
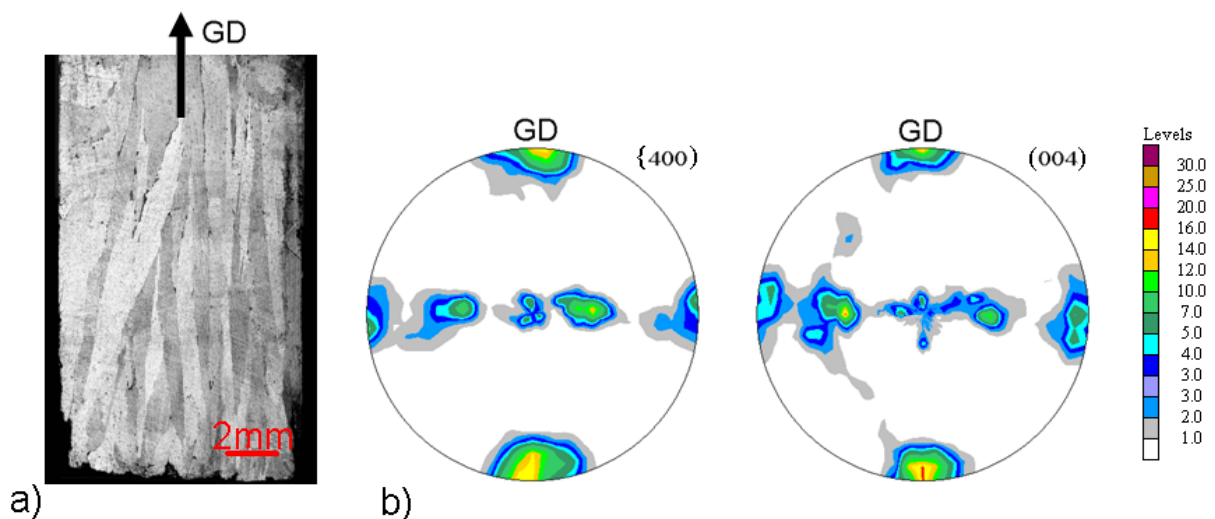

Figure 4.23: BSE image of the microstructure of a directionally solidified 5M Ni-Mn-Ga polycrystal (a).{400} and (004) pole figures of the tetragonal 5M phase in the directionally solidified sample measured with synchrotron radiation (intensities: 1.0, 2.0, 3.0 4.0, 8.0, 12.0, 16.0, 20.0, 24.0, 28.0 mrd, GD = growth direction)(b).

direction [79] yielding a <100> fibre texture. The directionally solidified sample is characterized by long columnar grains with a width of about 0.5 mm. To examine the texture of coarse-grained Ni-Mn-Ga alloys in a statistically relevant way, diffraction of HESR (100 keV) was applied. Due to the high penetration depth of high-energy X-rays and neutrons, texture measurements with these radiations in transmission allow for collecting orientation data from a large sample volume, i.e. $3 \times 3 \times 0.5 \, mm^3$ with a good grain statistics.

The directionally solidified material has a strong <100> fibre texture along the growth direction (GD) (Figs. 4.23b, 4.24). In the tetragonal 5M Ni-Mn-Ga phase three martensitic variants may exist. Because of symmetry (two directions of the tetragonal structure are equivalent) the number is reduced to two in the case of <100> fibre textures.

During formation of the martensitic phases a variant selection took place favouring one of the <100> directions parallel to GD (Fig. 4.24). The volume fractions (full width at half maximum of 20°) of the different variants are for the 5M structure: 21% [001], 74% [100], rest phone. The <100> fibre texture existing in the directionally solidified Ni-Mn-Ga alloy is typical for cast cubic crystals with the <100> fibre axis aligned along the temperature gradient determining GD [79]. The variant selection during the martensitic phase transformation is such that mainly the longest lattice parameter is parallel to GD.
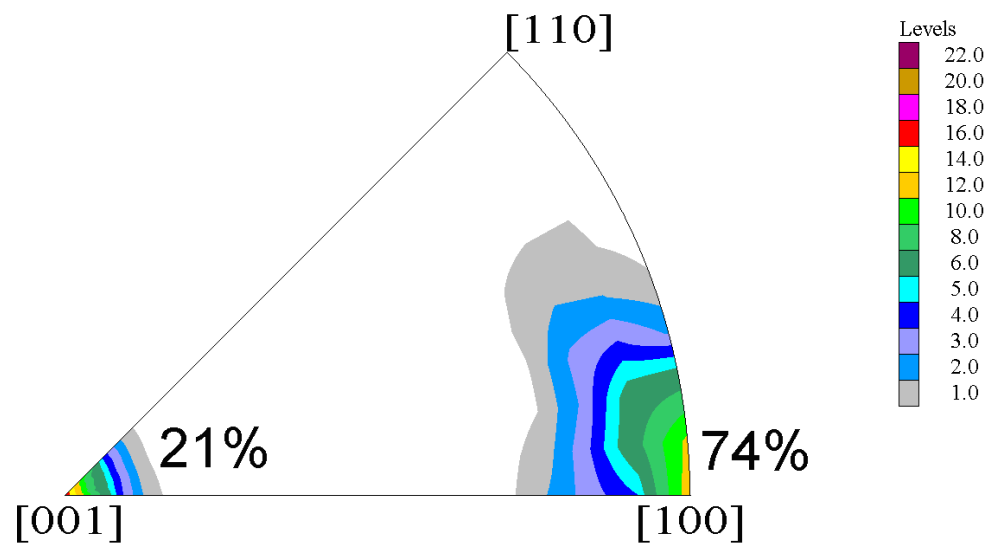
Figure 4.24: Inverse pole figure of GD of the tetragonal 5M phase in the directionally solidified sample. The volume fraction of different orientations along GD with a spread of 20° is given. The difference to 100% belongs to the rest of orientations.

4.6.2 Hot rolling texture

Another route to produce textures is plastic deformation by hot rolling. The ingot ($7.9 \times 11.9 \times 44\,mm^3$) canned in steel was rolled at a temperature of 1000°C up to 50% reduction and then air-cooled to room temperature. The microstructure of the hot rolled alloy is recrystallized with an equiaxed grain size of about 400 μm (Fig. 4.25). The texture of the 5M phase investigated by neutron diffraction is a weak {111}<112> rolling texture (Fig. 4.26). It has been formed by dynamic recrystallization during hot rolling in the B2 phase field. It is a typical recrystallization texture of body-centred cubic metals [80]. In comparison to directional solidification no obvious variant selection took place during phase transformation from the cubic L2$_1$ phase to the martensitic phases.
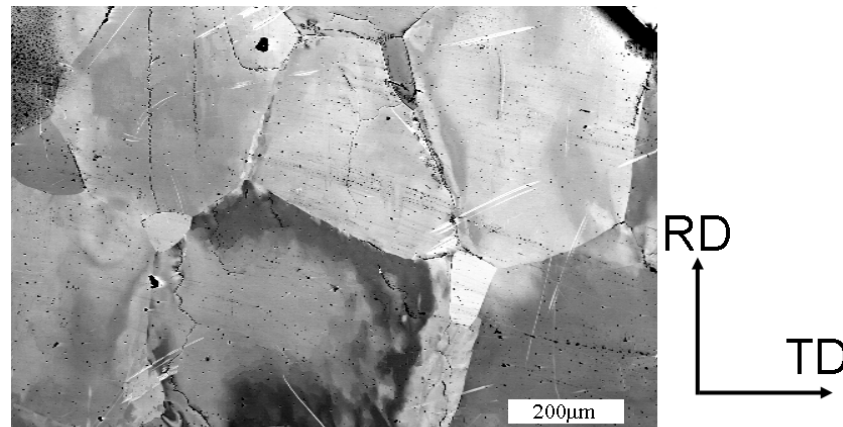
Figure 4.25: BSE image of the microstructure of hot rolled 5M Ni-Mn-Ga polycrystals (RD = rolling direction, TD = transverse direction)
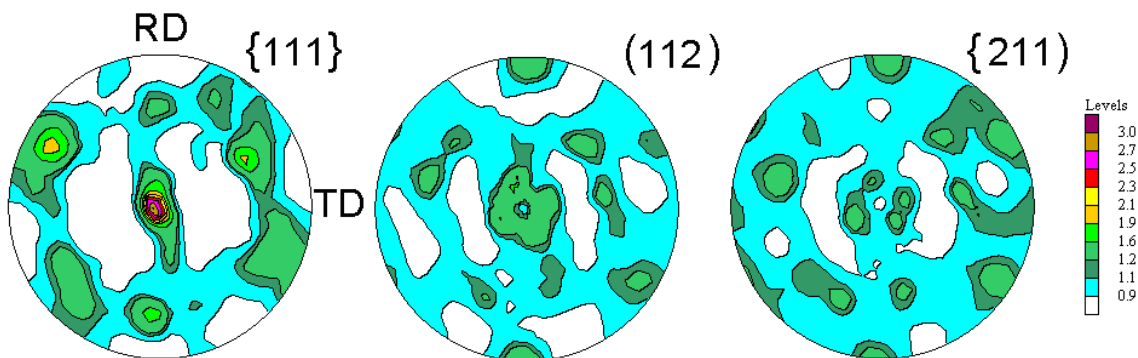
Figure 4.26: {112} and {111} pole figures of the tetragonal 5M phase in the hot rolled sample measured with neutron diffraction (RD = rolling direction, TD = transverse direction).

4.6.3 Hot extrusion texture

Hot rolling experiments at 1000°C have shown that plastic deformation of polycrystalline $Ni_{50}Mn_{29}Ga_{21}$ above the ordering temperature is possible in the B2' structure without brittle fracture. The same holds for HE. During extrusion the material mainly experiences axisymmetric tension. Orientation images obtained by EBSD in the central region of the rod (Fig. 4.27) show the grain structure after HE.
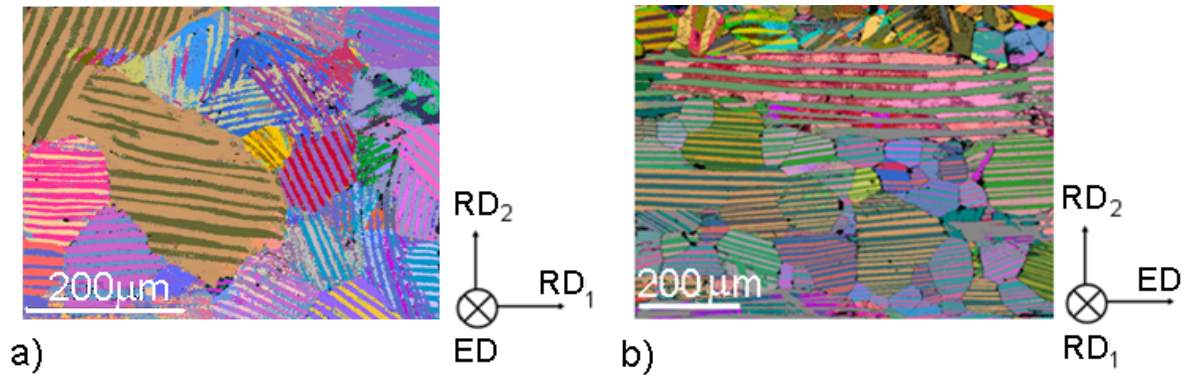
Figure 4.27: EBSD mappings of the hot extruded Ni-Mn-Ga sample taken in the central region of the rod normal to ED (a) and along ED (b), (ED = extrusion direction, RD = radial direction)

It is seen that dynamic recrystallization has taken place. Recrystallization leads to slightly elongated grains with a size of about 100 μm. The recrystallized grains contain a lot of twins with the trace of the twin boundaries preferentially aligned along ED (Fig. 4.27b). Moreover, a large BSE image of the microstructure also taken in the centre of the rod (Fig. 4.28) shows preferred alignment of the twin boundaries with their trace either parallel or
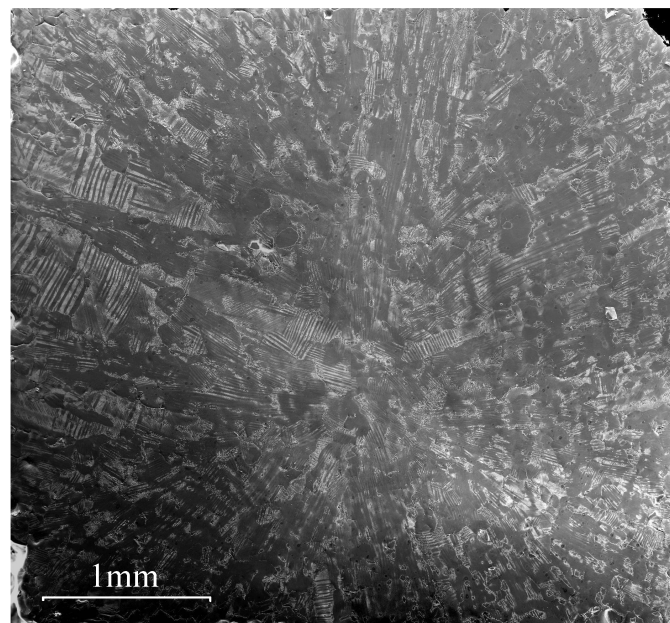
Figure 4.28: BSE image of the microstructure of the hot extruded 5M Ni-Mn-Ga polycrystal (cross-section normal to the extrusion direction, position 3 of Fig. 4.29)

perpendicular to the radial direction (RD). Therefore, as demonstrated in Fig. 4.29, five different samples were cut for local EBSD and synchrotron radiation measurements. These measurements reveal that the texture of the hot extruded sample is quite complex. It is
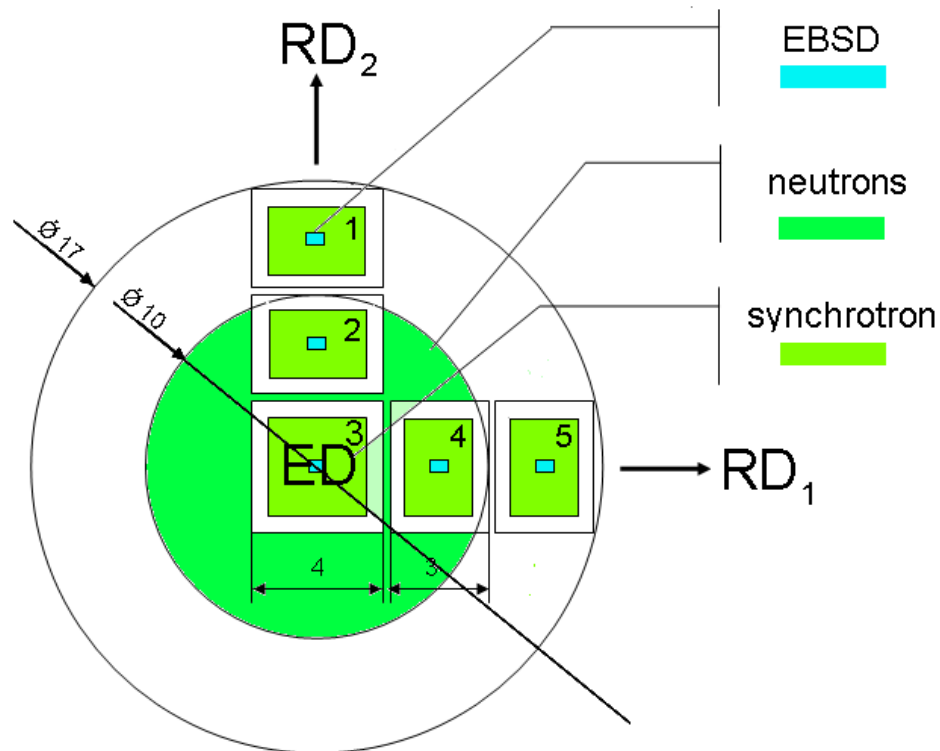
Figure 4.29: Areas in the cross-section of the hot extruded sample measured with different techniques of texture measurement (dimensions are given in mm)

composed of components related to RD rotating around the extrusion axis. Additionally, the dominant texture components change from the centre to the edge of the rod. To capture these changes, different texture measurement techniques have been applied in five different areas as shown in Fig. 4.29. The microstructure and pole figures measured with EBSD mappings and HESR (Figs. 4.30 and 4.31), show the cyclic nature of the microstructure and texture. The {111} pole figures from positions 1 and 2 are almost identical. Moreover, they resemble those from positions 4 and 5 rotated by 90° around the extrusion axis (Fig. 4.31). The same holds for the mictrustructure where the traces of the twin plane are mostly radially distributed (Fig. 4.30). Thus, the off-central regions do not have rotational symmetry typical for fibre textures. To describe the cyclic texture observed, the ODF and ideal components are more appropriate. To do so, the sample CS was chosen with X, Y, Z parallel to the RD_2, RD_1 and ED, respectively. RD_1 and RD_2, with RD_1 perpenticular to RD_2, are chosen arbitrarily. Such a convention allows presenting all observed components and fibre textures in a clearer way. The texture is represented by $\varphi_2 = 0°$ and $\varphi_2 = 45°$ ODF sections using monoclinic sample symmetry.

The ideal orientations of the measured components are shown in the key figures; for their designation see Table 4.1. It should be mentioned that the description used for F and J components does not correspond to the ideal orientations in simple shear deformation. This description is used here because of the same positions in the ODF. However, it has different physical meaning with respect to the stress-state. To distinguish between both cases the upper case letter "E" denotes extrusion. The subscript "A", "B" or "C" is added to describe different variants.

Table 4.1: Main ideal orientations in the 5M martensitic structure after HE in B2'

Component	Miller indices		Euler angles [°]		
	$\perp \mathrm{RD}_2$	$\parallel$ ED	φ_1	Φ	φ_2
C_A	(001)	[010]	90	90	0
	(001)	[100]	90	90	90
C_B	(100)	[010]	0	90	0
	(010)	[100]	0	90	90
C_C	(100)	[001]	0	0	0
	(010)	[001]	90	0	0
F_{E_A}	(001)	[110]	90	90	45
F_{E_B}	(100)	[011]	0	43.2	0
	(010)	[101]	0	43.2	90
	($0\bar{1}0$)	[101]	180	43.2	90
	($\bar{1}00$)	[011]	180	43.2	0
J_{E_A}	($\bar{1}\bar{1}2$)	[111]	90	53	45
J_{E_B}	($1\bar{2}1$)	[111]	29	53	45
J_{E_C}	($\bar{2}11$)	[111]	151	53	45
<100>$_A$ fibre	fibre	[100]	0 - 180	90	90
	fibre	[010]	0 - 180	90	0
<001>$_B$ fibre	fibre	[001]	0 - 180	0	0
<110>$_A$ fibre	fibre	[110]	0 - 180	90	45
<011>$_B$ fibre	fibre	[101]	0 - 180	43.2	90
	fibre	[011]	0 - 180	43.2	0
<111> fibre	fibre	<111>	0 - 180	53	45

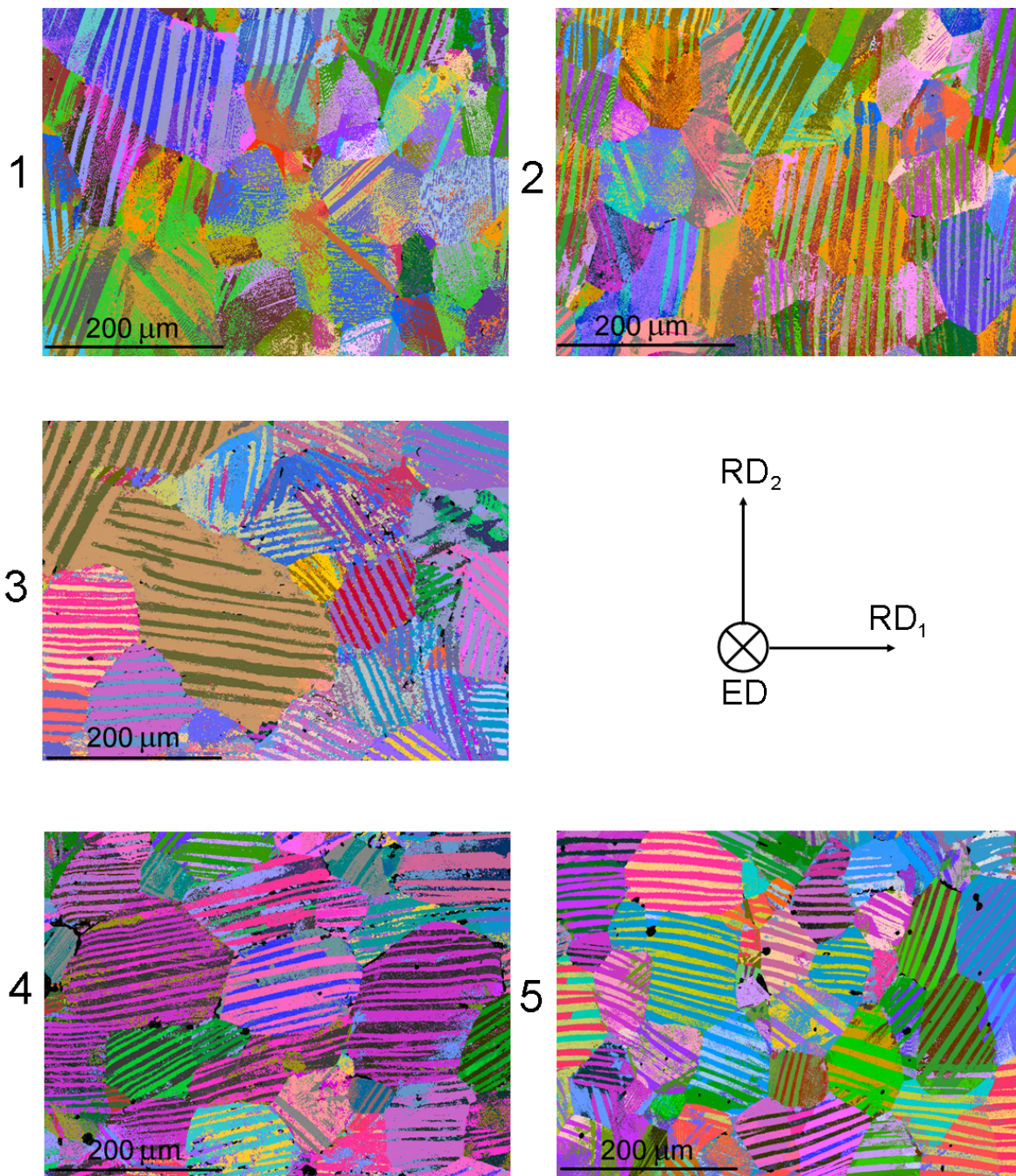**Figure 4.30:** EBSD mappings of the tetragonal 5M phase in the hot extruded sample taken in five positions according to Fig. 4.29 (ED = extrusion direction, RD = radial direction)

Typically, the deformation texture of B2 materials extruded through a round die is axisymmetric and consists of a <100>/<110> double fibre texture with <110> dominating [69]. It changes to a <111> fibre by static and/or dynamic recrystallization [81].
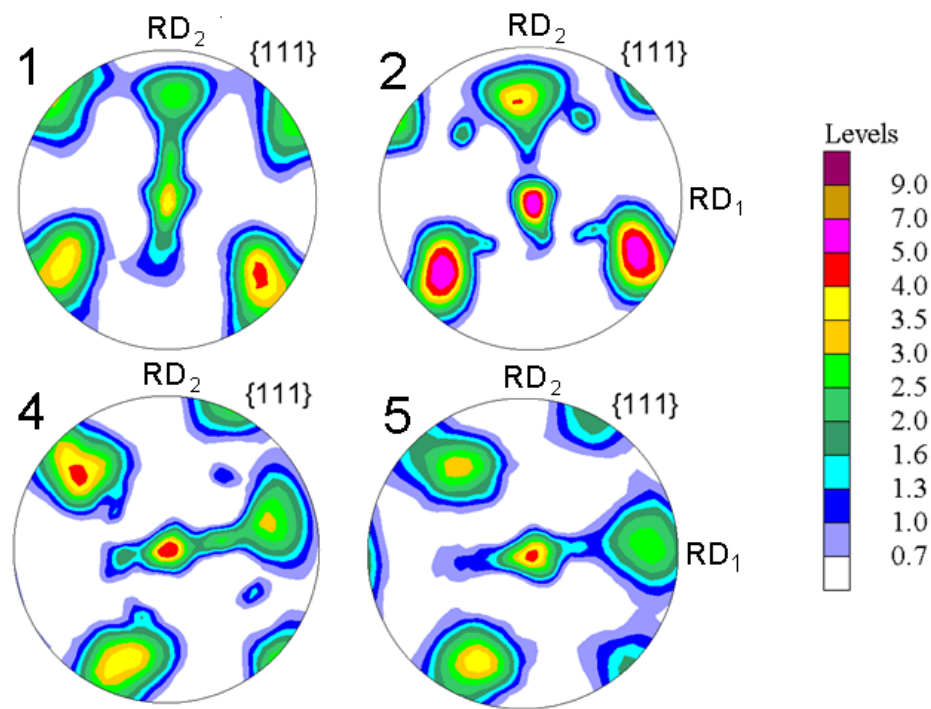
Figure 4.31: {111} pole figures of the tetragonal 5M phase in the hot extruded sample taken in positions 1, 2, 4 and 5 according to Fig. 4.29

As measured in the central part of the extruded rod (position 3) by synchrotron diffraction, the texture in this area is characterized by a $<111>/<110>$ double fibre texture and a cube component (Fig. 4.32). While in positions 1 and 2 strong J_E, weaker F_E and very weak cube components are found. In positions 4 and 5 these components are rotated by 90° around ED with respect to the positions 1 and 2 (Fig. 4.32). This clearly shows that the texture of the hot extruded $Ni_{50}Mn_{29}Ga_{21}$ is a "cyclic" fibre texture consisting of components related to RD rotated about ED. The radially distributed J and F cyclic components can also be observed in the global texture. To measure the global texture of the hot extruded material neutron diffraction was applied on a cylindrical sample with height and diameter of 10 mm cut from the center of the extruded rod (Fig. 4.29). The neutron texture measurement from such a large volume shows that HE produces a $<100>/<110>/<111>$ triple fibre texture with $<100>$ clearly dominating (Fig. 4.33).

Figure 4.32: ODF sections at $\varphi_2 = 0°$ and $\varphi_2 = 45°$ of the hot extruded 5M Ni-Mn-Ga alloy measured with synchrotron radiation at five positions (see Fig. 4.29). Key figure gives the ideal components in extrusion. Intensities are given in multiples of a random distribution (mrd).

The neutron texture measurement approximately corresponds to five positions measured

by synchrotron (Fig. 4.29) extended in ED, where the cyclic J_E and F_E components as a whole create the <111> and <110> fibres. The <100> fibre is mostly found in the center of the rod and less frequently in the off-central regions. It should be mentioned that no obvious variant selection is observed. The reason for the cyclic texture is the grain structure and texture of the initial cast material which typically consists of three zones (chill, columnar and equiaxed zone). The texture is random in the outer chill and inner equiaxed zone, while in the intermediate columnar zone it is a fibre with <100> aligned in radial direction parallel to the long axis of the columnar grains. During HE <110> and <111> are aligned parallel to ED creating the cyclic strong components F_E and J_E. Unfortunately, the initial microstructure was not investigated before extrusion, but the texture and microstructural observations suggest that the intermediate columnar zone dominates by volume (positions 1, 2, 4, 5) compared to the two other zones. The textures of the front and end part of the extruded rod are qualitatively comparable to that of the middle part.
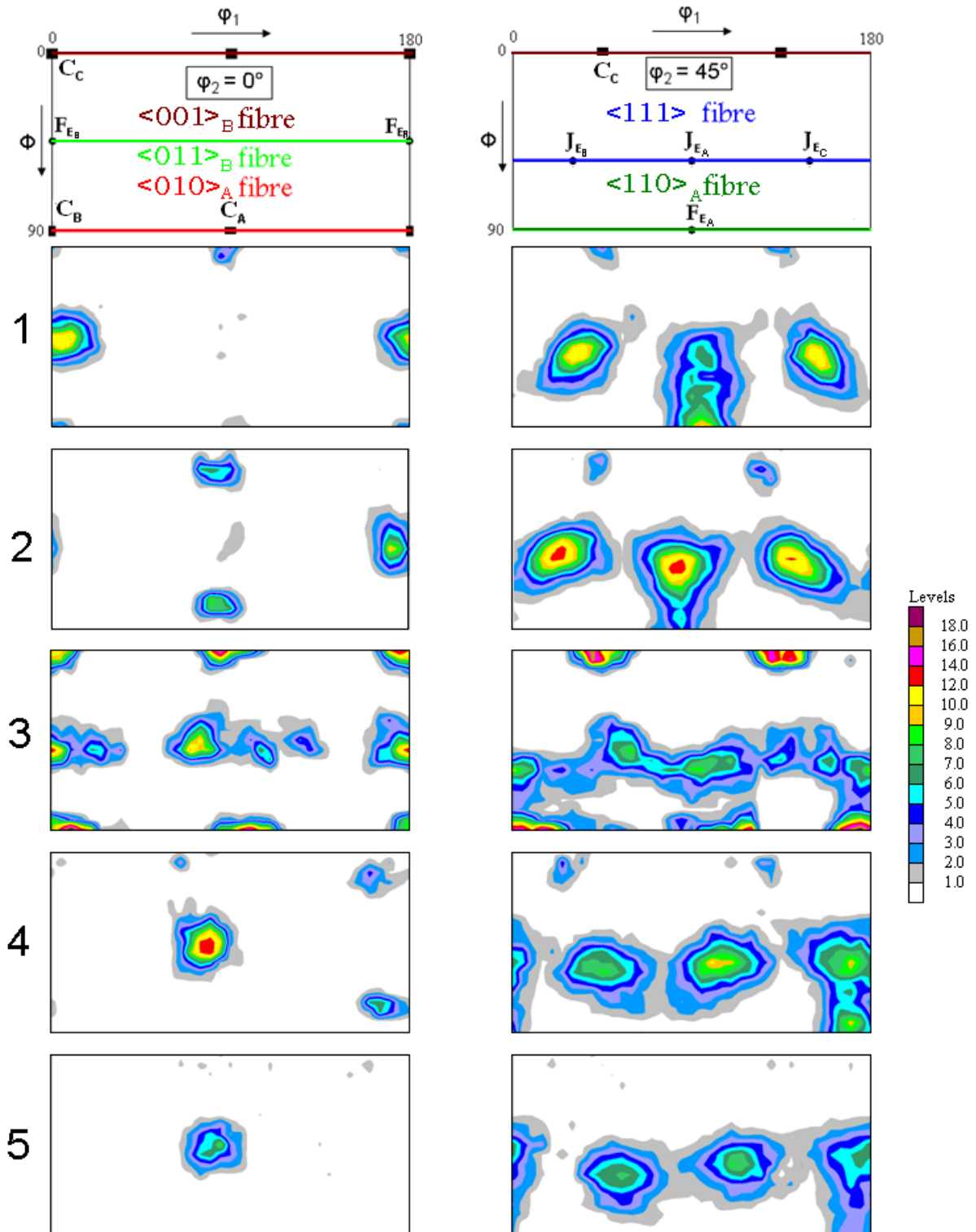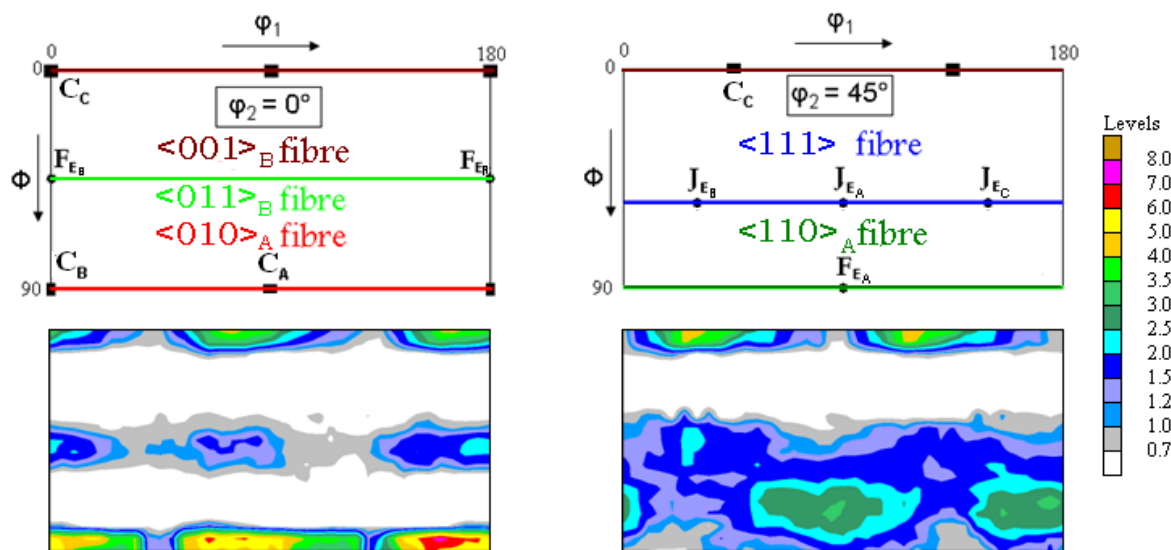

Figure 4.33: ODF sections at $\varphi_2 = 0°$ and $\varphi_2 = 45°$ of the hot extruded 5M Ni-Mn-Ga alloy measured with neutron diffraction. Key figure gives the ideal components in extrusion. Intensities are given in multiples of a random distribution (mrd).

4.6.4 High pressure torsion texture

The fourth fabrication process applied is high pressure torsion (HPT). As a starting material the hot extruded sample was used. High strain torsion of the sample with torsion

axis parallel to the extrusion axis was done with a Paterson rock deformation machine [66] at 1073 K under a confining pressure of 400 MPa. The maximum shear strain and shear strain rate applied were about 3 and $2 \times 10^{-4} s^{-1}$, respectively. The shear stress – shear strain curve for the surface of the sample was calculated from the measured torque and twist data according to the procedure given in [66, 67]. After some undefined oscillations the shear stress at a shear strain of about 2 reaches a steady state value of about 18 MPa, which is the maximum shear stress acting in the torsion sample (Fig. 4.34). The shear strain increases from zero in the centre of the bar to a maximum at the edge according to [68].
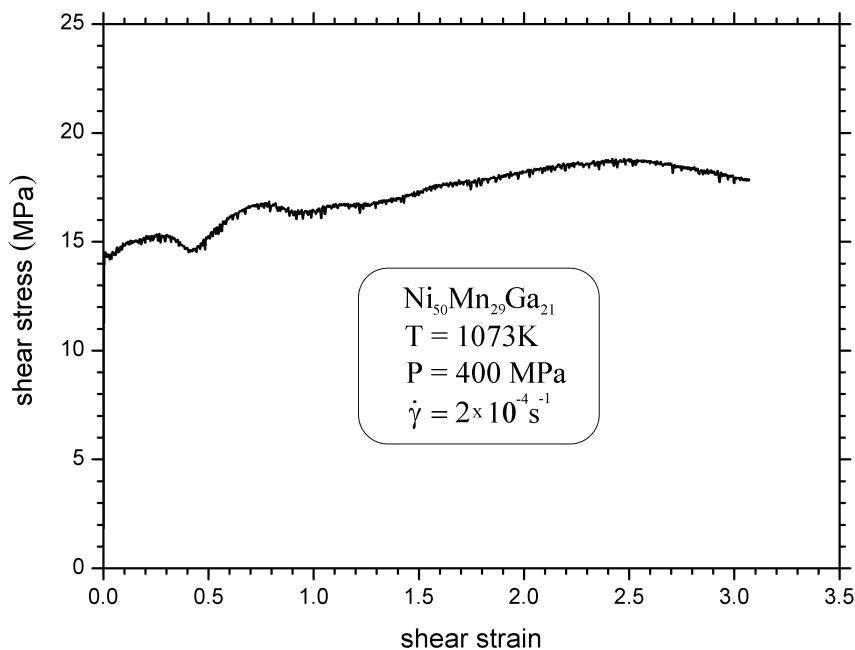
Figure 4.34: Shear stress - shear strain curve for 5M Ni-Mn-Ga deformed by HPT

The microstructure was investigated on longitudinal tangential sections cut at edge positions across the sample. The starting material as mentioned before is characterized by grains slightly elongated in the extrusion direction with a size of about 100 μm (Fig. 4.35a). The grains contain a lot of macro twins with the trace of the twin boundaries preferentially aligned along the extrusion direction. The grain size after torsion is about 250 μm (Fig. 4.35b) due to discontinuous dynamic recrystallization and strain-induced grain growth. The traces of the macro twins are aligned at about 0° and 45° with respect to the shear
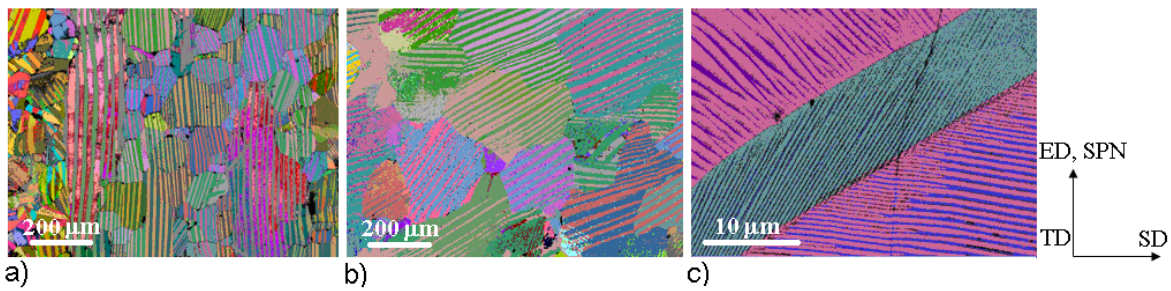
Figure 4.35: EBSD maps showing the microstructure of $Ni_{50}Mn_{29}Ga_{21}$ after hot extrusion (a) and after additional HPT at a shear strain of about 1.88 (b). At higher magnification micro twins (c) are detected within the macro twins shown in (b), (ED = extrusion direction, TD = transverse direction, SPN = shear plane normal, SD = shear direction).
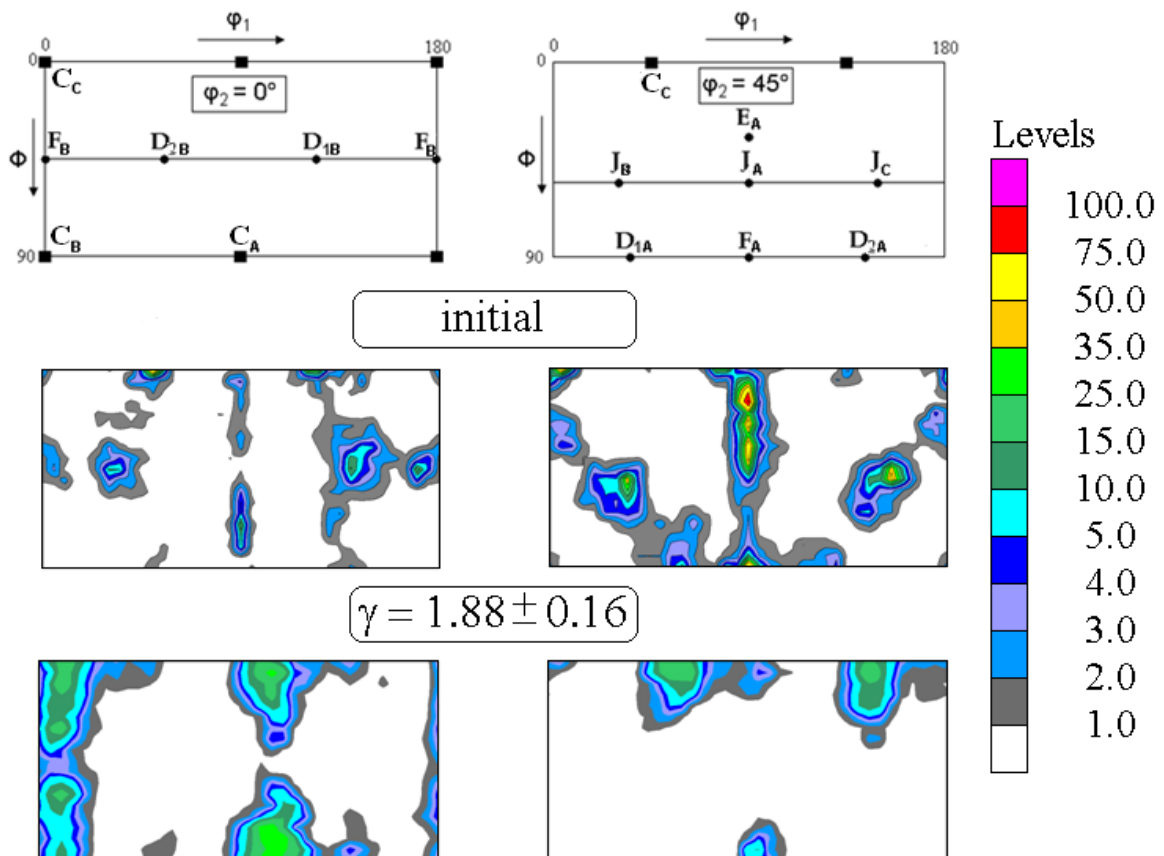
Figure 4.36: ODF sections at $\varphi_2 = 0°$ and $\varphi_2 = 45°$ of the initial hot extruded 5M Ni-Mn-Ga sample and after HPT at a shear strain of 1.88. Key figure gives the ideal components of simple shear of bct metals. Intensities are given in multiples of a random distribution (mrd).

direction. The texture of polycrystalline $Ni_{50}Mn_{29}Ga_{21}$ deformed by HPT at 1073K was investigated with HESR. The high penetration depth of HESR opens the possibility to investigate representative small sample volumes ($1.0 \times 1.2 \times 0.5 \, mm^3$) along the radial direction of the torsion samples in transmission starting at the middle of a pin of size $1.0 \times 1.2 \times 1.0 \, mm^3$. The value of the given shear strain corresponds to the middle of the respectively analyzed volume. The ODF was calculated from the measured pole figures ($\{400\}$, $\{220\}$ and $\{224\}$). The Euler angles were used in Bunge notation [77]. To account best for the monoclinic symmetry of simple shear, the crystal and sample reference systems have been defined as X $\parallel$ shear direction (SD), Y $\parallel$ shear plane normal (SPN), Z $\parallel$ transverse direction (TD) [82]. The textures are represented by $\varphi_2 = 0°$ and $\varphi_2 = 45°$ ODF sections, which for body-centred cubic (bcc) metals contain all major shear components [4.36], (Table 4.2).

Torsion changes the initial <100>/<110>/<111> extrusion cyclic fibre texture to a shear texture with a strong cube and a weak F component, Fig. 4.36. For designation of the simple shear components see Table 4.2. The ODF maxima of the cube and F components are 22 and 8 mrd, respectively. Both components are slightly deviated from the ideal positions in positive φ_1 direction, with the deviation being larger for the cube component. The results obtained on microstructure and texture development correlate quite well with those reported for the B2 structured intermetallic compound NiAl investigated in a wide temperature range [83]. There, it was found that at high temperature (above 1000 K) the cube component increased at the cost of F because of massive grain growth. Moreover, similar deviations were observed. In comparison to the textures already discussed, the texture after HPT seems to be more appropriate for MFIS in polycrystals because it is a biaxial texture consisting of a strong cube component (maximum intensity more than 22 mrd). Similar to the HE case, no obvious variant selection is observed.

Table 4.2: Main ideal orientations in simple shear deformation of bct metals (SP = shear plane, SD = shear direction).

Component	Miller indices		Euler angles		
	∥ SP	∥ SD	φ_1	Φ	φ_2
D_{1A}	$(1\bar{1}\bar{2})$	$[1\bar{1}1]$	33.8	90	45
D_{1B}	$(\bar{1}\bar{2}1)$	$[\bar{1}11]$	126.4	43.2	90
	$(2\bar{1}1)$	$[\bar{1}\bar{1}1]$	126.4	43.2	0
D_{2A}	$(1\bar{1}2)$	$[\bar{1}11]$	144.7	90	45
D_{2B}	$(\bar{1}21)$	$[\bar{1}\bar{1}1]$	53.8	43.2	90
	$(21\bar{1})$	$[1\bar{1}1]$	53.8	43.2	0
F_A	(110)	$[110]$	90	90	45
	(011)	$[100]$	0	43.2	0
F_B	(101)	$[010]$	0	43.2	90
	(101)	$[0\bar{1}0]$	180	43.2	90
	(011)	$[\bar{1}00]$	180	43.2	0
J_A	$(1\bar{1}0)$	$[\bar{1}\bar{1}2]$	90	53	45
J_B	$(10\bar{1})$	$[1\bar{2}1]$	29	53	45
J_C	$(01\bar{1})$	$[\bar{2}11]$	151	54.7	45
E_A	$(1\bar{1}0)$	$[\bar{1}\bar{1}1]$	90	34.8	45
E_B	$(10\bar{1})$	$[1\bar{1}1]$	37.7	64.8	26.6
E_C	$(0\bar{1}1$	$[\bar{1}11]$	142.2	64.8	63.4
C_A	(010)	$[001]$	90	90	0
	(100)	$[001]$	90	90	90
C_B	(010)	$[100]$	0	90	0
	(100)	$[010]$	0	90	90
C_C	(001)	$[100]$	0	0	0
	(001)	$[010]$	90	0	0

5

Conclusions and Outlook

The general conclusion drawn from this work is that a suitable type and strength of texture as well as a proper thermo-mechanical treatment increase the amount of MFIS in polycrystalline $Ni_{50}Mn_{29}Ga_{21}$. The particular results supporting this conclusion can be summarized as follows:

Investigation on microstructure

The initial microstructure of polycrystalline 5M Ni-Mn-Ga alloys is a typical self-accommodated martensitic microstructure containing different variants. The Ni-Mn-Ga polycrystals investigated consist of macro and micro twins with the twin planes determined as {1 0 1). The coarse twin lamellae extend through the whole parent austenitic grains while the fine lamellae frequently cross the coarse variants in a zig-zag manner with mirror symmetry. This kind of microstructure is observed in all polycrystals investigated. It should be mentioned that the fine twin lamellae can only be resolved by EBSD at high magnification. At first the coarse twin lamellae are formed and subsequently the fine twins develop. Besides the so called "twins within twins" structure another type of microstructure can be observed in $Ni_{50}Mn_{29}Ga_{21}$ alloys with {1 1 0) grain boundary which is not equivalent to the twin plane in the tetragonal system. However, the traces of these planes look like a mirror image with respect to the main twin boundary.

Close examination of the high resolution EBSD mapping reveals that more than just three orientations, as expected from the Bain model, exist in $Ni_{50}Mn_{29}Ga_{21}$. Each of the three Bain variants in different regions of the sample may be split according to specific twin relations which differ from each other by about few degrees creating a high number of variants. The model presented in this thesis is based on two different rotations which

multiply the number of possible variants to 96. Using this method, the simulated positions of the martensitic variants do not deviate more than 0.5° from the theoretical positions. Moreover, synchrotron diffraction experiments show that modulation takes place on {110) along <1 1 0]. During twin boundary motion the c-axis orientation changes and with this also the direction of modulation with respect to the initial single crystal reference system. This demonstrates that the direction of modulation is crystallographically fixed normal to the c-axis.

Training process

The training process, as the last step in the preparation procedure of Ni-Mn-Ga alloys, consists of multi-axis compression finally leading to a single-variant state. Compression of polycrystalline samples leads to the motion of those twin boundaries changing the volume fraction of particular martensitic variants in such a way that the shortest axis (c-axis) becomes preferentially aligned parallel to the compression axis. It allows reducing the twinning stress and maximizing the twinning strain. It is shown that the fastest way to train Ni-Mn-Ga 5M single or polycrystals is by successive compression just along two axes with respect to the main (macro) twins.

Texture analysis

Table 5.1 summarizes the texture of $Ni_{50}Mn_{29}Ga_{21}$ polycrystals observed so far for different fabrication processes and thermo-mechanical treatments. The analyses of global texture measurements by synchrotron radiation and neutrons of Ni-Mn-Ga subjected to DS and HR show a fibre or weak biaxial texture. The texture after HPT is characterized by a strong cube component which seems to be most suited for MFIS in $Ni_{50}Mn_{29}Ga_{21}$ polycrystals. The cyclic fibre texture of hot extruded material also allows finding off-center regions with two strong texture components, which are slightly differently oriented. Additionally, in Table 5.1 the measured textures are compared with literature results. As can be seen the measured textures coincide with those reported for related bcc metals and B2', B2 intermetallics.

Table 5.1: Main textures of $Ni_{50}Mn_{29}Ga_{21}$(RR = reduction ratio)

Process	Deformation parameters	Texture	Texture reference
directional solidification (DS)	cast on cold copper plate	<100> fibre	<100> fibre ($Ni_{48}Mn_{30}Ga_{22}$) [65]
hot rolling (HR)	1273 K 50% RR	weak {111}<112>	{111}<112> ($\alpha - Fe$, Mo, W) [80]
hot extrusion (HE)	1273 K 4/1 RR round die	<100><110><111> cyclic fibre texture	<100> fibre ($Ni_{49}Mn_{27.5}Ga_{23.5}$) [58]
high pressure torsion (HPT)	1073 K $\gamma = 1.88$	cube and F	cube and F (NiAl) [83]

Outlook

Further work to be done within this field is to study the interaction of the twin variants as well as their interaction with grain boundaries. Another task will also be to find the conditions of "safe" training. Therefore, training at higher temperatures is of great interest. It is also important to continue texture measurements on thermo-mechanically treated and mechanically trained Ni-Mn-Ga polycrystals with the aim to optimize MFIS.

Bibliography

[1] K. Ullakko, J. K. Huang, C. Kantner, R. C. O'Handley, and V. V. Kokorin. Large magnetic-field-induced strains in Ni_2MnGa single crystals. *Applied Physics Letters*, 69:1966–1968, 1996.

[2] S. J. Murray, M. Marioni, S. M. Allen, R. C. O'Handley, and T. A. Lograsso. 6% magnetic-field-induced strains by twin boundary motion in ferromagnetic Ni-Mn-Ga. *Applied Physics Letters*, 77:886–888, 2000.

[3] P. Müllner, V. A. Chernenko, M. Wollgarten, and G. Kostorz. Large cyclic deformation of a Ni-Mn-Ga shape memory alloy induced by magnetic fields. *Journal of Applied Physics Letters*, 92/11:6708–6713, 2002.

[4] O. Heczko, N. Scheerbaum, and O. Gutfleisch. *Nanoscale magnetic materials and applications - Magnetic shape memory phenomena.* Springer-Verlag, 2009.

[5] P. Müllner, V. A. Chernenko, and G. Kostorz. A microscopic approach to the magnetic-field-induced deformation of martensite (magnetoplasticity). *Journal of Magnetism and Magnetic Materials*, 267:325–334, 2003.

[6] A. Sozinov, A. A. Likhachev, N. Lanska, and K. Ullakko. Giant magnetic-field-induced strain in Ni-Mn-Ga seven-layered martensitic phase. *Applied Physics Letters*, 80:1746–1748, 2002.

[7] O. Heczko, A. Sozinov, and K. Ullakko. Giant field-induced reversible strain in magnetic shape memory alloys. *IEEE Transactions on Magnetics*, 36:3266–3268, 2000.

[8] E. C. Bain. The nature of martensite. *Transactions AIME*, 70:25–35, 1924.

[9] G. Kurdjumov and G. Sachs. Über den mechanismus der stahlhärtung. *Zeitschrieft für Physik*, 63:225–243, 1930.

[10] Z. Nishiyama. X-ray investigation of the mechanism of the transformation from faced-centred cubic lattice to body centred cubic. *Science Reports Tohoku Imperial University*, 23:1934–1935, 1930.

[11] G. Wassermann. *Archiv für das Eisenhüttenwesen*, 16:647–649, 1933.

[12] V. A. Cherneko. Compositional instability of ß-phase in Ni-Mn-Ga alloys. *Scripta Materialia*, 40:523–527, 1999.

[13] V. A. Cherneko, E. Cesari, V. V. Kokorin, and I. N. Vitenko. The development of new ferromagnetic shape memory alloys in Ni-Mn-Ga system. *Scripta Metallurgica et Materialia*, 33:1239, 1995.

[14] S. K. Wu and S. T. Yang. Effect of composition on transformation temperatures of Ni-Mn-Ga shape memory alloys. *Materials Letters*, 57:4291–4296, 2006.

[15] P. J. Brown, J. Crangle, T. Kanomata, M. Matsumoto, K. U. Neumann, B. Ouladdiaf, and K. R. A. Ziebeck. The crystal structure and phase transitions of the magnetic shape memory compound Ni$_2$MnGa. *Journal of Physics*, 14:10159–10171, 2002.

[16] R. W. Overholser, M. Wuttig, and D. A. Neumann. Chemical ordering in Ni-Mn-Ga heusler alloys. *Scripta Materialia*, 40:1095–1102, 1999.

[17] V. V. Martynov. X-ray diffraction study of thermally and stress-induced phase transformations in single crystalline Ni-Mn-Ga alloys. *Journal de Physique IV*, 5:5–13, 1995.

[18] J. Pons, V. A. Chernenko, S. Santamarta, and E. Cesari. Crystal structure of martensitic phases in Ni-Mn-Ga shape memory alloys. *Acta Materialia*, 48:3027–3038, 2000.

[19] A. Sozinov, A. A. Likhachev, and K. Ullakko. Magnetic and magnetomechanical properties of Ni-Mn-Ga alloys with easy axis and easy plane of magnetization. *Proceedings of SPIE*, 4333:189–196, 2001.

[20] V. V. Martynov and V. V. Kokorin. The crystal structure of thermally- and stress-induced martensites in Ni_2MnGa single crystals. *Journal de Physique III*, 2:739–749, 1992.

[21] A. T. Zayak, P. Entel, and J. Hafner. A first-principles investigation of tetragonal and orthorhombic deformations in the ferromagnetic heusler alloy Ni_2MnGa. *Journal de Physique IV*, 112:985–988, 2003.

[22] A. T. Zayak, P. Entel, J. Enkovaara, A. Ayuela, and R. M. Nieminen. First-principles investigations of homogeneous lattice-distortive strain and shuffles in Ni_2MnGa. *Journal of Physics - Condensed Matter*, 15:159–164, 2003.

[23] A. T. Zayak and P. Entel. Role of shuffles and atomic disorder in Ni-Mn-Ga. *Materials Science and Engineering A*, 378:419–423, 2004.

[24] J. Pons, R. Santamarta, V. A. Chernenko, and E. Cesari. HREM study of martensitic phases in Ni-Mn-Ga alloys. *Materials Chemistry and Physics*, 81:457–459, 2003.

[25] J. Pons and S. Santamarta. Long-period martensitic structures of Ni-Mn-Ga alloys studied by high-resolution transmission electron microscopy. *Journal of Applied Physics*, 97:083516–083522, 2005.

[26] J. W. Christian and S. Mahajan. Deformation twinning. *Progress in Materials Science*, 39:1–157, 1995.

[27] Y. Chu. Structural and magnetic phase transitions in Ni-Mn-Ga ferromagnetic shape memory alloys. *IEEE Transactions on Magnetic*, 37:2666–2668, 2001.

[28] A. N. Vasilev, A. D. Bozhko, V. V. Khovailo, I. E. Dikshtein, V. G. Shavrov, V. D. Buchelnikov, M. Matsumoto, S. Suzuki, T. Takagi, and J. Tani. Structural and magnetic phase transitions in shape memory alloys. *Physical Review B*, 59:1113–1120, 1999.

[29] H. Morito, A. Fujita, K. Fukamichi, R. Kainuma, K. Ishida, and K. Oikawa. Magnetocrystalline anisotropy in single-crystal Co-Ni-Al ferromagnetic shape memory alloy. *Applied Physics Letters*, 79:3290–3292, 2001.

[30] T. Kannomata, K. Shirakawa, and T. Kaneko. Effect of hydrostatic pressure on the curie temperature of the heusler alloys Ni_2MnZ (Z=Al, Ga, In, Sn and SB). *Journal of Magnetism and Magnetic Materials*, 65:76–82, 1987.

[31] N. Lanska, O. Soderberg, A. Sozinov, Y. Ge, K. Ullakko, and V. K. Lindroos. Composition and temperature dependence of the crystal structure of Ni-Mn-Ga alloys. *Journal of Applied Physics*, 95:8074–8078, 2004.

[32] C. Jiang, Y. Muhammed, L. Deng, W. Wu, and H. Xu. Composition dependence on the martensitic structures of the Mn-rich NiMnGa alloys. *Acta Materialia*, 52:2779–2785, 2004.

[33] U. Gaitzsch, M. Pötschke, S. Roth, N. Mattern, B. Rellinghaus, and L. Schultz. Structure formation in martensitic $Ni_{50}Mn_{30}Ga_{20}$ MSM alloy. *Journal of Alloys and Compounds*, 443:99–104, 2007.

[34] A. A. Likhachev, A. Sozinov, and K. Ullakko. Different modeling concepts of magnetic shape memory and their comparism with some experimental results obtained in Ni-Mn-Ga. *Materials Science and Engineering*, 378:513–518, 2004.

[35] A. A. Likhachev and K. Ullakko. Influence of external stress on thereversibility of magnetic-field-controlled shape memory effect in Ni-Mn-Ga. *Proceedings of SPIE*, 4333:197–203, 2001.

[36] A. Sozinov, A. A. Likhachev, N. Lanska, and K. Ullakko. Crystal. *Journal of Alloys and Compounds*, 38:2814–2816, 2002.

[37] L. Straka, N. Lanska, K. Ullakko, and A. Sozinov. Twin microstructure dependent mechanical response in Ni-Mn-Ga single crystals. *Applied Physics Letters*, 96(13), 2010.

[38] O. Heczko and L. Straka. Temperature dependence and temperature limits of magnetic shape memory effect. *Journal of Applied Physics*, 94:7139–7143, 2003.

[39] O. Söderberg, L. Straka, V. Novak, O. Heczko, S. P. Hannula, and V. K. Lindroos.

Tensile/compressive behaviour of non-layered tetragonal nimnga alloy. *Materials Science and Engineering A*, 386:27–33, 2004.

[40] N. Okamoto, T. Fukuda, T. Kakeshita, and T. Takeushi. Magnetocrystalline anisotropy and twinning stress of 10M and 2M martensites in Ni-Mn-Ga system. *Materials Science Forum*, 512:195–200, 2006.

[41] N. Okamoto, T. Fukuda, and T. Kakeshita. Temperature dependence of rearrangement of martenite variants by magnetic field in 10M, 14M and 2M martensites of Ni-Mn-Ga. *Materials Science and Engineering A*, 306:481–482, 2008.

[42] O. Heczko, L. Straka, N. Lanska, K. Ullakko, and J. Enkovaara. Temperature variation of structure and magnetic properties of Ni-Mn-Ga magnetic shape memory alloy. *Journal of Magnetism and Magnetic Materials*, 91:242–245, 2002.

[43] S. Rajasekhara and P. J. Ferreira. A dislocation model for the magnetic field induced shape memory effect in Ni_2MnGa. *Scripta Materialia*, 53:817–822, 2005.

[44] X. Wang and J. Zhang. In situ high-energy X-ray studies of magnetic-field-induced phase transition in a ferromagnetic shape memory Ni-Co-Mn-In alloy. *Acta Materialia*, 55:5169–5179, 2007.

[45] M. Han, J. C., M. A. Bennett, Gharghouri, J. Chen, and C. V. Hyatt. Understanding modulated twin transition at the atomic level. *Acta Materialia*, 55:1731–1740, 2007.

[46] R. C. O'Handley. Discussion session at the workshop on magnetic shape memory alloys. *Ascona, Switzerland*, 11-16 Sept. 2005.

[47] Y. Murakami, D. Shindo, M. Suzuki, M. Ohtsuka, and K. Itagaki. Magnetic domain structure in $Ni_{53.6}Mn_{23.4}Ga_{23.0}$ shape memory alloy films studied by electron holography and lorentz microscopy. *Acta Materialia*, 51:485–494, 2003.

[48] K. Ullakko, A. Sozinov, and P. Yakovenko. *ArXiv:cond-mat/0004211 v1*, 2000.

[49] K. Ullakko, Y. Ezer, A. Sozinov, G. Kimmel, P. Yakovenko, and V. K. Lindroos. Magnetic-field-induced strains in polycrystalline Ni-Mn-Ga at room temperature. *Scripta Matererialia*, 44:475–480, 2001.

[50] M. A. Meyers, O. Vöhringer, and V. A. Lubarda. The onset of twinning in metals: a constitutive description acta materialia. *Acta Materialia*, 49:4025–4039, 2001.

[51] R. Chulist, M. Pötschke, A. Böhm, H.-G. Brokmeier, U. Garbe, T. Lippmann, C.-G. Oertel, and W. Skrotzki. Cast and rolling textures of Ni-Mn-Ga alloys. *MRS Proceedings 1050E*, Warrendale PABB09:03, 2008.

[52] M. Pasquale, C. P. Sasso, S. Besseghini, F. Passaretti, E. Villa, and V. A. Chernenko. Effect of texturing on the magnetically activated properties of polycrystalline NiMnGa alloys. *Journal de Physique IV*, 11:305–311, 2001.

[53] F. Albertini, S. Besseghini, A. Paoluzi, L. Pareti, M. Pasquale, F. Passaretti, C. P. Sasso, A. Stantero, and E. Villa. Structural, magnetic and anisotropic properties of Ni_2MnGa melt-spun ribbons. *Journal of Magnetism and Magnetic Materials*, 242-245:1412–1424, 2002.

[54] D. Y. Cong, Y. D Wang, P. Zetterström, R. L. Peng, R. Delaplane, X. Zhao, and L. Zuo. Crystal structures and textures of hot forged $Ni_{48}Mn_{30}Ga_{22}$ alloy. *Materials Science and Technology*, 21:1412–1414, 2005.

[55] S. Besseghini, E. Villa, F. Passarati, M. Pini, and F. Bonfanti. Plastic deformation of NiMnGa polycrystals. *Materials Science and Engineering A*, 378:415–418, 2004.

[56] B. Lu, H. B. Wang, Y. Liu, and H. l. Wang. Formation of texture of $Ni_{48}Mn_{31}Ga_{21}$ polycrystalline alloy by thermal simulation pack rolling technology. *Transactions of the Nonferrous Metals Society of China*, 16:843–847, 2006.

[57] R. Chulist, A. Böhm, T. Lippmann, W. Skrotzki, W. G. Drossel, and R. Neugebauer. Twinning behaviour of textured polycrystalline Ni-Mn-Ga alloy after hot extrusion. *Materials Science Forum*, 635:195–199, 2010.

[58] H. Morawiec, J. Lelatko, T. Goryczka, K. Prusik, St. Piechota, and D. Stroz. Extruded rods with <001> axial texture of polycrystalline Ni-Mn-Ga alloys. *Materials Science Forum*, 635:189–194, 2010.

[59] R. Chulist, W. Skrotzki, C.-G. Oertel, A. Böhm, T. Lippmann, and E. Rybacki. Microstructure and texture in $Ni_{50}Mn_{29}Ga_{21}$ deformed by high-pressure torsion. *Scripta Materialia*, 62:650–653, 2010.

[60] F. Thoss, M. Pötschke, U. Gaitzsch, J. Freudenberger, W. Anwand, S. Roth, B. Rellinghaus, and L. Schultz. Grain growth in Ni-Mn-Ga alloys. *Journal of Alloys and Compounds*, 488:420–424, 2009.

[61] R. Chulist, M. Pötschke, C.-G. Oertel T. Lippmann, and W. Skrotzki. Deformation twinning in polycrystalline Ni-Mn-Ga alloys. *Journal of Physics: Conference Series*, 240:012024–012027, 2010.

[62] R. Chulist, W. Skrotzki, C.-G. Oertel, A. Böhm, and M. Pötschke. Change in microstructure during training of a $Ni_{50}Mn_{29}Ga_{21}$ bicrystal. *Scripta Materialia*, 63:548–551, 2010.

[63] U. Gaitzsch, S. Roth, B. Rellinghaus, and L. Schultz. Adjusting the crystal structure of NiMnGa shape memory ferromagnets. *Journal of Magnetism and Magnetic Materials*, 305:275–277, 2006.

[64] U. Gaitzsch, M. Pötschke, S. Roth, B. Rellinghaus, and L. Schultz. A 1% magnetostrain in polycrystalline 5M Ni-Mn-Ga. *Acta Materialia*, 57:365–370, 2009.

[65] M. Pötschke, U. Gaitzsch, B. Rellinghaus S. Roth, and L. J. Schultz. Preparation of melt textured Ni-Mn-Ga. *Journal of Magnetism and Magnetic Materials*, 316:383–385, 2007.

[66] M. S. Paterson and D. L. Olgaard. Rock deformation tests to large shear strains in torsion. *Journal of Structural Geology*, 22:1341–1358, 2000.

[67] B. Klöden, C.-G. Oertel, E. Rybacki, and W. Skrotzki. Torsional creep of polycrystalline NiAl. *Scripta Materialia*, 52:289–293, 2005.

[68] J. G. Ramsay and M. I. Huber. *The Techniques of Modern Structural Geology*. Academic Press, London, 1983.

[69] R. Tamm W. Skrotzki and C.-G. Oertel. Effects of thermomechanical processing on texture formation in iron aluminides. *Materials Science Forum*, 426:3593–3598, 2003.

[70] L. Wcislak, H. Klein, H.J. Bunge, U. Garbe, T. Tschentscher, and J.R. Schneider. Texture analysis with high-energy synchrotron radiation. *Journal of Applied Crystallography*, 35:82–85, 2002.

[71] H. J. Bunge. *Texture Analysis in Materials Science: Mathematical Methods.* Culliver Verlag Göttingen, 1993.

[72] K. Pawlik and P. Ozga. Labotex: The texture analysis software. *Göttinger Arbeiten zur Geologie und Paläontologie*, SB4:146–147, 1999.

[73] R. V. Kohn and S. Müller. Branching of twins near an austenite-twinned martensite interface. *Philosophical Magazine A*, 66:697–715, 1992.

[74] A. Sozinov, A. A. Likhachev, and K. Ullakko. Giant field-induced reversible strain in magnetic shape memory NiMnGa alloy. *IEEE Transactions on Magnetics*, 36:3266–3268, 2000.

[75] Y. Ge, H. Jiang, A. Sozinov, O. Soderberg, N. Lanska, E. I. Kauppinem J. Keranen, V. K. Lindroos, and S. P. Hannula. Crystal structure and macrotwin interface of five-layered martensite in NiMnGa magnetic shape memory alloy. *Materials Science and Engineering A*, 438:961–964, 2006.

[76] M. Hatherley and W. B. Hutchinson. *An Introduction to Textures in Metals.* Chamefeon Press Ltd. London, 1979.

[77] H. J. Bunge. *Texture Analysis in Materials Science: Mathematical Methods.* Butterworths London, 1982.

[78] J. Hansen, J. Pospiech, and K. Lücke. *Tables for Texture Analysis of Cubic Crystals.* Springer Berlin, 1978.

[79] G. Wassermann and J. Grewen. *Texturen metallischer Werkstoffe.* Springer, 1962.

[80] D. Raabe and K. Lücke. Rolling and annealing textures of bcc metals. *Materials Science and Engineering A*, 157-162:597–610, 1994.

[81] W. Skrotzki, K. R. Tamm, Kegler, and C.-G. Oertel. Deformation and recrystallization textures in iron aluminides. *Materials Science Forum: Microstructure and Texture in Steels*, Part V:379–391, 2009.

[82] J. Baczynski and J. J. Jonas. Texture development during the torsion testing of α - iron and IF steels. *Acta Materialia*, 44:4273–4288, 1996.

[83] B. Klöden, C.-G. Oertel, E. Rybacki, and W. Skrotzki. Texture formation and swift effect in high strain torsion of NiAl. *Journal of Engineering Materials and Technology*, 131:011101.1–9, 2009.

List of publications

R. Chulist, M. Pötschke, A. Böhm, H.-G. Brokmeier, U. Garbe, T. Lippmann, C.-G. Oertel, and W. Skrotzki. Cast and rolling textures of Ni-Mn-Ga alloys. *MRS Proceedings* 1050*E Warrendale*, PA BB09–03 2008.

R. Chulist, M. Pötschke, T. Lippmann, C.-G. Oertel, and W. Skrotzki. Deformation twinning in polycrystalline Ni-Mn-Ga alloys. *Journal of Physics: Conference Series,* 240:012024–27 2009.

R. Chulist, M. Pötschke, T. Lippmann, C.-G. Oertel, and W. Skrotzki. On the role of twinning in Ni-Mn-Ga magnetic shape memory alloys. *15thInternational Symposium on Plasticity & Its Current Applications,* ISBN: 0-9659463-9-8:322–324 2009.

R. Chulist, A. Böhm, T. Lippmann, W. Skrotzki, W. G. Drossel, and R. Neugebauer. Twinning behaviour of textured polycrystalline Ni-Mn-Ga alloy after hot extrusion. *Materials Science Forum*, 635:195–199 2010.

R. Chulist, W. Skrotzki, C.-G. Oertel, A. Böhm, and T. Lippmann. Microstructure and texture in $Ni_{50}Mn_{29}Ga_{21}$ deformed by high-pressure torsion. *Scripta Materialia*, 62:650–653 2010.

R. Chulist, C.-G. Oertel, W. Skrotzki, and T. Lippmann. Direction of modulation during twin boundary motion. *Scripta Materialia*, 62:235–237 2010.

R. Chulist, W. Skrotzki, C.-G. Oertel, A. Böhm, and M. Pötschke. Change in microstruc-

ture during training of a Ni$_{50}$Mn$_{29}$Ga$_{21}$ bicrystal. *Scripta Materialia*, 63:548–551 2010.

Acknowledgement

First of all I would like to thank my supervisor Prof. Dr. Werner Skrotzki for the patient guidance, support, encouragement and advice he provided throughout my time as his student. Especially, I am grateful for many conversations that clarified my thinking on many scientific topics and for the care with which he reviewed my thesis. I would also like to thank Dr. Carl-Georg Oertel for wise advices, help with various scientific applications and technical problems. I am indebted to many of my colleagues from the Institute of Structural Physics and the Priority Program (SPP 1239) which invested much time and effort to support my investigations. Special thanks go to Dr. Stefan Roth, Dr. Andrea Böhm, Dr. Benoit Beausir and Martin Pötschke for a helpful and effective collaboration. I am also grateful to Prof. Dr. Heinz-Günter Brokmeier and Dr. Thomas Lippmann for support in texture measurements with neutron diffraction and high energy synchrotron radiation. They were always willing to share their extensive research experience. I wish to thank my family for providing a loving environment for me, especially my wife Katarzyna, my parents, sister and brother. The work was financially supported by the Deutsche Forschungsgemeinschaft through SPP 1239.

Erklärung

Ich erkläre hiermit an Eides statt, dass ich die vorliegende Arbeit ohne unzulässige Hilfe Dritter und ohne Benutzung anderer als der angegebenen Hilfsmittel angefertigt habe; die aus anderen Quellen direkt oder indirekt übernommenen Daten und Konzepte sind unter Angabe des Literaturzitats gekennzeichnet. Die Arbeit wurde bisher weder im Inland noch im Ausland in gleicher oder ähnlicher Form einer anderen Prüfungsbehörde vorgelegt.

Die Dissertation wurde an der TU Dresden unter der wissenschaftlichen Betreuung von Prof. Dr. Werner Skrotzki und Dr. Carl-Georg Oertel angefertigt. Die Promotionsordnung der Fakultät für Mathematik und Naturwissenschaften vom 20.03.2000 erkenne ich an.

Datum   Unterschrift